Title
Application of the Floxin gene targeting technology reveals that Ofd1 controls centriole length

Author
Singla, Veena

Publication Date
2010

Peer reviewed|Thesis/dissertation

Application of the Floxin gene targeting technology reveals that *Ofd1* controls centriole length

by

Veena Singla

DISSERTATION

Submitted in partial satisfaction of the requirements for the degree of

DOCTOR OF PHILOSOPHY

in

CELL BIOLOGY

in the

ACKNOWLEDGEMENTS

I approached my first day of grad school with trepidation, feeling out of place, nervous and unsure of what I was doing. Emerging from the belly of the whale into the light at last, I welcome the opportunity to thank those who helped me along the way and made my little contribution to science possible. By little, I do not mean diminutive, but rather, something incremental that others can hopefully build upon…because that's the way science really works. I also mean cute, because small things are adorable.

Back in the day, it was just the four of us in lab, so it was a good thing we all got along so well. I owe a lot of my training to one Dr. Kevin Corbit, who was generous with his time and an excellent, patient teacher. We could also pass downtime during washes by making animal sounds and plotting the creation of our next ungodly hybrid creature. He was always willing to help me troubleshoot protocols and his extensive knowledge of technical and scientific literature gave him the well-earned name Kevinpedia.

I met Jeremy at my second official UCSF event: Granlibakken Tetrad retreat, 2003. He gave a poster about a system for working with embryonic stem cells. I was hooked, not just by the science, but also by his enthusiasm, excitement, and charisma. Anyone who knows Jeremy will agree that he is brilliant; an informal lab survey revealed 100% agreement that he would get a Nobel someday. But to truly be a good mentor takes smarts and then some. Lucky for me Jeremy has the then some…I think one of his best qualities is his stoic yet unflappable optimism, which is essential when you think you've been scooped or your month long experiment didn't work. I could always depend on him to be the one reasonable person in my life, a reliable island of sanity in a sea of crazy. I

admire his boldness, confidence and creativity in science. His guidance has made possible my current, and future, success.

Even when nothing is working and life is going to hell, I can always count on my girls in lab to commiserate, cheer me up, and make me a drink (not necessarily in that order). Nicole and Julie, you preserved my sanity by giving me some weekends off- I love how we got each other's backs in the SCSCSC! Hard days in lab are a lot easier to get through with (a) bad music (b) drinking and (c) happy hour to look forward to at the end of the day…Nicole and Victoria, I don't think I could have made it through some days without you lovely ladies around. Inside and outside of lab, you've always been supportive, generous, and willing to listen to me whine. I am so lucky to count you as my friends. I love you girls!

Lani- you have helped me in so many ways, scientifically and as a friend. I firmly believe that shameless public drunkenness is something to be shared…good thing someone agrees with me.

Favorite class sub-group (A): Matt, Holly, Emma. Started as a study group, but we got along so well we never stopped hanging out. Thanks for being there to listen through all my hard times, and all the awesome birthday lunches.

Favorite class sub-group (B): Emma, Monica, Georgette; otherwise known as Arts and Culture Sundays. Most people hate Sunday evenings because it means the end of the weekend. I looked forward to them because it meant I got to see some of my favorite people in the world, eat a fabulous meal, and reset for the week. No matter how I felt going in, I always felt better going out. We have supported each other through a lot, and I know I can count on these girls always.

Jesahel, I love the way you manage to accomplish what you want no matter what life throws at you. You've helped me face difficult times with compassion and humor, and I am so grateful for you.

Any time of day or night, if I need to talk to someone, I can call Grace. We've known each other going on 13 years now, and regardless of what changes, what's important always stays the same.

Somehow I found someone that's part wholesome, subversive, and ridiculous in equal measure to share my time with. Rego, you are my favorite fuzzy and one and only house Turk.

Finally, I have to thank my parents, for making my achievements possible in so many ways. I know that life is not always fair and there will undoubtedly be tough times ahead…but knowing I have all these wonderful people with me will make those times easier to face.

ACKNOWLEDGEMENT OF PUBLISHED MATERIAL

Chapter one of this thesis contains material adapted from "Floxin, a resource for genetically engineering mouse ESCs." Veena Singla, Julie Hunkapiller, Nicole Santos, Allen D. Seol, Andrew R. Normal, Paul Wakenight, William C. Skarnes, and Jeremy F. Reiter. *Nature Methods*. 2010. January, 7(1): 50-2. Chapter two of this thesis contains material adapted from "The primary cilium as the cell's antenna: signaling at a sensory organelle." Veena Singla and Jeremy F. Reiter. *Science*. 2006. August, 4; 313 (5787): 629-33. and "*Ofd1*, a human disease gene, regulates the length and distal structure of centrioles." Veena Singla, Miriam Romaguera-Ros, Jose Manuel Garcia-Verdugo, and Jeremy F. Reiter. *Developmental Cell*. 2010. March, 16; 18(3): 410-424.

Application of the Floxin gene targeting technology reveals that *Ofd1* controls centriole length

Veena Singla

ABSTRACT

We describe here a resource of mouse embryonic stem (ES) cell lines that contain gene trap insertions capable of post-insertional modification. We demonstrate Floxin technology for efficient targeted modification of gene trap alleles. Loss-of-function gene trap mutations created with the pGTLxf and pGTLxr vectors are reverted and new DNA sequences inserted into the locus using Cre recombinase and a shuttle vector, pFloxin. As proof-of-principle, we used this strategy to create targeted modification of several gene trap alleles. pFloxin-contained DNA constructs are efficiently and precisely inserted, and are regulated by endogenous promoters. Possible applications include the generation of point mutations, humanized alleles, tagged alleles and insertion of non-homologous constructs such as fluorescent reporters. The resource contains ES cell lines with compatible gene traps in more than 4,500 genes, enabling the high-throughput modification of many genes in mouse ES cells.

Centrosomes and their component centrioles represent the principal microtubule organizing centers of animal cells. Here we show that the gene underlying Orofaciodigital Syndrome 1, *Ofd1*, is a component of the distal centriole that controls centriole length. In the absence of *Ofd1*, distal regions of centrioles, but not procentrioles, elongate abnormally. These long centrioles are structurally similar to normal centrioles, but contain destabilized microtubules with abnormal post-translational modifications. *Ofd1* is also important for centriole distal appendage formation and centriolar recruitment

of the intraflagellar transport protein Ift88. To model OFD1 Syndrome in embryonic stem cells, we replaced the *Ofd1* gene with missense alleles from human OFD1 patients. Distinct disease-associated mutations cause different degrees of excessive or decreased centriole elongation, all of which are associated with diminished ciliogenesis. Our results indicate that Ofd1 acts at the distal centriole to build distal appendages, recruit Ift88, and stabilize centriolar microtubules at a defined length.

TABLE OF CONTENTS

LIST OF TABLES

Chapter 1

Chapter 2

LIST OF FIGURES

Chapter 1

Chapter 2

CHAPTER 1: Floxin, a resource for genetically engineering mouse ESCs.

INTRODUCTION

Genetic modification of mouse embryonic stem cells (ESCs) and mice is an important source of insight into the functions of mammalian genes. Loss of function studies provide valuable initial information about gene function, but a full understanding of gene structure and function requires study of alleles other than the null allele. The most widely applied approaches for genetic modification of mouse ESCs are transgene insertion and homologous recombination. These methods allow creation of loss of function and other alleles, but there are limitations associated with both.

Transgenes are useful for expression of new alleles, but these constructs integrate at a random location in the genome. As such, transgenes are subject to position effects and can interfere with the function of neighboring genes. Large regions of known or possible regulatory elements can be included in a transgene construct, but control of native regulatory elements is lost. Transgene insertion is not a reproducible process.

Targeted mutations, either loss of function ('knock out') or insertion of new constructs ('knock in'), can be created by homologous recombination, but the process is extremely laborious from construct design to end product. It takes from several months to a year, and on average, only about 1.5% of clones screened will have correctly integrated the construct (Lu et al., 2003). Additionally, different constructs must be created for each gene. These factors limit the throughput of this technology for individual researchers. Large scale efforts such as the NIH Knockout Mouse Project (KOMP) and the European Conditional Mouse Mutagenesis (EUCOMM) Program have developed more high-

throughput pipelines, but these modifications do not permit expression of new alleles at the targeted loci (Collins et al., 2007).

A complementary approach to generating loss-of-function mutations in ESCs is gene trapping (Hansen et al., 2003; Mitchell et al., 2001; Stanford et al., 2006). Gene trapping in ESCs offers a high-throughput method to generate random insertional mutations that are immediately accessible to molecular characterization (Stanford et al., 2001). Gene trap vectors interfere with gene function by co-opting splicing; integration of a vector containing a strong splice acceptor creates a fusion between 5' exons of the endogenous gene and a gene trap open reading frame encoding a reporter gene and polyadenylation signal (Gossler et al., 1989; Skarnes et al., 1992; von Melchner et al., 1992). The most widely used reporter system for gene trapping is βgeo, a fusion between β-galactosidase and neomycin phosphotransferase (Friedrich and Soriano, 1991). Gene trap insertions accurately report the expression pattern of the trapped gene and are highly mutagenic, almost always resulting in the generation of null alleles (Mitchell et al., 2001).

Gene trap lines have been created and characterized using high-throughput methods (Hansen et al., 2008; Horn et al., 2007; Townley et al., 1997; Wiles et al., 2000; Zambrowicz et al., 1998). Existing gene trap lines are described in the International Gene Trap Consortium (IGTC) database (www.genetrap.org), and have been used extensively to generate mutant mouse lines for phenotypic analysis (Leighton et al., 2001; Mitchell et al., 2001; Nord et al., 2006; Zambrowicz et al., 2003).

Below, we describe the gene trap vectors *pGTLxf* and *pGTLxr*, which allow post-insertional modification of the trapped locus using an accompanying technology called

Floxin (Flanked lox site insertion), based on recombination mediated cassette exchange (RMCE).

We show that the Floxin technology allows for reversion of the gene trap mutation and targeted insertion of new DNA constructs at eight genomic loci. Insertion is highly efficient, representing an eighty-fold improvement over average homologous recombination integration rates. Using the Floxin technology, one individual can create targeted alleles representative of the null, wild type, and other desired variations within weeks.

RESULTS

Overview of the Floxin gene trap and vector designs

We show a schematic of mutation, reversion, and modification of a generic, autosomal *Your Favorite Gene* (*YFG*) (**Fig. 1a-d**). A *pGTLxf* or *pGTLxr* gene trap in an intron of *YFG* results in expression of an YFG-βgeo fusion protein in the gene trap line $YFG^{Gt/+}$ (**Fig. 1a**). To revert this loss-of-function mutation, transiently expressed Cre excises the floxed splice acceptor, leaving a single Lox71 site (**Fig. 1b**) (Sauer, 1993). In the absence of the splice acceptor, $YFG^{Rev/+}$ cells lose *βgeo* expression and reactivate *YFG* expression.

pFloxin vectors contain a Lox66 site (**Fig. 1c**) so that Cre-mediated recombination between the *pFloxin* Lox66 and genomic Lox71 site of revertant cells results in directional insertion of the *pFloxin* sequence (**Fig. 1d**). Recombination between Lox66 and Lox71 sites produces one inactive Lox site and one LoxP site (**Fig. 1d**), making integration irreversible (Albert et al., 1995).

Floxin vectors also include a splice acceptor to permit expression of defined sequences at the modified locus (**Fig. 1c-d**). The *pFloxin-YFG-Flag* inserted cDNA is spliced so that the inserted sequence is expressed as a fusion with upstream exons from the endogenous promoter. The other Floxin vector, *pFloxin-IRES-HA-YFG*, contains an IRES element to initiate translation of an amino-terminally tagged version of YFG. The line $YFG^{IRES\text{-}HA\text{-}YFG/+}$ expresses full length *HA-YFG* under the control of the endogenous promoter and the IRES element. The Floxin vectors also include *βActin* promoters that reactivate *βgeo* expression and thus permit pharmacological selection of correct insertions (**Fig. 1c-d**).

RMCE has been shown previously to function robustly in ESCs with varied vector designs (Araki et al., 1999; Hardouin and Nagy, 2000; Osipovich et al., 2005; Schnutgen et al., 2005; Taniwaki et al., 2005; Xin et al., 2005). To date, the BayGenomics and Sanger Institute gene trap efforts have generated 24,149 gene trap cell lines with the *pGTLxf* and *pGTLxr* vectors, representing 4,528 individual genes (Skarnes et al., 2004). This resource of gene trap cell lines represents genes covering a wide array of cellular components and processes (**Supplementary 1**). A database of the gene trap alleles and the corresponding cell lines are accessible to the community through the IGTC (www.genetrap.org).

Cre-mediated reversion of gene trap mutations

Here, we demonstrate modification of eight genomic loci: *Sall4*, *Suz12*, *Ofd1*, *Gli2*, *Tardbp*, *Sntb2, Pex14* and *Tet1*. MGI allele names are included (**Supplementary Table**

1). *Ofd1*^{Gt} cells are hemizygous as the *Ofd1* gene is X-linked and the E14 gene trap ESCs are male. Consequently, *Ofd1*^{Gt} cells do not produce any Ofd1 protein (**Fig. 1e**).

To remove the exogenous splice acceptor, we electroporated gene trap cells with an expression construct for nuclear Cre recombinase. On average, 45% of colonies screened showed proper excision of the splice acceptor (**Table 1**). Revertant cells no longer displayed β-galactosidase activity or neomycin resistance (**Fig. 2a, Supplementary 2d**), and reversion caused loss of the *βgeo* transcript (**Supplementary 2e**). Genomic PCR and Southern blot confirmed correct excision of the splice acceptor in revertant cells (**Supplementary 2f-g**).

Gene trap vectors can insert in a concatamer fashion, creating multiple possibilities for Lox site recombination with expression of Cre. However, we have found that the process of reversion collapses concatamer insertions down to a single insertion with a high frequency, thus allowing application of the Floxin process to these alleles (**Supplementary 3**).

Floxin-mediated insertion of new DNA sequences at gene trap loci

Using the Floxin strategy, we generated cell lines expressing wild type Ofd1, Suz12, Sall4, Gli2, or Tardbp with carboxy-terminal tags, and lines expressing *eGFP* at the *Sntb2*, *Pex14*, or *Tet1* genomic loci. Revertant lines were co-electroporated with the appropriate *pFloxin* or *pFloxin-IRES* construct and a nuclear Cre expression construct and selected with neomycin. On average, 86% of resultant ESC colonies contained the correctly integrated pFloxin construct (**Table 2**), and β-galactosidase activity was re-activated (**Fig. 2a**). Genomic PCR and Southern blot confirmed integration in Floxin cell

lines (**Supplementary 2g, Supplementary 4a-c**). These data indicate that Floxin-mediated targeted insertion occurs efficiently and accurately in many different genomic contexts.

Expression and function of reverted and Floxin proteins

Quantitative RT-PCR and immunoblot indicated that revertant alleles are expressed at wild type levels in *Sall4*$^{Rev/+}$ and *Suz12*$^{Rev/+}$(**Fig. 2b and Supplementary 4d**). In contrast, immunoblot indicated that *Ofd1*^{Rev} cells expressed lower levels of Ofd1 (at the expected size of 110 kD) than wild type cells (**Fig. 2c**). RT-PCR and sequencing indicated that the reduced *Ofd1* expression is attributable to the use of cryptic splice acceptor sites present in the *βgeo* cassette (data not shown). Northern blot revealed that *βgeo* transcript is detectable in a subset of revertant lines (**Supplementary 2e**). The use of these cryptic splice acceptor sites in certain revertant cell lines suggests that locus-dependent factors affect the restoration of normal expression. *Ofd1* is essential for the formation of the primary cilium (Ferrante et al., 2006), and wild type ESCs possessed primary cilia whereas *Ofd1*^{Gt} cells do not. *Ofd1*^{Rev} cells possessed primary cilia, indicating that reversion of the gene trap mutation restored gene function (**Fig. 2d**).

Floxin-inserted alleles were expressed at levels equivalent to the revertant alleles. The tagged alleles for both *Sall4*$^{Sall4TAP/+}$ and *Suz12*$^{Suz12TAP/+}$ were expressed at wild type levels (**Fig. 2b and Supplementary 4d**). Although immunoblot showed that Ofd1-Myc protein levels were less than wild type (**Fig. 2c**), production of Ofd1-Myc was sufficient to support ciliogenesis (**Fig. 2e**). Ofd1-Myc, like endogenous Ofd1, localized to the centrosome as assessed by immunofluorescence detection (**Fig. 2f**). Thus, Floxin-

inserted Ofd1 constructs, like the revertant allele, are functional but expressed at lower levels than the wild type allele.

Suz12-TAP, like endogenous Suz12, localized to the nucleus (**Fig. 2g**). ESC differentiation led to downregulation of endogenous Suz12 and Suz12-TAP to similar extents (**Fig. 2h**) (Pasini et al., 2007). Together, these data indicate that Floxin cells produce modified proteins that function and are regulated similar to wild type proteins.

In addition to tagged versions of endogenous genes, the Floxin technology can insert exogenous DNA into loci. *Sntb2*$^{IRESeGFP/+}$, *Pex14*$^{IRESeGFP/+}$ and *Tet1*$^{IRESeGFP/+}$ lines expressed eGFP under the control of endogenous regulatory elements (**Supplementary 4e**).

The presence of vector sequences may affect normal gene expression (Wilson and Kola, 2001). Therefore, we included Frt sites in the gene trap and Floxin vectors to allow for Flp-mediated removal of the *βActin* promoter and *βgeo* cassette (**Supplementary 5a**). To remove the *βActin-βgeo* cassette, we electroporated *Ofd1*^{Ofd1myc} or *Gli2*$^{Gli2TAP/+}$ cells with a mouse codon optimized FLP (FLPo) expression construct (Raymond and Soriano, 2007). On average, 51% of ESC clones assayed showed excision of the *βActin-βgeo* cassette (*Δβgeo)*, identified by loss of β-galactosidase activity (**Fig. 2a**, **Supplementary 5b**). Genomic PCR verified correct excision (**Supplementary 5c**). Removal of vector sequences increased the expression of Ofd1-Myc (**Supplementary 5d**).

To assess whether the genetic manipulations associated with gene trapping, reversion, and the Floxin process affected ESCs, we performed karyotyping and evaluated pluripotency by three methods. The five Floxin lines evaluated showed normal euploid karyotypes (**Supplementary 6** and data not shown). All Floxin lines had normal

ESC colony and cell morphology (**Supplementary 7a**). Additionally, Floxin lines had expression levels similar to wild type ESCs for three regulators of pluripotency, *Oct4*, *Sox2* and *Nanog* (**Supplementary 7b**). The Floxin lines also possessed the ability to differentiate into cell types that express *Fgf5*, *Afp* and *T/Brachyury*, markers of embryonic ectoderm, endoderm and mesoderm, respectively (**Supplementary 7c**). While these assays suggest that the Floxin process does not adversely affect ESC pluripotency, germline competency of Floxin cells has not been systematically evaluated. Other studies have shown that three genetic manipulations do not necessarily limit germline transmission (Hardouin and Nagy, 2000; Nagy et al., 1993).

DISCUSSION

A detailed understanding of gene function requires the generation of a range of alleles. The Floxin strategy described here allows for high throughput modification of ESC loci harboring insertions of the *pGTLxf* or *pGTLxr* gene trap vectors. The Floxin system allows for Cre-mediated reversion of the gene trap mutation and subsequent insertion of new DNA of interest into the genomic locus. Genes of interest are cloned with standard molecular biology techniques into *pFloxin* shuttle vectors.

Unanswered Questions and Future Improvements

Reversion restores wild type expression of the endogenous trapped allele and abrogates *βgeo* expression for the majority of the gene trap lines studied. However, in a subset of the lines studied ($Ofd1^{Rev}$ and $XD052^{Rev}$), reversion only partially restored wild type expression of the allele (**Fig. 2c, Supplementary 7d**). Additionally, some lines

continued to express *βgeo* after reversion as assayed by either RT-PCR (*Ofd1*^{Rev}, data not shown) or Northern blot (*Flna*^{Rev}, **Supplementary 1e**). The chromosomal location of the trap in all of these cases is the X chromosome. This suggests the possibility of specific factors unique to the X chromosome that cause a greater use of cryptic splice sites in the *βgeo* cassette for this particular chromosomal location. To determine if this is the case would require further study of revertant alleles located on the X chromosome. If chromosomal location were not the primary factor affecting use of cryptic splice sites, it may be interesting to determine what other features of gene location and/ or sequence determine splicing efficiency of different sites.

Regardless of the mechanism that determines cryptic splicing in various lines, it may be useful to remove this variable all together in future lines by eliminating cryptic splice sequences from future Floxin-compatible gene trap vectors. To redesign the *pGTLxf/r* gene trap vectors for possible use in creating human gene trap ESC lines, one could employ a similar method as used to construct FLPo (Raymond and Soriano, 2007).

Applications and advantages of the Floxin system

We have demonstrated the generation of tagged or reporter alleles at eight loci, and shown how the technology can be used to model a human genetic disease in ESCs, study protein localization, and report on the dynamics of protein expression (**Supplementary Table 2**). The gene trap allele can also be converted into a wide variety of other tailored alleles, such as missense, deletion, and domain swap alleles. Additionally, the Floxin technology is convenient for insertion of non-homologous DNA sequences into endogenous loci, such as demonstrated with *eGFP*. This approach could

be utilized for generating alleles expressing other exogenous proteins such as Cre, rtTA, ΦC31 integrase, Alkaline phosphatase, or Diptheria toxin under the control of tissue- or cell type-specific promoters.

The Floxin strategy has several advantages over transgene insertion, homologous recombination, and other approaches for manipulating the ESC genome (Araki et al., 1999; Hardouin and Nagy, 2000; Osipovich et al., 2005; Taniwaki et al., 2005). First, unlike homologous recombination, the Floxin strategy does not require cloning of large pieces of DNA sequence ('homologous arms'). Second, unlike transgenes, Floxin alleles are created in the native genomic context. Third, each modification causes the presence or absence of βgeo expression, assisting in the selection or identification of the desired cells. Fourth, reversion allows for confirmation that observed cellular phenotypes are due to the gene trap mutation, as demonstrated for the role of *Ofd1* in ciliogenesis. Fifth, inserted DNA sequences can be expressed either as a direct fusion to upstream exons, or as a separate cistron. Sixth, Frt sites allow for removal of the *βActin-βgeo* cassette, abrogating interference from vector prokaryotic sequences. Lastly, the Floxin technology is compatible with the extensive collection of 24,149 characterized and validated gene trap lines available to the community.

The Floxin strategy of reversion and new DNA insertion are both highly efficient and reproducible at a variety of loci. By avoiding the most laborious aspects of traditional gene replacement strategies, the Floxin system allows new alleles to be engineered with minimal effort.

MATERIALS AND METHODS

Cell Lines and Cell Culture

Ofd1^{Gt} (RRF427), *Sall4*$^{Gt/+}$(XE027), *Suz12*$^{Gt/+}$(XG122), *Gli2*$^{Gt/+}$ (XG045), and *Tardbp*$^{Gt/+}$ (RRB030) E14 ESC lines were obtained from BayGenomics. *Sntb2*$^{Gt/+}$ (XC195), *Pex14*$^{Gt/+}$ (XC197), *Tet1*$^{Gt/+}$ (XD006), *Flna*^{Gt} (XC373), *Btf3*$^{Gt/+}$ (XD028), *Nsd1*$^{Gt/+}$ (XC030), and *XD052*^{Gt} (XD052) were provided by W.C.S. Cells were cultured on 0.1% gelatin in GMEM supplemented with 10% FBS, glutamine, pyruvate, NEAA, βME, and LIF.

Plasmids and Vector Construction

pPGK-NLS-Cre expresses a fusion of the bacteriophage P1 recombinase Cre with a SV40 large T antigen nuclear localization signal (Gu et al., 1993). *pFloxin* vectors were built from the *pBluescript* backbone by adding an *Engrailed2* splice acceptor sequence, multiple cloning site polylinker, SV40 polyA signal and, in the case of *pFloxin-IRES*, an IRES. All *pFloxin* constructs were produced in *rec*A1 Stbl2 cells (Invitrogen) according to manufacturer's protocol, except cultures were grown at 37° in LB medium. GenBank accession numbers for *pFloxin*, *pFloxin-IRES*, *pFloxin-TAP*, and *pFloxin-IRES-eGFP* are EU916834, EU916835, EU916836, and GQ357182 respectively. The vector *pFloxin-MCS2-IRES-MCS* (GenBank number GU180239) with two multiple cloning sites and an IRES allows insertion of homologous cDNA as well as a reporter regulated by the same promoter.

cDNA constructs and cloning

Suz12 and *Sall4* cDNAs were gifts from Miguel Ramalho-Santos. To make $Sall4^{Sall4TAP/+}$ and $Suz12^{Suz12TAP/+}$ cell lines, primers were used to amplify and add appropriate restriction sites to exons 2-4 of *Sall4*, and exons 8-16 of *Suz12* (**Supplementary Table 3**). The cDNAs were then cloned into *pFloxin-TAP*, in frame with the TAP tag. *Ofd1* cDNA was cloned from RNA of E11.5 mouse embryos using 1 Step RT-PCR kit (Invitrogen). Further amplification and addition of the Myc tag was performed with the Expand High Fidelity kit (Roche). Quik Change II XL site directed mutagenesis kit (Stratagene) was used to repair missense mutations introduced during PCR. Final products were confirmed by sequencing.

Electroporation and Selection

For reversion: 60 μg of *pGK-NLS-Cre* DNA was ethanol precipitated, and the pellet washed 3 times with 70% ethanol. The pellet was dried in tissue culture hood for 30' at room temperature and resuspended in 100 μL calcium-magnesium free PBS overnight at room temperature. On the morning of electroporation, new media was added to the gene trap cells grown to 70-90% confluency in a T75 flask. After 3-4 hours, cells were trypsinized, counted, and washed with PBS. 10^7 cells were added to a chilled electroporation cuvette with DNA and electroporated at 240 V, 500 μF, exponential (Bio-Rad GenePulser Xcell). Electroporated cells were incubated 20' at room temperature, and 10^5 cells were split evenly between 10 10-cm plates. Colonies were picked and transferred to a 48 well plate after 3-5 days.

For Floxin: *pGK-NLS-Cre* and *pFloxin* DNA were prepared as above. We electroporated revertant cell lines with both DNAs as above, except 10^7 cells were plated evenly between 6 10-cm plates. We began selection with 150-350 μg/mL G418 (Invitrogen) one day after electroporation, and picked colonies after 6-7 days.

For FLP removal of vector sequence: 120 μg *pPGK-FLPo* (Addgene plasmid 13793) was prepared as above (Raymond and Soriano, 2007). We electroporated and plated Floxin cell lines as described in the reversion section above.

See supplementary experimental procedures for detailed protocol.

β-galactosidase Activity Assays

Galacto-Light Plus System (Applied Biosystems) was used to assay cell lysates from a 24 or 48-well plate according to manufacturer's protocol.

Quantitative PCR

RNA was extracted from ESCs or embryoid bodies using RNeasy Plus (Qiagen). First strand cDNA synthesis was performed using extracted RNA with iScript (Biorad) or First Strand cDNA Synthesis (Fermentas). Transcript levels were measured in triplicate using a 7300 Real-time PCR machine (Applied Biosystems) and then normalized to *βActin* levels.

Antibodies

Antibodies to Ofd1 were generated by Covance by immunizing rabbits with the peptide [H]-CDTYDQKLKTELLKYQLELKDDYI–[NH2] corresponding to amino acids 340-

362 of murine Ofd1. Antibody was used at 1:5000 for Western blotting and 9.2 μg for IP. Other antibodies used were: acetylated Tubulin (Sigma T6793) used at 1:1000, γ–Tubulin (Santa Cruz sc-7396) 1:200, GFP (Aves Labs GFP-1020) 1:500, Centrin1 (Abcam ab11257) 1:200, Suz12 (Santa Cruz sc-46264) 1:200, Flag (Sigma F7425) 1:500 for IF. Flag resin (Sigma) was used for IP. Myc antibody (Novus Biologicals NB600-335) was used at 1:1000 for immunoblotting, 1:200 for IF, and 3 μg for IP. TAP antibody (GenScript A00683) was used at 1:500 for immunoblotting. Secondary antibodies were conjugated with Alexa Fluor 488 or 555 (Invitrogen) and used at 1:400.

Immunofluorescence and Microscopy

For ESC ciliation studies: ESCs were plated on coverslips coated with poly-D-lysine and 1% Matrigel (BD) and treated with 0.5 mM mimosine (Sigma) overnight to arrest cells. Cells were fixed 5' in 4% PFA, washed in PBS, and fixed 2-3' in -20° methanol. The cells were then washed in PBS with 0.1% Triton-X100 (PBST), blocked in 2% BSA in PBST, and incubated with primary antibodies in block for 1 hr at RT. The cells were washed in PBST, incubated with secondary antibodies in block for 30' at RT, and mounted with Vectashield hardset with DAPI (Vector labs). Slides were viewed on Deltavision microscope (Applied Precision) and images were processed with Deltavision and Metamorph (Molecular Devices) software.

For GFP staining: Cells were plated on coverslips as above and cultured overnight. Cells were fixed 5' in 4% PFA and stained as above. Slides were viewed on an Axio Observer D1 (Zeiss) microscope and images were processed with Axiovision (Zeiss), ImageJ (NIH), and Metamorph (Molecular Devices) software.

For TAP staining: Cells were plated on coverslips as above and cultured overnight. The cells were fixed in 100% methanol for 5'and stained as above. Slides were viewed on Nikon C1 confocal and images were processed with Nikon EZ-C1 software.

For cellular morphology assessment: Cells were plated in 6 well plates and viewed on an Axio Observer D1 (Zeiss) microscope.

ESC differentiation

ESCs were plated in suspension culture in ultra-low adherence six well plates (Corning) at $5x10^5$ per well (Suz12-TAP differentiation) or 10^6 per well in duplicate (pluripotency assessment) to induce embryoid body formation. Suspension media consisted of 10% FBS, nonessential amino acids, pyruvate, glutamine, and βME in GMEM and was changed every other day. For Suz12-TAP differentiation, protein lysate was collected on 0, 4, 8, and 12 days following initial plating. For pluripotency assessment, RNA was collected 7 days after plating.

SUPPLEMENTARY EXPERIMENTAL PROCEDURES

Detailed protocol for electroporation and selection

Protocol for Creating Revertant cell line

Prepare pGK-NLS-Cre DNA at least one day before you want to electroporate cells.

1. Ethanol precipitate 60 μg of DNA

Add all following washes in tissue culture hood to keep DNA sterile

2. wash pellet 2x 1 mL 70% ethanol, spin down max speed, 5' at 4 degree after each wash

3. aspirate second wash, add 1 mL 70% ethanol, dislodge pellet by vortex or flicking tube, incubate 10' 4 degree on shaker or nutator to wash pellet really well, spin down 5' 4 degree max speed

4. aspirate supe

5. let dry in hood with lid of tube open, 30' at room temp (RT)

6. add 100 μL PBS (Calcium and magnesium free (CMF-PBS)), pipet up down to break up the pellet. let resuspend in the hood at RT over night.

7. can store DNA at 4 degree if cells are not ready yet

Electroporation

* Gene trap cell line should be about 70-90% confluent in a T75 on the morning of. Feed cells in the morning, wait 3-4 hours. Chill electroporation cuvette on ice.

1. Trypsinize and count cells. Collect about 1.4E7 cells and spin down.

2. wash cells 1x with 10 mL CMF-PBS. spin down.

3. Resuspend cells in 1 mL CMF-PBS

4. add 100 μL DNA to chilled cuvette, then add 700 μL cells (1E7 cells) carefully, avoiding bubbles.

5. electroporate at 240 V, 500 uF, exponential.

6. incubate cuvette at RT in hood 20'

7. Take 1E5 cells of the electroporation reaction and split evenly between 10 10-cm plates. (can freeze down rest of reaction)

8. because you cannot select the cells with drug (reversion eliminates G418 resistance), you must pick colonies before the cells become too confluent, usually

about 3-5 days. The colonies will be small.

Correct reversion will create a cell line with the following characteristics:

-sensitive to G418

-does not express βgeo

-should express your gene of interest from both copies in the genome, the allele with the gene trap and the allele without the gene trap

Picking Colonies

Prepare 48 well plates to pick into. We usually get plenty of usable clones if we pick 2 48-well plates (96 clones) total.

Use dissecting scope in hood (wipe down really well with 70% EtOH, and then UV for 15 min)

Remove media and add 10 mL PBS

Scrape/ aspirate center of each colony with a pipettor set at 50 μL, into 48 well plate.

When you have picked the number of colonies you want, add 50 μL 4x trypsin (0.1% trypsin) to each well.

Incubate 37 degree, 2-3'

Add 1 mL complete media, pipet up and down 3-4x each well to break up cells.

Protocol for Creating Floxin cell line

Follow protocol for making revertant cell line above, except you will precipitate 60 μg each of pGK-NLS-Cre and your pFloxin DNA. Resuspend in separate tubes, 100 μL CMF-PBS each.

* Revertant cell line should be about 70-90% confluent in a T75 on the morning of. Feed cells in the morning, wait 3-4 hours. chill electroporation cuvette on ice.

Electroporation: Follow protocol for making revertant cell line above, except you will collect 1.67E7 cells, and then take 600 μL of cells (1E7 cells) to electroporate after adding 100 μL each DNA (200 μL total) to cuvette.

Also, plate the entire electroporation reaction, split evenly between 6 10-cm plates.

The next day after electroporation:

1. Begin selection with G418. I highly recommend doing a kill curve on the revertant ES cells with each new lot of G418, as the strength varies considerably from batch to batch. We have used from 150-350 μg/ mL G418 to select. (Note- I have found that some revertant cells are slightly more resistant to G418 than WT cells due to cryptic splicing in the gene trap. Also, anything lower than 150 μg/ mL G418 is generally too low)
2. Change media every day until colonies start to form, usually about 6-7 days.
3. Follow protocol for picking colonies above.

Correct Floxin will create a cell line with the following characteristics:

-resistant to G418

-expresses βgeo from β*Actin* promoter

-expresses inserted construct from gene-trap locus promoter

REFERENCES

Albert, H., Dale, E.C., Lee, E., and Ow, D.W. (1995). Site-specific integration of DNA into wild-type and mutant lox sites placed in the plant genome. Plant J *7*, 649-659.

Araki, K., Imaizumi, T., Sekimoto, T., Yoshinobu, K., Yoshimuta, J., Akizuki, M., Miura, K., Araki, M., and Yamamura, K. (1999). Exchangeable gene trap using the Cre/mutated lox system. Cell Mol Biol (Noisy-le-grand) *45*, 737-750.

Collins, F.S., Rossant, J., and Wurst, W. (2007). A mouse for all reasons. Cell *128*, 9-13.

Ferrante, M.I., Zullo, A., Barra, A., Bimonte, S., Messaddeq, N., Studer, M., Dolle, P., and Franco, B. (2006). Oral-facial-digital type I protein is required for primary cilia formation and left-right axis specification. Nat Genet *38*, 112-117.

Friedrich, G., and Soriano, P. (1991). Promoter traps in embryonic stem cells: a genetic screen to identify and mutate developmental genes in mice. Genes Dev *5*, 1513-1523.

Gossler, A., Joyner, A.L., Rossant, J., and Skarnes, W.C. (1989). Mouse embryonic stem cells and reporter constructs to detect developmentally regulated genes. Science *244*, 463-465.

Gu, H., Zou, Y.R., and Rajewsky, K. (1993). Independent control of immunoglobulin switch recombination at individual switch regions evidenced through Cre-loxP-mediated gene targeting. Cell *73*, 1155-1164.

Hansen, G.M., Markesich, D.C., Burnett, M.B., Zhu, Q., Dionne, K.M., Richter, L.J., Finnell, R.H., Sands, A.T., Zambrowicz, B.P., and Abuin, A. (2008). Large-scale gene trapping in C57BL/6N mouse embryonic stem cells. Genome Res *18*, 1670-1679.

Hansen, J., Floss, T., Van Sloun, P., Fuchtbauer, E.M., Vauti, F., Arnold, H.H., Schnutgen, F., Wurst, W., von Melchner, H., and Ruiz, P. (2003). A large-scale, gene-driven mutagenesis approach for the functional analysis of the mouse genome. Proc Natl Acad Sci U S A *100*, 9918-9922.

Hardouin, N., and Nagy, A. (2000). Gene-trap-based target site for cre-mediated transgenic insertion. Genesis *26*, 245-252.

Horn, C., Hansen, J., Schnutgen, F., Seisenberger, C., Floss, T., Irgang, M., De-Zolt, S., Wurst, W., von Melchner, H., and Noppinger, P.R. (2007). Splinkerette PCR for more efficient characterization of gene trap events. Nat Genet *39*, 933-934.

Leighton, P.A., Mitchell, K.J., Goodrich, L.V., Lu, X., Pinson, K., Scherz, P., Skarnes, W.C., and Tessier-Lavigne, M. (2001). Defining brain wiring patterns and mechanisms through gene trapping in mice. Nature *410*, 174-179.

Lu, Z.H., Books, J.T., Kaufman, R.M., and Ley, T.J. (2003). Long targeting arms do not increase the efficiency of homologous recombination in the beta-globin locus of murine embryonic stem cells. Blood *102*, 1531-1533.

Mitchell, K.J., Pinson, K.I., Kelly, O.G., Brennan, J., Zupicich, J., Scherz, P., Leighton, P.A., Goodrich, L.V., Lu, X., Avery, B.J*., et al.* (2001). Functional analysis of secreted and transmembrane proteins critical to mouse development. Nat Genet *28*, 241-249.

Nagy, A., Rossant, J., Nagy, R., Abramow-Newerly, W., and Roder, J.C. (1993). Derivation of completely cell culture-derived mice from early-passage embryonic stem cells. Proc Natl Acad Sci U S A *90*, 8424-8428.

Nord, A.S., Chang, P.J., Conklin, B.R., Cox, A.V., Harper, C.A., Hicks, G.G., Huang, C.C., Johns, S.J., Kawamoto, M., Liu, S*., et al.* (2006). The International Gene Trap Consortium Website: a portal to all publicly available gene trap cell lines in mouse. Nucleic Acids Res *34*, D642-648.

Osipovich, A.B., Singh, A., and Ruley, H.E. (2005). Post-entrapment genome engineering: first exon size does not affect the expression of fusion transcripts generated by gene entrapment. Genome Res *15*, 428-435.

Pasini, D., Bracken, A.P., Hansen, J.B., Capillo, M., and Helin, K. (2007). The polycomb group protein Suz12 is required for embryonic stem cell differentiation. Mol Cell Biol *27*, 3769-3779.

Raymond, C.S., and Soriano, P. (2007). High-efficiency FLP and PhiC31 site-specific recombination in mammalian cells. PLoS ONE *2*, e162.

Sauer, B. (1993). Manipulation of transgenes by site-specific recombination: use of Cre recombinase. Methods Enzymol *225*, 890-900.

Schnutgen, F., De-Zolt, S., Van Sloun, P., Hollatz, M., Floss, T., Hansen, J., Altschmied, J., Seisenberger, C., Ghyselinck, N.B., Ruiz, P.*, et al.* (2005). Genomewide production of multipurpose alleles for the functional analysis of the mouse genome. Proc Natl Acad Sci U S A *102*, 7221-7226.

Skarnes, W.C., Auerbach, B.A., and Joyner, A.L. (1992). A gene trap approach in mouse embryonic stem cells: the lacZ reported is activated by splicing, reflects endogenous gene expression, and is mutagenic in mice. Genes Dev *6*, 903-918.

Skarnes, W.C., von Melchner, H., Wurst, W., Hicks, G., Nord, A.S., Cox, T., Young, S.G., Ruiz, P., Soriano, P., Tessier-Lavigne, M.*, et al.* (2004). A public gene trap resource for mouse functional genomics. Nat Genet *36*, 543-544.

Stanford, W.L., Cohn, J.B., and Cordes, S.P. (2001). Gene-trap mutagenesis: past, present and beyond. Nat Rev Genet *2*, 756-768.

Stanford, W.L., Epp, T., Reid, T., and Rossant, J. (2006). Gene trapping in embryonic stem cells. Methods Enzymol *420*, 136-162.

Taniwaki, T., Haruna, K., Nakamura, H., Sekimoto, T., Oike, Y., Imaizumi, T., Saito, F., Muta, M., Soejima, Y., Utoh, A.*, et al.* (2005). Characterization of an exchangeable gene trap using pU-17 carrying a stop codon-beta geo cassette. Dev Growth Differ *47*, 163-172.

Townley, D.J., Avery, B.J., Rosen, B., and Skarnes, W.C. (1997). Rapid sequence analysis of gene trap integrations to generate a resource of insertional mutations in mice. Genome Res *7*, 293-298.

von Melchner, H., DeGregori, J.V., Rayburn, H., Reddy, S., Friedel, C., and Ruley, H.E. (1992). Selective disruption of genes expressed in totipotent embryonal stem cells. Genes Dev *6*, 919-927.

Wiles, M.V., Vauti, F., Otte, J., Fuchtbauer, E.M., Ruiz, P., Fuchtbauer, A., Arnold, H.H., Lehrach, H., Metz, T., von Melchner, H.*, et al.* (2000). Establishment of a gene-trap sequence tag library to generate mutant mice from embryonic stem cells. Nat Genet *24*, 13-14.

Wilson, T.J., and Kola, I. (2001). The LoxP/CRE system and genome modification. Methods Mol Biol *158*, 83-94.

Xin, H.B., Deng, K.Y., Shui, B., Qu, S., Sun, Q., Lee, J., Greene, K.S., Wilson, J., Yu, Y., Feldman, M.*, et al.* (2005). Gene trap and gene inversion methods for conditional gene inactivation in the mouse. Nucleic Acids Res *33*, e14.

Zambrowicz, B.P., Abuin, A., Ramirez-Solis, R., Richter, L.J., Piggott, J., BeltrandelRio, H., Buxton, E.C., Edwards, J., Finch, R.A., Friddle, C.J.*, et al.* (2003).

Wnk1 kinase deficiency lowers blood pressure in mice: a gene-trap screen to identify potential targets for therapeutic intervention. Proc Natl Acad Sci U S A *100*, 14109-14114.

Zambrowicz, B.P., Friedrich, G.A., Buxton, E.C., Lilleberg, S.L., Person, C., and Sands, A.T. (1998). Disruption and sequence identification of 2,000 genes in mouse embryonic stem cells. Nature *392*, 608-611.

Figure 1. The Floxin strategy for reversion and modification of gene trap loci.

(**a**) In the wild type allele of *Your Favorite Gene* (*YFG*), exons 1 and 2 are spliced together and translated to produce full length YFG protein (right). Dashed lines indicate splicing. In the gene trap line $YFG^{Gt/+}$, a gene trap vector *pGTLxf* or *pGTLxr* has inserted into the intron. The gene trap splice acceptor, flanked by Lox71 and LoxP sites, co-opts splicing to create a fusion between *βgeo* and the 5' endogenous exon. (**b**) To revert the gene trap mutation, Cre recombines the Lox71 and LoxP sites, excising the splice acceptor and leaving a Lox71 site. In the absence of the gene trap splice acceptor, wild type expression of *YFG* is restored. (**c**) For Floxin-mediated cassette insertion, revertant cells are co-electroporated with a Cre expression plasmid and a *pFloxin* vector carrying the DNA sequence of interest. *pFloxin-YFG-Flag* carries the cDNA for exon 2 of YFG with a C-terminal Flag tag, and *pFloxin-IRES-HA-YFG* carries the full-length cDNA for YFG with an N-terminal HA tag. Recombination between the Lox71 and Lox66 sites irreversibly integrates the pFloxin construct into the genomic locus. (**d**) The Floxin cell lines express tagged YFG under the control of endogenous regulatory elements and re-express *βgeo* from the *βActin* promoter. (**e**) Immunoblots with Ofd1 and Actin antibodies on lysates from wild type and $Ofd1^{Gt}$ ESCs. We loaded 10 μg protein per lane.

Figure 1

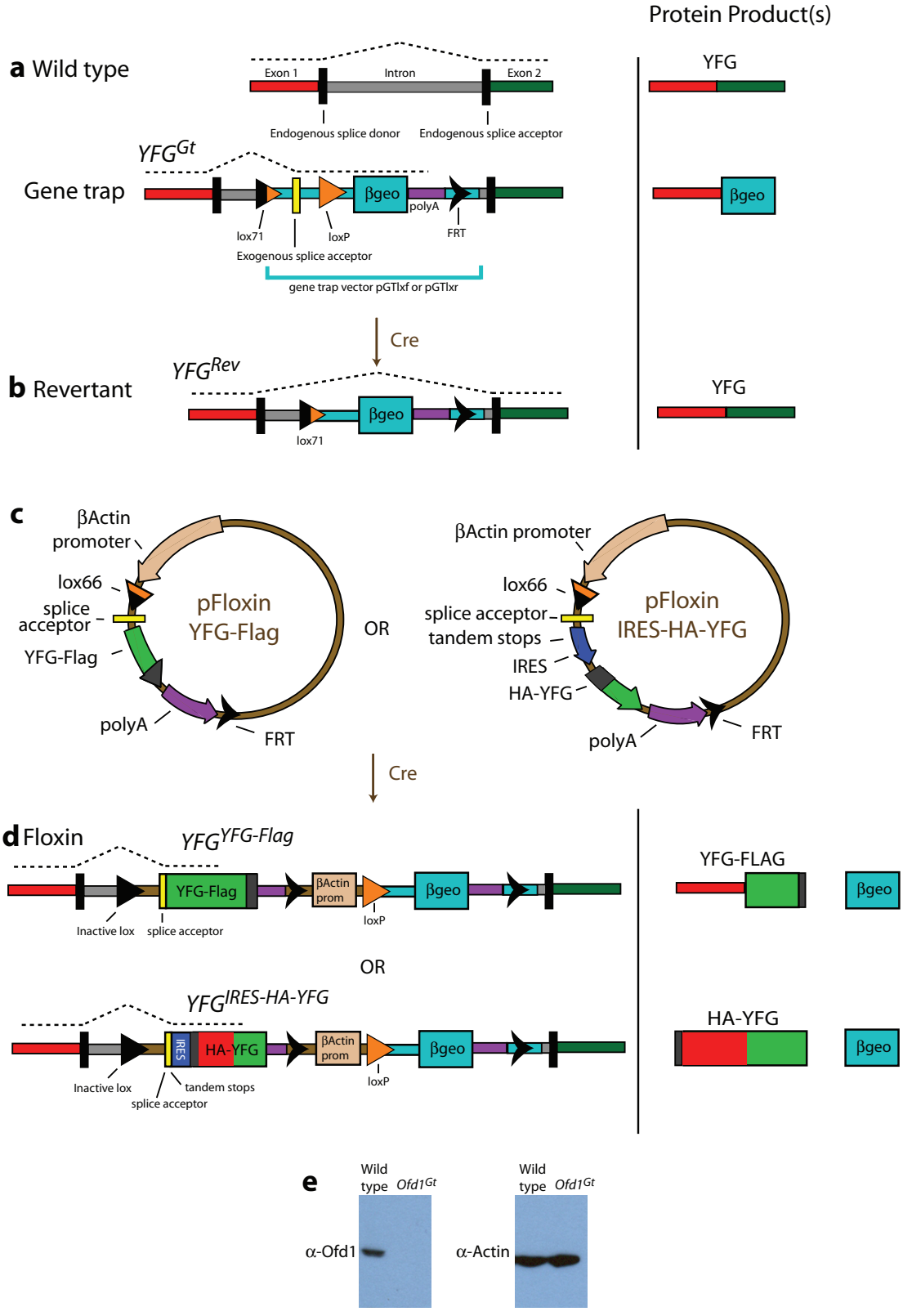
Protein Product(s)
a Wild type
Exon 1
Intron
Exon 2
Endogenous splice donor
Endogenous splice acceptor
YFG
YFG^Gt
Gene trap
βgeo
polyA
lox71
loxP
FRT
Exogenous splice acceptor
gene trap vector pGTlxf or pGTlxr
βgeo
Cre
b Revertant
YFG^Rev
βgeo
lox71
YFG
c
βActin promoter
lox66
splice acceptor
YFG-Flag
polyA
FRT
pFloxin YFG-Flag
OR
βActin promoter
lox66
splice acceptor
tandem stops
IRES
HA-YFG
polyA
FRT
pFloxin IRES-HA-YFG
Cre
d Floxin
YFG^YFG-Flag
YFG-Flag
βActin prom
βgeo
Inactive lox
splice acceptor
loxP
YFG-FLAG
βgeo
OR
YFG^IRES-HA-YFG
IRES
HA-YFG
βActin prom
βgeo
Inactive lox
tandem stops
splice acceptor
loxP
HA-YFG
βgeo
e
Wild type
Ofd1^Gt
α-Ofd1
Wild type
Ofd1^Gt
α-Actin

Figure 2. Efficient reversion of gene trap mutations and Floxin-mediated engineering of new alleles.

(**a**) β-galactosidase activity in cell lines of the indicated genotypes RLU, relative luciferase units. Error bars indicate standard deviation (*n* = 3*)*. (**b**) Immunoblots showing Suz12 (left and middle, 20 μg protein per lane) detected with antibodies to Suz12 and TAP, and Sall4 (right; immunoprecipitated (IP) with an antibody to Flag from 500 μg for each cell line) detected with an antibody to TAP in the cell lines of the indicated genotypes. (**c**) Immunoblots showing expression of Ofd1 in $Ofd1^{Rev}$ cells (left, IP with an Ofd1 antibody from 4 mg of total protein for each cell line and detected with an Ofd1 antibody) and full length Myc-tagged Ofd1 in Floxin cells (middle, 25 μg per lane; right, IP with a Myc antibody from 800 μg total protein for each cell line and detected with an Ofd1 antibody). (**d, e**) Representative fluorescence micrographs of cell lines of the indicated genotypes. Cilia (acetylated tubulin), centrosomes (γ-Tubulin), DAPI (DNA). (**f**) Representative fluorescence micrograph showing Ofd1-Myc (Myc), centrosome (Centrin), and DAPI (DNA) staining. (**g**) Representative fluorescence micrograph showing Suz12-TAP (Flag), centrosomes (acetylated tubulin), and DAPI (DNA) staining. Scale bars 5 μm, inset 1 μm. (**h**) Immunoblot showing wild type Suz12 and Suz12-TAP detected with an antibody to Suz12 upon differentiation of $Suz12^{Suz12TAP/+}$ cells for the indicated number of days. We loaded 3 μg protein per lane.

Figure 2

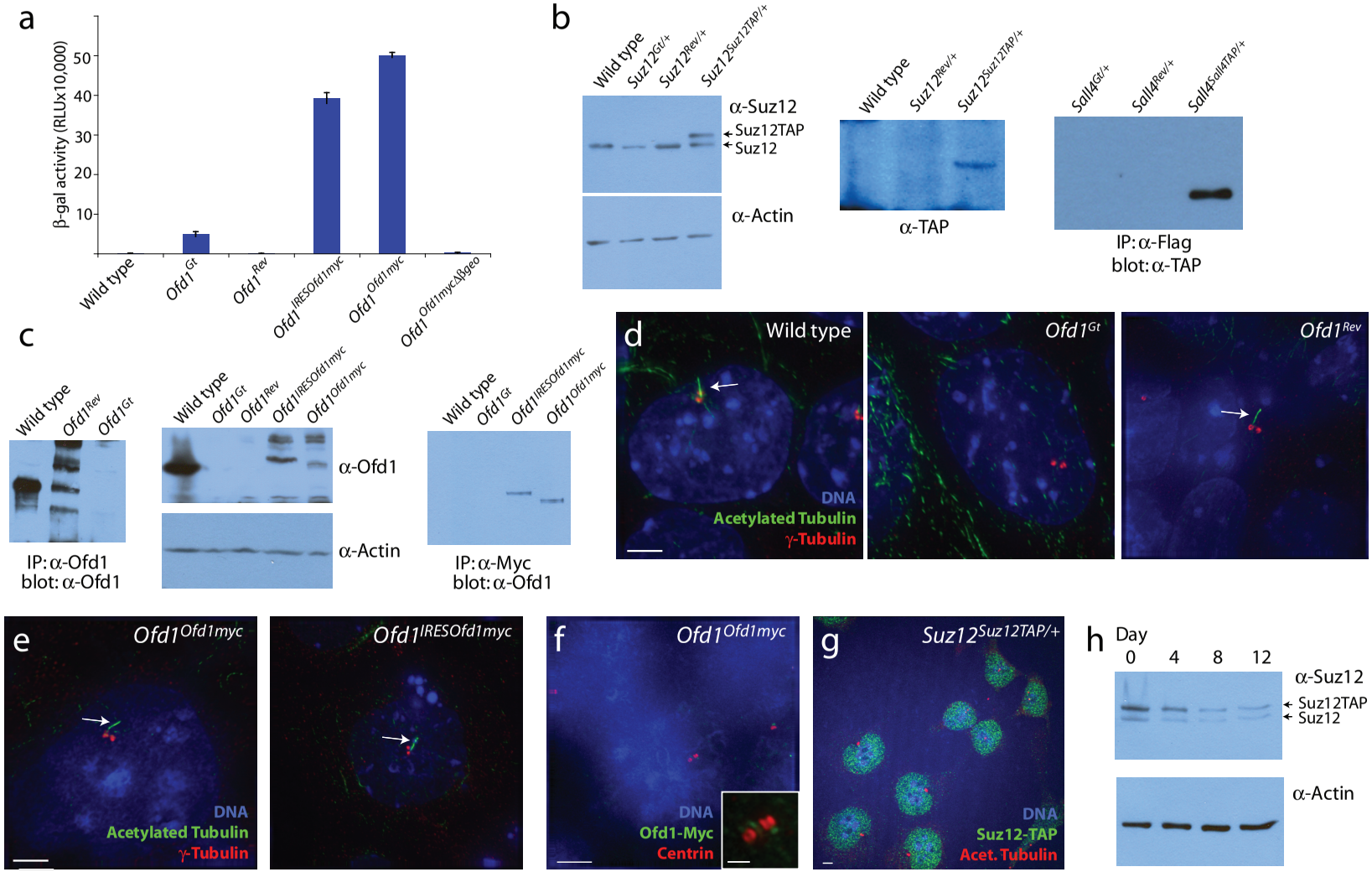
a
β-gal activity (RLUx10,000)
50
40
30
20
10
Wild type
Ofd1Gt
Ofd1Rev
Ofd1IRESOfd1myc
Ofd1Ofd1myc
Ofd1Ofd1mycΔBgeo
b
Wild type
Suz12Gt/+
Suz12Rev/+
Suz12Suz12TAP/+
α-Suz12
Suz12TAP
Suz12
α-Actin
Wild type
Suz12Rev/+
Suz12Suz12TAP/+
α-TAP
Sall4Gt/+
Sall4Rev/+
Sall4Sall4TAP/+
IP: α-Flag
blot: α-TAP
c
Wild type
Ofd1Rev
Ofd1Gt
IP: α-Ofd1
blot: α-Ofd1
Wild type
Ofd1Gt
Ofd1Rev
Ofd1IRESOfd1myc
Ofd1Ofd1myc
α-Ofd1
α-Actin
Wild type
Ofd1Gt
Ofd1IRESOfd1myc
Ofd1Ofd1myc
IP: α-Myc
blot: α-Ofd1
d
Wild type
Ofd1Gt
Ofd1Rev
DNA
Acetylated Tubulin
γ-Tubulin
e
Ofd1Ofd1myc
Ofd1IRESOfd1myc
DNA
Acetylated Tubulin
γ-Tubulin
f
Ofd1Ofd1myc
DNA
Ofd1-Myc
Centrin
g
Suz12Suz12TAP/+
DNA
Suz12-TAP
Acet. Tubulin
h
Day
0
4
8
12
α-Suz12
Suz12TAP
Suz12
α-Actin

Supplementary Figure 1. Gene ontogeny analysis of Floxin compatible genes reveals that a wide variety of genes involved in all aspects of cell function are accessible.

Supplementary Figure 1

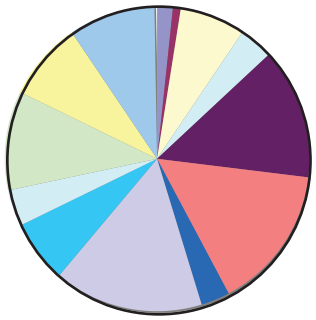

cell adhesion	2%
cell-cell signalling	1%
cell cycle and proliferation	9%
death	5%
cell organization and biogenesis	18%
protein metabolism	20%
DNA metabolism	4%
RNA metabolism	20%
other metabolic processes	9%
stress response	5%
transport	14%
developmental processes	11%
signal transduction	12%

Process

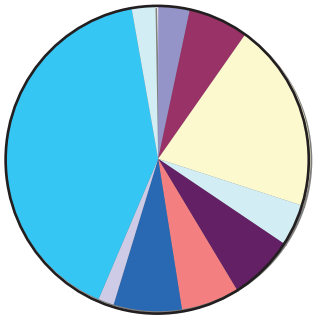

extracellular matrix	3%
plasma membrane	6%
other membranes	18%
cytosol	4%
cytoskeleton	6%
mitochondrion	5%
ER/ Golgi	6%
translational apparatus	2%
nucleus	36%
other cytoplasmic organelles	2%

Components

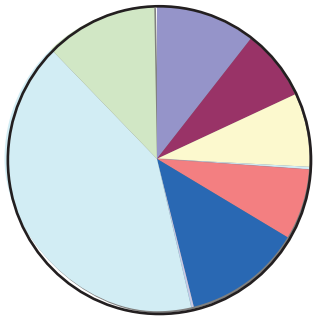

signal transduction activity	6%
transporter activity	4%
enzyme regulator activity	4%
extracellular structural	.05%
cytoskeletal activity	4%
transcription regulatory	7%
nucleic acid binding activity	22%
kinase activity	7%

Functions

Supplementary Figure 2. **Reversion removes the splice acceptor, restores neomycin sensitivity, and abrogates βgeo expression.**

(**a-c**) Schemas of *Ofd1*, *Suz12*, and *Sall4* loci showing locations of diagnostic PCR primers and band sizes (dark red), Southern probes (dashed lines), and expected Southern product sizes in kB (black). For *Ofd1*, the 5' probe is located in the intron upstream of the gene trap insertion site, and the 3' probe spans part of exon 4 and intron 4, downstream of the gene trap insertion site. Black arrows indicate BglII cut sites for Southern. Diagram is not to scale. (**d**) Whereas gene trap cell lines are resistant to G418, revertant cell lines display wild type G418 sensitivity. Live cells are stained blue. (**e**) Northern blot with a probe against *βgeo* transcript reveals that all gene trap lines ($Nsd1^{Gt/+}$, $Pex14^{Gt/+}$, $Flna^{Gt}$, $Tet1^{Gt/+}$, $Btf3^{Gt/+}$, and $XD052^{Gt}$) produce *βgeo* message, while the revertant (Rev) lines show loss of *βgeo* message. The presence of some *βgeo* message in $Flna^{Rev}$ cells indicates the use of a cryptic splice acceptor site in this revertant cell line. (**f**) PCR primers B and C span the region of the gene trap containing the splice acceptor. Gene trap lines have a product of 500 bp, whereas revertant lines, with the splice acceptor excised, have a product size of 160 bp. Genomic PCR with primers B and C demonstrates removal of the splice acceptor in $Ofd1^{Rev}$, $Suz12^{Rev/+}$, and $Sall4^{Rev/+}$cells. (**g**) Southern blot with 5' and 3' probes outside of the modified region confirms the excision of the splice acceptor in $Ofd1^{Rev}$ cells and correct integration into the *Ofd1* genomic locus of *pFloxin-Ofd1-Myc* or *pFloxin-IRES-Ofd1-Myc*.

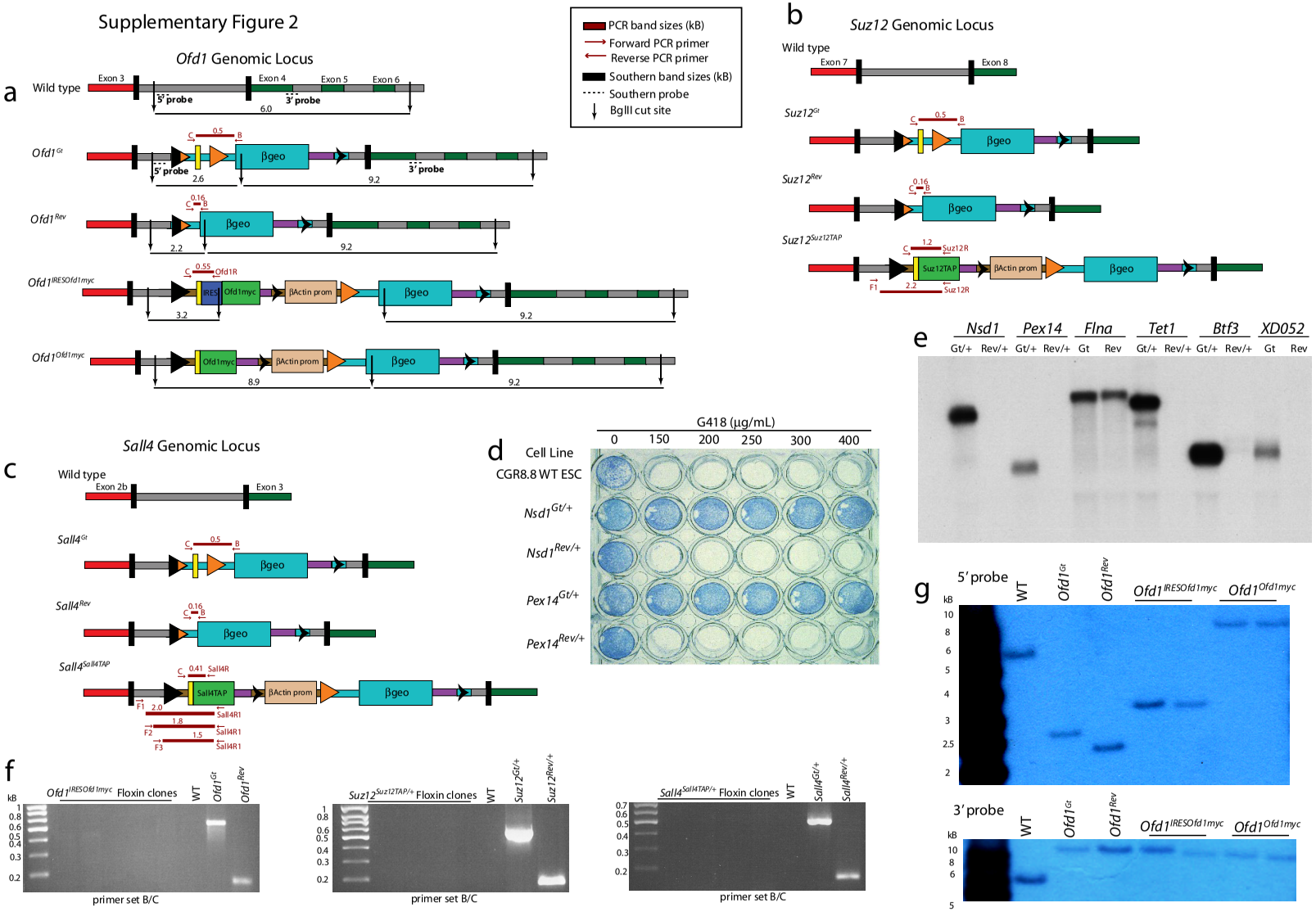
Supplementary Figure 2
PCR band sizes (kB)
Forward PCR primer
Reverse PCR primer
Southern band sizes (kB)
Southern probe
BglII cut site
a
Ofd1 Genomic Locus
Wild type
Exon 3
Exon 4
Exon 5
Exon 6
5' probe
3' probe
6.0
Ofd1Gt
βgeo
2.6
9.2
Ofd1Rev
2.2
Ofd1IRESOfd1myc
Ofd1R
IRES
Ofd1myc
βActin prom
3.2
Ofd1Ofd1myc
8.9
b
Suz12 Genomic Locus
Exon 7
Exon 8
Suz12Gt
Suz12Rev
Suz12Suz12TAP
Suz12R
Suz12TAP
c
Sall4 Genomic Locus
Exon 2b
Sall4Gt
Sall4Rev
Sall4Sall4TAP
Sall4R
Sall4TAP
Sall4R1
d
Cell Line
CGR8.8 WT ESC
Nsd1Gt/+
Nsd1Rev/+
Pex14Gt/+
Pex14Rev/+
G418 (μg/mL)
0
150
200
250
300
400
e
Nsd1
Pex14
Flna
Tet1
Btf3
XD052
Gt/+
Rev/+
Gt
Rev
f
Ofd1IRESOfd1myc Floxin clones
WT
Ofd1Gt
Ofd1Rev
kB
primer set B/C
Suz12Suz12TAP/+ Floxin clones
Suz12Gt/+
Suz12Rev/+
Sall4Sall4TAP/+ Floxin clones
Sall4Gt/+
Sall4Rev/+
g
5' probe
Ofd1IRESOfd1myc
Ofd1Ofd1myc
3' probe

Supplementary Figure 3: Reversion reduces concatamer insertions to a single insertion with high frequency.

(**a**) Southern blot with a probe against the Engrailed2 intronic sequence, present in the endogenous Engrailed2 locus, as well as in the gene trap vector. All revertant lines show a smaller size band consistent with Cre excision of the splice acceptor sequence, while lines 1 and 5 also show a larger band due to Class 2 recombination. (**b**) Southern blot with a probe against the Engrailed2 splice acceptor sequence, present in the endogenous Engrailed2 locus, as well as in the gene trap vector. No bands are present in the revertant lines due to Cre excision of this sequence. (**c**) Southern blot with a probe against the pUC sequence, present in the gene trap vector. All lines except 1 and 5 show one band, consistent with Class 1 recombination. (**d**) Diagram of Nsd1 genomic loci. Class 1 recombination reduces the concatamer insertion to a single insertion while Class 2 recombination excises the individual splice acceptor sequences. Black arrows indicate BglII cut sites.

Supplementary Figure 3

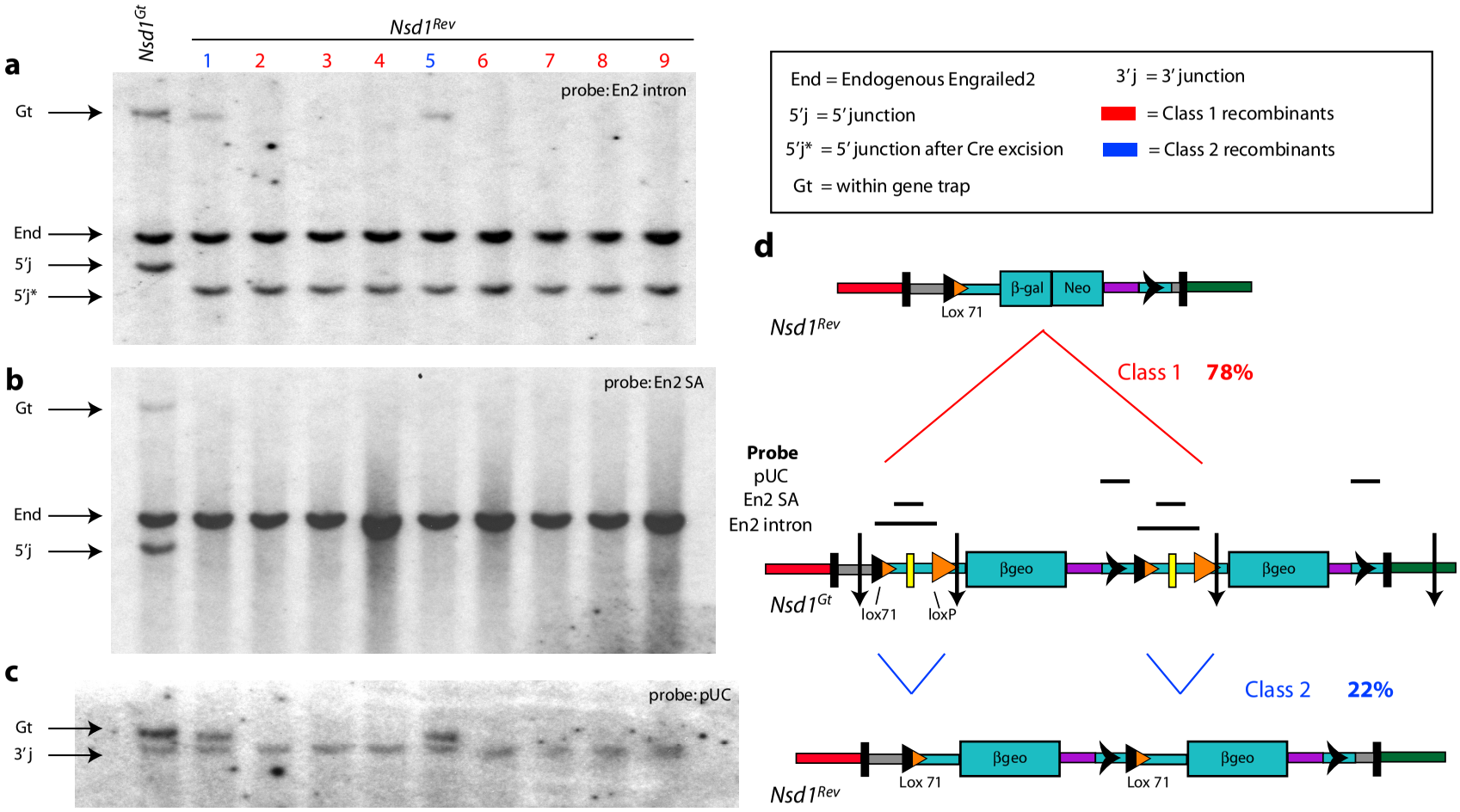

Supplementary Figure 4. The Floxin process precisely integrates DNA.

(**a**) Genomic PCR reveals correct integration of pFloxin constructs in multiple clones in *Ofd1*, *Suz12* and *Sall4* cell lines. PCR primer sets have a forward primer C in the newly integrated splice acceptor sequence, and a reverse primer (Ofd1 R, Suz12 R, or Sall4 R) in the pFloxin cDNA sequence. Primer locations are indicated in Supp. 1a-c. (**b-c**) Genomic PCR with a forward primer in the intronic region 5' of the insertion site and a reverse primer in the pFloxin cDNA sequence confirms correct integration at *Suz12* or *Sall4* in multiple Floxin lines. Primer locations are indicated in Supp. 1B-C. (**d**) qRT-PCR indicates that Suz12 and Sall4 revertant and Floxin cells express close to wild type levels of message. Similar levels of Sall4 message may be present in all cell lines due to autoregulation (Wu et al., 2006). **(E)** eGFP expression in $Sntb2^{lRESeGFP/+}$, $Pex14^{lRESeGFP/+}$ and $Tet1^{lRESeGFP/+}$ Floxin cell lines. eGFP (green), nuclei (DAPI, blue). Scale bar 5 μm.

Wu, Q., Chen, X., Zhang, J., Loh, Y.H., Low, T.Y., Zhang, W., Zhang, W., Sze, S.K., Lim, B., and Ng, H.H. (2006). Sall4 interacts with Nanog and co-occupies Nanog genomic sites in embryonic stem cells. J Biol Chem *281*, 24090-24094.

Supplementary Figure 4

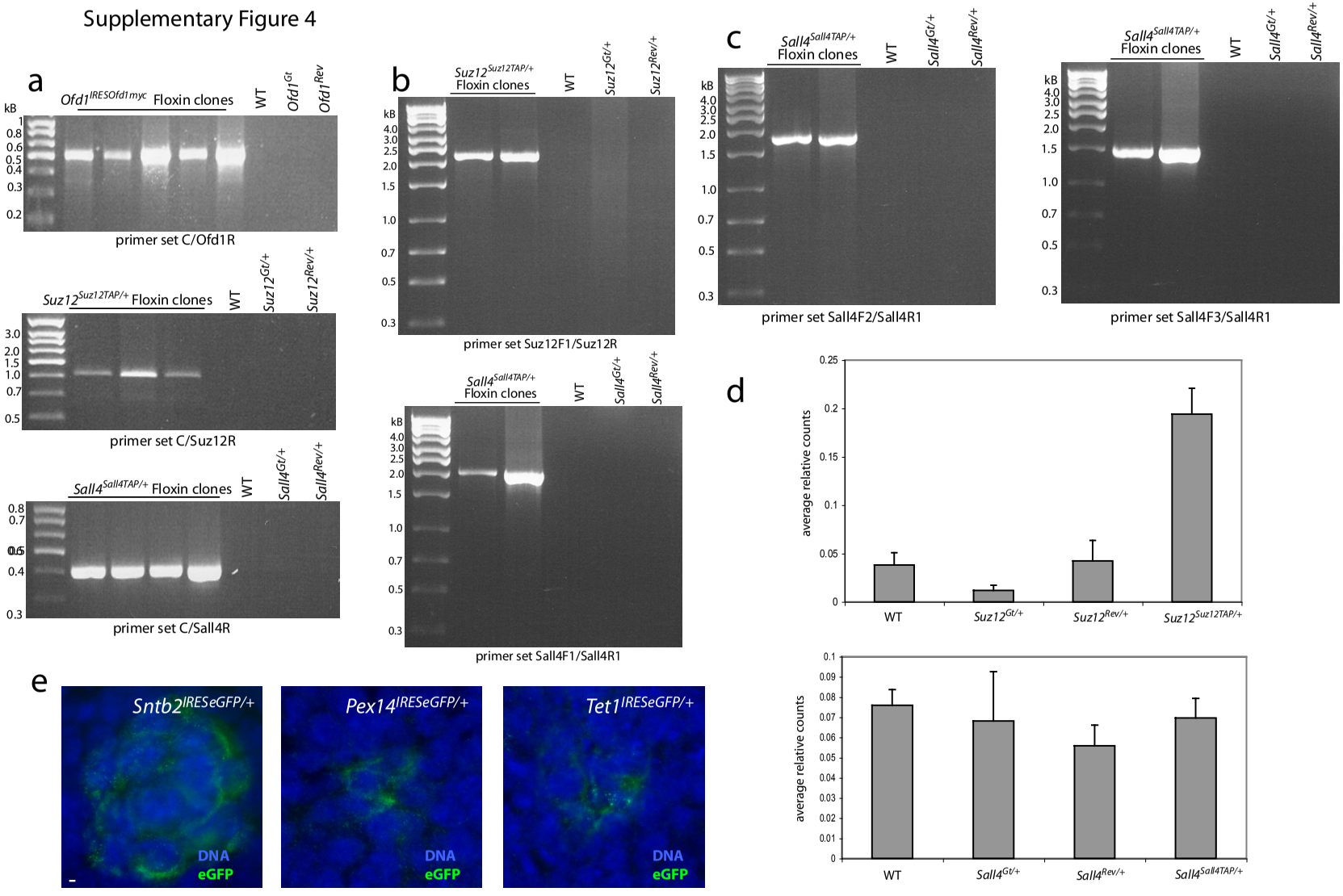

Supplementary Figure 5. FLP mediated removal of the βActin-βgeo cassette.

(**a**) FLPo recombination of FRT sites excises the β-Actin-*βgeo* cassette. Locations of diagnostic PCR primers shown (dark red). *Ofd1*^{Ofd1mycΔβgeo} cells continue to express Ofd1-Myc, but no longer express *βgeo*. (**b**) Quantitation of β-Actin-βgeo cassette excision efficiency for two genomic loci. Clones were screened for absence of β-galactosidase activity. (**c**) Genomic PCR reveals correct excision of β-Actin-*βgeo* in the Δβgeo cell line. Image was digitally manipulated to change order of lanes. (**d**) Deletion of the β-Actin-*βgeo* cassette increases expression of Ofd1. Densitometric quantitation is normalized to Actin. 20 μg protein per lane.

Supplementary Figure 5

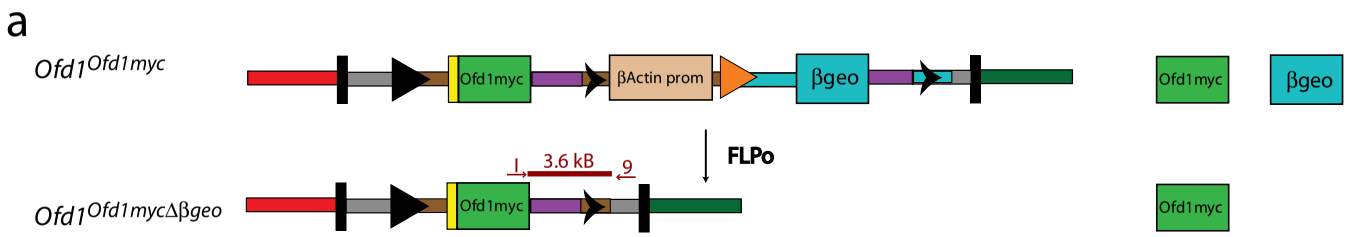

b

Cell line	% with correct Flp-out
Ofd1^{Ofd1mycΔβgeo}	37
Gli2$^{Gli2TAPΔβgeo/+}$	64
Average	51

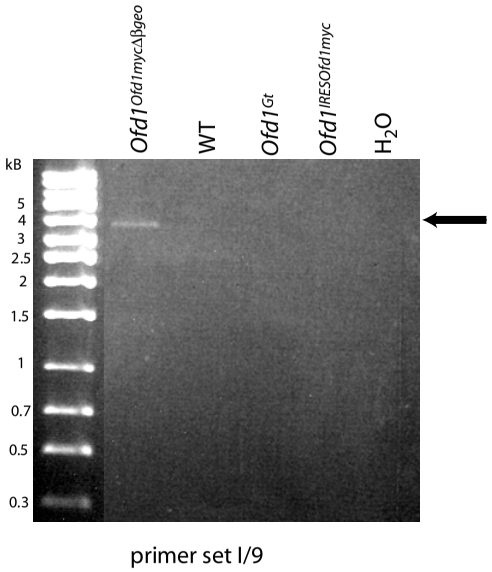

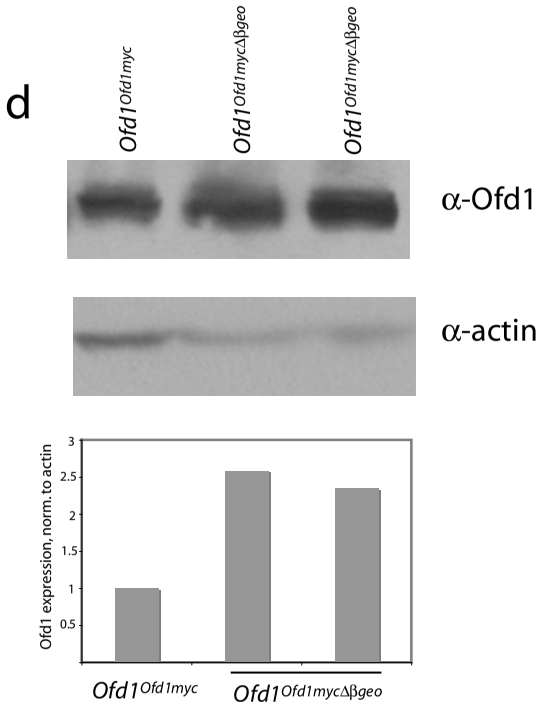

Supplementary Figure 6. Floxin cells have normal euploid karyotypes.

Representative karyotypes from cells of the indicated genotypes. Scale bar 15 μm.

Supplementary Figure 6

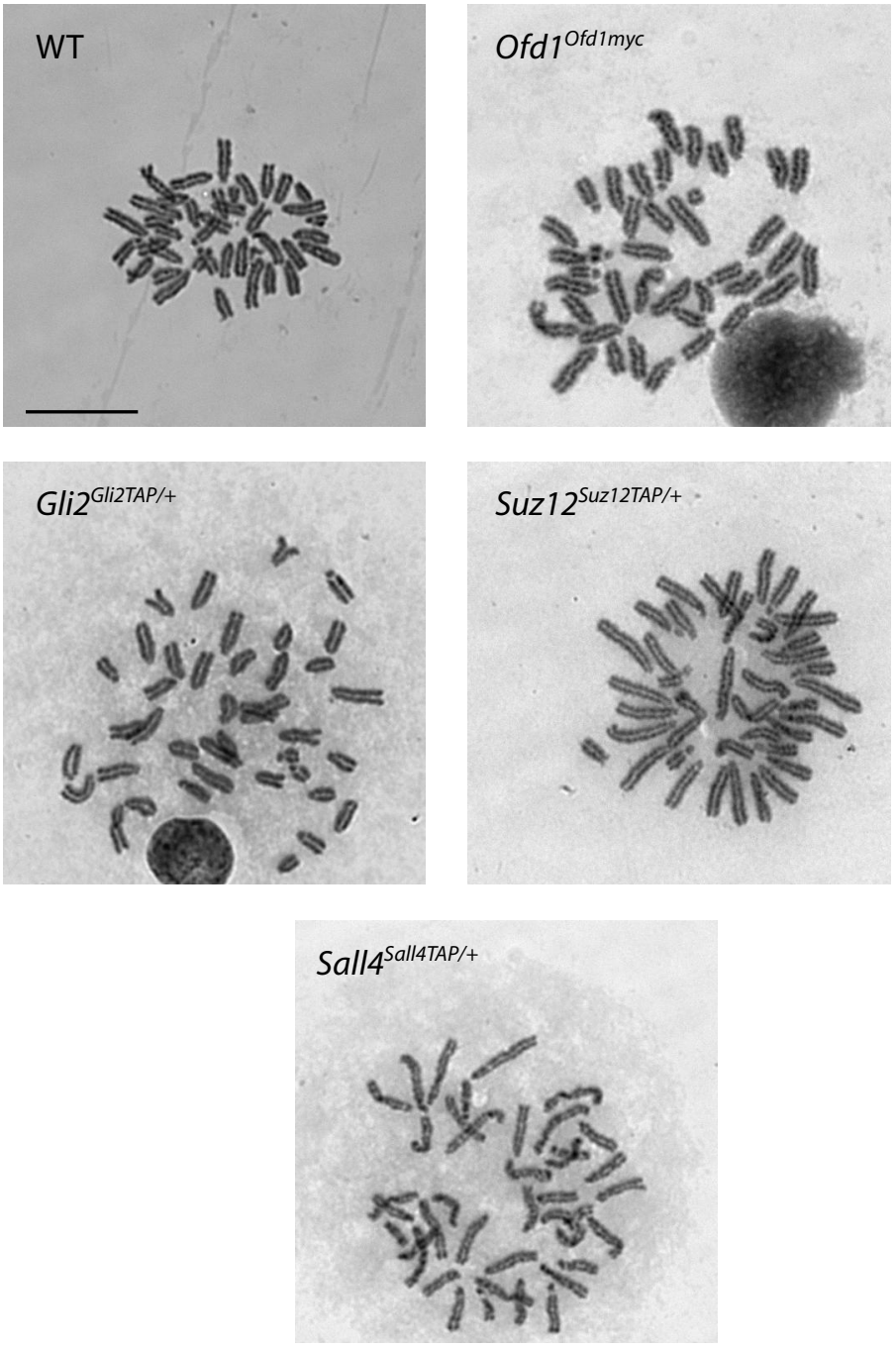

Supplementary Figure 7. ESCs retain pluripotency after Floxin.

(**a**) Floxin cell lines show typical ESC colony and cellular morphology. Scale bar 100 μm. (**b**) Floxin ESCs and WT ESCs have similar expression levels of the pluripotency regulators *Sox2*, *Oct4*, and *Nanog*, as assessed by quantitative RT-PCR. (**c**) Quantitative RT-PCR assessment of *Fgf5*, *T/Brachyury*, and *Afp* expression levels in EBs generated from WT and Floxin ESC lines after 7 days of differentiation. Expression was scored as positive if greater than 10 fold than undifferentiated WT ESCs. (**d**) Northern blot with a probe against XD052 transcript using RNA from the indicated cell lines.

Supplementary Figure 7

a

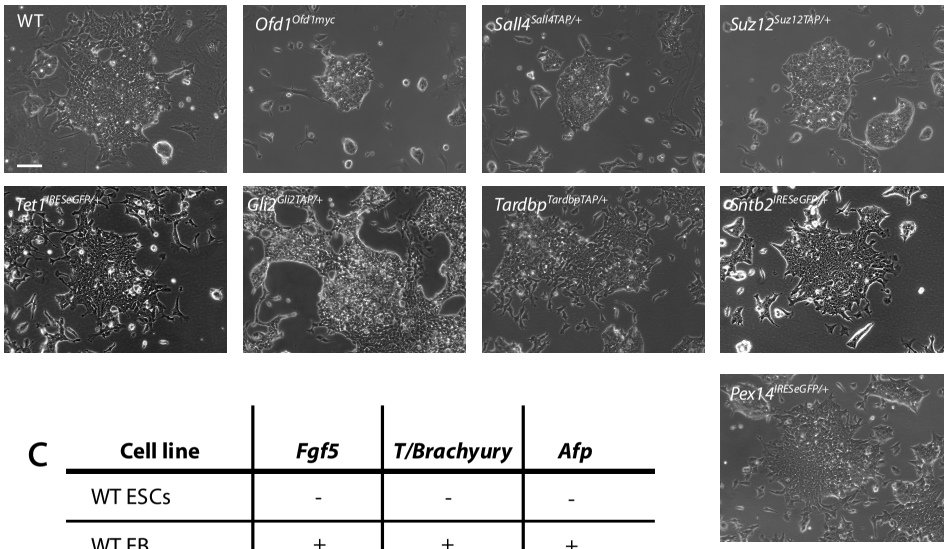

b

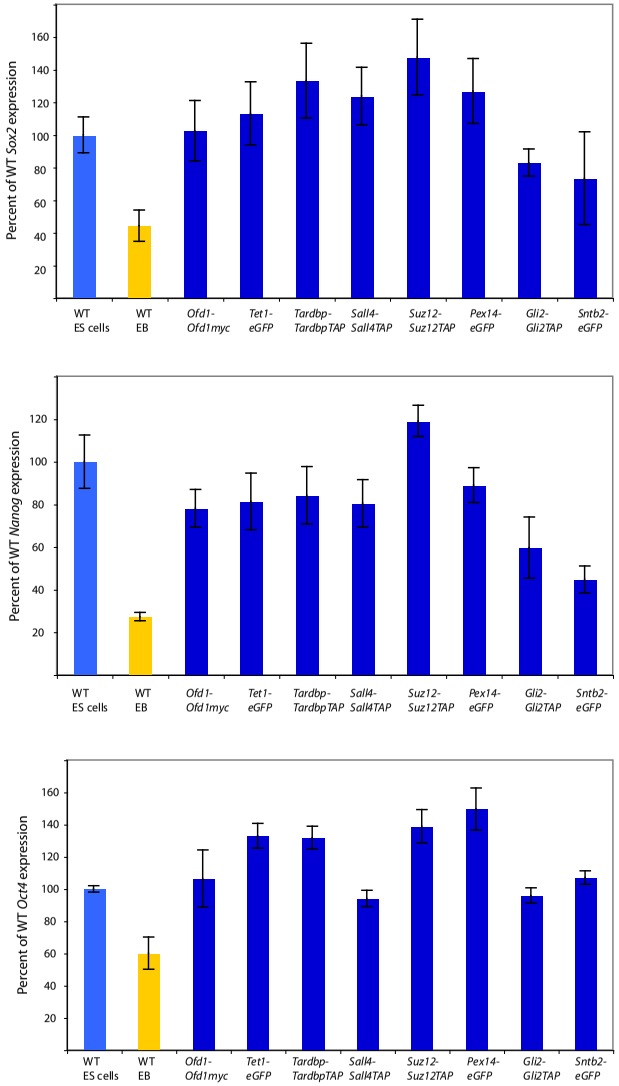

c

Cell line	*Fgf5*	*T/Brachyury*	*Afp*
WT ESCs	-	-	-
WT EB	+	+	+
Ofd1^{Ofd1myc}	+	+	+
Tet1$^{IRESeGFP/+}$	+	+	+
Tardbp$^{TardbpTAP/+}$	+	+	+
Sall4$^{Sall4TAP/+}$	+	+	+
Suz12$^{Suz12TAP/+}$	+	+	+
Pex14$^{IRESeGFP/+}$	+	+	+
Gli2$^{Gli2TAP/+}$	+	+	+
Sntb2$^{IRESeGFP/+}$	+	+	+

d

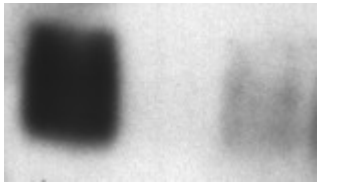

Table 1. Efficiency of reversion at eight gene trap loci.

Cell line	% with correct reversion	Chromosome
Ofd1^{Rev}	62	X
Sall4$^{Rev/+}$	45	2
Suz12$^{Rev/+}$	74	11
Gli2$^{Rev/+}$	74	1
Tardbp$^{Rev/+}$	33	4
Sntb2$^{Rev/+}$	27	8
Pex14$^{Rev/+}$	24	4
Tet1$^{Rev/+}$	18	10
Average	**45**	

Table 2. Efficiency of correct Floxin-mediated engineering of new alleles.

Cell line	% with correct Floxin
Ofd1^{IRESOfd1myc}	92
Ofd1^{Ofd1myc}	73
Sall4$^{Sall4TAP/+}$	89
Suz12$^{Suz12TAP/+}$	91
Gli2$^{Gli2TAP/+}$	88
Tardbp$^{TardbpTAP/+}$	68
Sntb2$^{IRESeGFP/+}$	100
Pex14$^{IRESeGFP/+}$	89
Tet1$^{IRESeGFP/+}$	80
Average	**86**

Supplementary Table 1. MGI nomenclature for alleles.

Allele	MGI nomenclature
Ofd1^{Gt}	*Ofd1*$^{Gt(RRF427)Byg}$
Ofd1^{Rev}	*Ofd1*$^{Gt(RRF427)Byg+}$
Ofd1^{Ofd1myc}	*Ofd1*$^{Gt(RRF427)Byg.tm1(Ofd1myc)Reit}$
Ofd1^{IRESOfd1myc}	*Ofd1*$^{Gt(RRF427)Byg.tm2(Ofd1myc)Reit}$
Ofd1$^{Ofd1myc\Delta\beta geo}$	*Ofd1*$^{Gt(RRF427)Byg.tm3(Ofd1myc)Reit}$
Sall4^{Gt}	*Sall4*$^{Gt(XE027)Byg}$
Sall4^{Rev}	*Sall4*$^{Gt(XE027)Byg+}$
Sall4^{Sall4TAP}	*Sall4*$^{Gt(XE027)Byg.tm1(Sall4TAP)Reit}$
Suz12^{Gt}	*Suz12*$^{Gt(XG122)Byg}$
Suz12^{Rev}	*Suz12*$^{Gt(XG122)Byg+}$
Suz12^{Suz12TAP}	*Suz12*$^{Gt(XG122)Byg.tm1(Suz12TAP)Reit}$
Gli2^{Gt}	*Gli2*$^{Gt(XG045)Byg}$
Gli2^{Rev}	*Gli2*$^{Gt(XG045)Byg+}$
Gli2^{Gli2TAP}	*Gli2*$^{Gt(XG045)Byg.tm1(Gli2TAP)Reit}$
Tardbp^{Gt}	*Tardbp*$^{Gt(RRB030)Byg}$
Tardbp^{Rev}	*Tardbp*$^{Gt(RRB030)Byg+}$
Tardbp^{TardbpTAP}	*Tardbp*$^{Gt(RRB030)Byg.tm1(TardbpTAP)Reit}$
Sntb2^{Gt}	*Sntb2*$^{Gt(XC195)Byg}$
Sntb2^{Rev}	*Sntb2*$^{Gt(XC195)Byg+}$
Sntb2^{IRESeGFP}	*Sntb2*$^{Gt(XC195)Byg.tm1(eGFP)Reit}$
Pex14^{Gt}	*Pex14*$^{Gt(XC197)Byg}$
Pex14^{Rev}	*Pex14*$^{Gt(XC197)Byg+}$
Pex14^{IRESeGFP}	*Pex14*$^{Gt(XC197)Byg.tm1(eGFP)Reit}$
Tet1^{Gt}	*Tet1*$^{Gt(XD006)Byg}$
Tet1^{Rev}	*Tet1*$^{Gt(XD006)Byg+}$
Tet1^{IRESeGFP}	*Tet1*$^{Gt(XD006)Byg.tm1(eGFP)Reit}$

Supplementary Table 2. Proposed applications of the Floxin technology. Demonstrated applications are shown in green.

Supplementary Table 2

	Types	Comments
Model Genetic Diseases	• **Dominant** and recessive genetic diseases -insertion of mutant alleles • Cell based assays -**cellular phenotype**	• **Ofd1 controls ciliogenesis in ES cells** • Dominant genetic disease -model with wild type and mutant alleles -differentiate to desired cell type to study
Protein Function Studies	• **Pluripotent and/ or differentiated cells** • **Localization** • Interacting partners -mass spectrometry -biochemical assays	• Allele types -**tagged** -mutant -domain swaps, etc. • **Transcription factors**, other regulators
Protein Biochemical Studies	• Purification -in vitro assays: kinase, etc. • Post-translational modifications • Structure/ function analysis	• Study phosphorylation, glycosylation, protein cleavage -in different cell types • Mutate consensus sites
Reporter Genes	• Mark specific stem cell populations -lineage analysis -pure populations by sorting • Report on pluripotent or differentiated status	• Genes required for maintenance of stem cell character are well represented among gene trap lines
Genomic Scale Studies	• chromatin state and transcription • genomic stability, loss of heterozygosity • nuclear localization and transcriptional state	• **Demonstrated for loci on chromosomes X, 1, 2, 4, 8, 10, 11** • Gene traps distributed on chromosomes throughout the genome, easily insert reporter genes for readout of transcription
Directed Differentiation	• Activated or dominant-negative alleles • Non-homologous constructs	

Supplementary Table 3. PCR primer sequences

Experiment or Primer name	**Sequence**
Cloning Sall4 cDNA	forward 5'-TACCAGGTCGTACCAGCCTCCCT-3' reverse 5'-TACTAGTGCTGACAGCAATCTTATTTT-3'
Cloning Suz12 cDNA	forward 5'-TACCAGGTGTCAGTGAAGAACTTCCA-3' reverse 5'-TACTAGTGAGTTTTTGTTTCTTGCTCT-3'
Cloning Ofd1 cDNA- step 1	forward mOFD1 5'-TCCGTCTTTATTCCGTCCAG-3' reverse mOFD1 5'CCAGAAAAACAAGAACACATATTACG-3'
Cloning Ofd1 cDNA- step 2	forward mOfd1 5'- GACGAGTTAGGGGCTGAATG-3' reverse mOFD1 from above
Cloning Ofd1 cDNA- step 3	forward mOfd1 from above and reverse Ofd1Myc 5'-TTACAAGTCCTCTTCAGAAATGAGCTTT TGCTCCCACATGTCATCTGGTTCTTC-3'
Primer B	5'-GTTTTCCCAGTCACGACGTT-3'
Primer C	5'-AACAAACTTGGCCTCACCAG-3'
Primer D	5'-CCAAAAGACGGCAATATGGT-3'
Suz12F1	5'-GCTGGCCATGGTAGTTTGTT-3'
Suz12R	5'-TCGCGATTTCGTTTTCTTCT-3'
Sall4F1	5'-CCGGAGAGAGACCTTACGTG-3'
Sall4F2	5'-GGCTACCTCAAAAGCTCACG-3'
Sall4F3	5'-AGGGGAGAGACCATTCCAGT-3'
Sall4R	5'-GGCTGTGCTCGGATAAATGT-3'
Sall4R1	5'-CGGAGATCTCGTTGGTCTTC-3'
Primer I	5'-AAGGCATAATGAACGGCAAG-3'
Primer 9	5'-ATCTGGTGAACCAGTGGCTA-3'
For Southern 5' probe	forward 5'-GCAGAGTCCCACACTGTCAA-3' reverse 5'-GCCTAGGACTCACCAAGCTG-3'
For Southern 3' probe	forward 5'-TCATTCGGATTAACCCCTCA-3' reverse 5'-GTTCCATTTGAGGGGGCTAT-3'
Quantitative PCR	
β-Actin	F: CACAGCTTCTTTGCAGCTCCTT R: CGTCATCCATGGCGAACTG
Suz12	F: GTGCACTCTGAACTGCCGTA R: CCGGTCCATTTCGACTAAAA
Sall4	F: CTCATGGGGCCAACAATAAC R: CGGAGATCTCGTTGGTCTTC
Sox2	F: AAGGGTTCTTGCTGGGTTTT R: AGACCACGAAAACGGTCTTG
Oct4	F: CCAATCAGCTTGGGCTAGAG R: CTGGGAAAGGTGTCCCTGTA
Nanog	F: GCTCAGCACCAGTGGAGTATCC R: TCCAGATGCGTTCACCAGATAG
Fgf5	F: TGCATCTGCTCTGCTCTAAGAAA R: TCATCACATTCCCGAATTAAGCT
T/Brachyury	F: CTGGGAGCTCAGTTCTTTCGA R: GAGGACGTGGCAGCTGAGA
Afp	F: TGAAGCAAGCCCTGTGAACTC R: TCAGAAAACTGGTGATGCATAGC

Chapter 2: *Ofd1*, a human disease gene, regulates the length and distal structure of centrioles

INTRODUCTION

The centrosome: much more than mitosis

Centrosomes organize the microtubule cytoskeleton of animal cells and are most famous for their role in mitosis (Badano et al., 2005; Mikule et al., 2007; Nigg, 2004). A centrosome is present at each pole of a mitotic cell, nucleating and anchoring both spindle and astral microtubules. Perhaps less well known are the functions of centrosomes during interphase, when they play critical roles in the processes of cellular migration and cell polarity/ shape determination (Nigg and Raff, 2009). Centrioles are the functional hub of the centrosome and have a complex structure based upon a central core of microtubules arranged in a nine-fold triplet pattern. In a G1 or G0 cell, the centrosome consists of two centrioles, the mother and daughter, and pericentriolar material (Figure iA). In contrast to most cellular microtubules, which display dynamic instability and range widely in length, centriolar microtubules undergo regulated growth to a characteristic length, are extremely stable, and display numerous posttranslational modifications (PTMs) including acetylation and polyglutamylation (Bettencourt-Dias and Glover, 2009; Kochanski and Borisy, 1990). The centriole also exhibits polarity, with the microtubule minus ends defining proximal and the plus ends defining distal (Bornens, 2002).

The proximal and distal ends of centrioles are structurally and functionally distinct. By transmission electron microscopy (TEM), the distal lumen of both mother

and daughter centrioles contains electron dense material (Vorobjev and Chentsov, 1980). Additionally, the mother centriole is longer than the daughter and possesses two sets of projections at the distal end called subdistal and distal appendages (Chretien et al., 1997; Paintrand et al., 1992) (Figure iB).

The proximal end of the mother and daughter centrioles is the site at which a single new centriole, termed a procentriole, begins to grow during the process of centrosome duplication in S phase. The microtubules of procentrioles grow to a defined length before entry into mitosis, but these new centrioles must pass through the G2 phase of the next cell cycle before they achieve their full length. In the process of centriole maturation, the centriole grows and acquires the properties of a mother centriole, including appendages (Azimzadeh and Bornens, 2007). The distal and subdistal appendages are required for ciliogenesis, another important centrosomal function (Graser et al., 2007; Ishikawa et al., 2005).

Primary cilia: the cell's "antenna"

Primary cilia project from the surface of many vertebrate cells and transduce signals essential for normal development and adult tissue homeostasis (Sharma et al., 2008) (Figure ii). Cilia can be viewed as specialized cellular compartments or organelles. All cilia are generated during interphase from a plasma membrane–associated mother centriole (Figure iiA-B). During interphase, the centriole moves to the plasma membrane and templates the nucleation of the axoneme, the structural core of the cilium. Construction of the axoneme requires intraflagellar transport (IFT), a bidirectional transport system discovered in the green alga *Chlamydomonas* [reviewed in (Rosenbaum

and Witman, 2002)] (Figure iiC). Because no protein synthesis occurs within cilia, IFT is needed to move the organelle's structural components from the cell body to the ciliary tip (the anterograde direction) where axoneme synthesis occurs. This anterograde movement of the IFT complex is driven by the heterotrimeric motor Kinesin-2 (Kozminski et al., 1995) and, at least in the nematode *C. elegans*, by the kinesin OSM-3 (Snow et al., 2004). IFT returns proteins from the cilium to the cell body by means of a retrograde movement driven by a dynein motor (Pazour et al., 1998). IFT also brings signaling proteins to the cilium. For example, adhesion of the flagella of two *Chlamydomonas* gametes activates an IFT-dependent signaling pathway, resulting in cell fusion (Pan and Snell, 2003).

Structural elements contribute to the specialization of the ciliary environment. Among these elements are the terminal plate at the distal end of the basal body and the transitional fibers at the base of the cilium, which may physically restrict entrance of proteins into the cilium (Anderson, 1972)(Figure iiB). The most prominent structural element is the axoneme, consisting of nine doublet microtubules that originate at the triplet microtubules of the basal body centriole and extend the length of the cilium. Most motile cilia have an additional central microtubule pair (the 9+2 microtubule arrangement). Primary cilia are usually immotile, and they lack this central pair (the 9+0 arrangement). The motile primary cilia present on the node, a specialized signaling structure in the early mammalian embryo, are an exception (Figure iiD). The twirling of these primary cilia creates a leftward flow of the surrounding fluid and this flow is essential for the development of the left-right axis (Nonaka et al., 1998).

The primary cilium has several characteristics that make it an ideal cellular location for sensing and transducing signals. It extends into the extracellular space,

affording access to environmental signals. Its elongated geometry provides a high surface-to-volume ratio that may promote interaction of transmembrane receptors with downstream signaling machinery. Finally, the regulated entry of proteins into the cilium confers the advantages of specialization and compartmentalization. Evolution appears to have made use of these characteristics to adapt the cilium for the interpretation of information both from the environment and from other cells.

Cilia in sensation and signaling

Primary cilia play essential roles in odorant reception and photoreception (Benton et al., 2006; Marszalek et al., 2000). In addition to sensing odorants and light, cilia can sense movement. During normal kidney function, urine flows over kidney epithelial cells, bending their primary cilia. A ciliary mechanosensory complex translates this deflection into signals associated with the control of cellular growth and differentiation. Defects in ciliary mechanosensation underlie polycystic kidney disease (PKD), the most common monogenic disorder (Bisceglia et al., 2006; Nauli et al., 2003). PKD causes formation of large cysts, ultimately leading to kidney failure.

A clue that vertebrate cilia may be involved not only in sensing environmental inputs but also in transducing intercellular signals came from the surprising finding that mutations in genes encoding IFT components severely disrupt mammalian Hedgehog (Hh) signal transduction (Huangfu et al., 2003). Hh family members are secreted lipoproteins that regulate tissue patterning, cell proliferation, and many other biological processes [reviewed in (Lum and Beachy, 2004)]. Primary cilia are required to coordinate key steps of the vertebrate Hh signaling pathway (Wong and Reiter, 2008). Ciliary

dysfunction therefore can affect many Hh-mediated processes, such as patterning of the neural tube and limbs during development, and tumorigenesis in the adult (Wong et al., 2009). Cilia also regulate the PDGFαα and Wnt signaling pathways, both of which, like Hh, regulate cellular growth, differentiation, and tissue patterning (Corbit et al., 2008; Schneider et al., 2005).

Recently, it has become clear that defects in cilia underlie a group of genetic syndromes known as ciliopathies (Table 1). Ciliopathies include PKD, Bardet-Biedl syndrome, and Orofaciodigital syndrome 1 (OFD1) (Badano et al., 2006; Christensen et al., 2007). These diseases are heterogeneous, but often share the phenotypes of cystic kidneys, polydactyly, CNS malformations, and skeletal defects, thus leading to the idea that ciliopathies are different clinical entities that "share a common cellular defect and an overlapping set of phenotypes" (Cardenas-Rodriguez and Badano, 2009). The pleiotropic effect of mutations in centrosomal and ciliary genes likely reflects the involvement of cilia in diverse sensory modalities and signaling pathways.

OFD1 mutations cause ciliopathies

Mutations in the *OFD1* gene can cause X-linked Joubert syndrome, Simpson-Golabi-Behmel syndrome type 2, or OFD1 syndrome (Budny et al., 2006; Coene et al., 2009). OFD1 is rare, occurring about one in every 250,000 live births. The syndrome shows an X-linked dominant inheritance pattern with lethality in males, though about 75% of cases are sporadic (Morisawa et al., 2004). Heterozygous females present with a variable phenotype including malformations of the face, oral cavity and digits, CNS defects, and often polycystic kidney disease (Ferrante et al., 2001). The *Ofd1* gene

product localizes to the centrosome, is part of the centriolar proteome, and is required for formation of primary cilia (Ferrante et al., 2006; Keller et al., 2005; Romio et al., 2004). Mouse embryos with a targeted disruption of the *Ofd1* gene show abnormal left-right axis specification and Hh signaling, consistent with the requirement for primary cilia in these processes. However, it was unknown how Ofd1 acts at the centrosome to promote ciliogenesis.

Here we show that Ofd1 associates with the distal ends of centriolar microtubules and constrains mother and daughter centriole elongation. We demonstrate that Ofd1 is necessary for distal appendage formation and Ift88 recruitment, two processes essential for cilium formation. We also model effects of *Ofd1* human mutations in mouse embryonic stem (ES) cells, revealing that each disease-associated mutation differentially affects centriole length and ciliogenesis.

RESULTS

Ofd1 is required for centriole length control

To understand how Ofd1 contributes to normal centrosome structure and function, we characterized male murine ES cells with a gene trap mutation in the *Ofd1* locus, $Ofd1^{Gt}$ cells. As *Ofd1* is located on the X chromosome, these $Ofd1^{Gt}$ cells are hemizygous for *Ofd1* and do not produce Ofd1 protein (Figure 1A).

TEM of asynchronously growing cells revealed abnormally long centriole-like structures in 35% of cells lacking Ofd1, but never in wild type cells (Figure 1B). The mean length of wild type centrioles was 412 nm, whereas the *Ofd1* mutant centrioles averaged 685 nm, and were sometimes more than a micron long. In contrast to the wild

type centrioles which showed little variation in length (SD = 32 nm), the mutant centrioles varied widely in length (SD = 201 nm). The long *Ofd1* mutant centrioles had the microtubule composition and morphology of normal size centrioles, with distinct proximal and distal ends (Figure 1B), and recruited centrosomal and centriolar proteins including Pericentrin, acetylated tubulin, γ-tubulin, and Centrin (Figure 1C). The long *Ofd1* mutant centrioles also possessed known centriole-specific proteins, including Ninein, CP110, and Cep97 (Kleylein-Sohn et al., 2007; Mogensen et al., 2000; Piel et al., 2000; Spektor et al., 2007) (Figure S1A-C). Thus, Ofd1 is essential for the regulation of centriole length.

Recent work has shown that CP110 is also required for centriole length control (Kohlmaier et al., 2009; Schmidt et al., 2009; Tang et al., 2009). CP110 and Cep97 showed normal levels and localization on both normal size and long centrioles of *Ofd1* mutant cells, indicating that centriole elongation defects were not due to misregulation of the centriolar localization of these proteins. Transverse TEM sections showed that, like wild type centrioles, both the long and normal sized centrioles of *Ofd1* mutant cells contained triplet microtubules (Figure 1D, Figure S1D).

Centrioles have critical roles in the mitotic and microtubule organizing functions of centrosomes, as well as in promoting procentriole formation. The doubling time of $Ofd1^{Gt}$ cells was not different from wild type cells (Figure S1E). Additionally, wild type and $Ofd1^{Gt}$ cells had similar cell cycle phase distributions (Figure S1F).

Furthermore, loss of Ofd1 did not affect the interphase microtubule array or mitotic spindle structures (Figure S1G). $Ofd1^{Gt}$ cells showed no changes in normal centrosome or procentriole number, indicating that *Ofd1* is not required for centriole

duplication (Figure S1G-I). Both TEM and localization of procentriole components showed that long *Ofd1* mutant centrioles were associated with the normal number of procentrioles (Figure S1H-I), indicating that long mutant centrioles were capable of promoting normal centriole duplication. Microtubule nucleation and anchoring abilities of wild type and $Ofd1^{Gt}$ centrosomes were examined by using nocodazole treatment to depolymerize microtubules, and then observing microtubule regrowth and anchoring 30 seconds to 15 minutes following nocodazole removal (Figure S1J, and data not shown). Loss of Ofd1 did not affect microtubule nucleation or anchoring. Taken together, these data indicate that centriole duplication, microtubule organization and the mitotic functions of centrosomes do not depend on Ofd1.

Ofd1 localizes to the distal ends of all centrioles

To determine where within the centrosome Ofd1 localizes, we generated an antibody to Ofd1. The antibody recognized the centrosome of wild type cells, but not of $Ofd1^{Gt}$ cells (Figure 2A-B). Similarly, preimmune serum did not recognize the centrosome, confirming the specificity of the Ofd1 antibody (Figure 2A). In asynchronous cells, Ofd1 was present as two or four dots within the centrosome(s) (Figure 2B). In synchronized cells, Ofd1 localized to centrosomes throughout the cell cycle, appearing most intense during S/G2 and diminishing at mitosis (Figure S2A).

Closer inspection of wild type ES cells revealed that Ofd1 was associated with mother, daughter and procentrioles (Figure S2B). In cells in which the mother centriole extended a cilium, Ofd1 localized to the base of the cilium (Figure 2B-C). Similar localization to centrioles and the cilium base was seen in fibroblast, kidney, bone and

retinal cell lines of mouse or human origin (Figure S2C). To further assess Ofd1 centriolar association, we induced centriole overduplication by arresting U2OS cells in S phase (Habedanck et al., 2005). Consistent with findings in other cells, Ofd1 associated with all centrioles, including supernumerary centrioles, in arrested U2OS cells (Figure S2D).

We have developed a technology, called Floxin, to engineer ES cell gene trap loci (Singla et al., 2009). Floxin enables efficient targeted insertion of DNA constructs into gene trap loci. Using the Floxin approach, we introduced a carboxy-terminal Myc tagged version of wild type *Ofd1* (Ofd1-Myc knock-in) at the endogenous locus ($Ofd1^{Ofd1myc}$ cells). Inserting an *Ofd1-Myc* gene into the native genomic context and under control of endogenous regulatory elements restored Ofd1 protein expression and prevented long centriole formation (Figure S2E-F). However, Ofd1-Myc Floxin cells expressed reduced levels of protein as compared to wild type (Singla et al., 2009). Localization of the Myc tag of Ofd1 confirmed that Ofd1 localized to centrioles and the cilium base (Figure 2C). Additionally, of the $Ofd1^{Ofd1myc}$ cells that were ciliated, Ofd1-Myc also localized to about 50% of cilia, either along the cilium or at the tip (Figure S2G). Ciliary localization of Ofd1 was never seen when staining $Ofd1^{Ofd1myc}$ or wild type cells with Ofd1 antibody, suggesting that both antibodies recognize Ofd1 protein at the centrosome, while ciliary Ofd1 can only be detected by staining against the C-terminal Myc tag. Ciliary localization of Ofd1 has also been reported in renal proximal tubule epithelial cells using an antibody generated against the C-terminal portion of the protein (Romio et al., 2004).

To ascertain where Ofd1 localizes on procentrioles, we examined three markers of procentrioles: Sas-6, Poc5, and CP110, which associate with the proximal, distal and very

distal ends of procentrioles, respectively (Azimzadeh et al., 2009; Kleylein-Sohn et al., 2007; Strnad et al., 2007). Ofd1 localized to the procentriole distal end, in a domain between Poc5 and CP110 (Figure 2D-F).

We next examined the localization of Ofd1 on mother and daughter centrioles. Costaining with Rootletin or Poc1, which mark the proximal ends of mother and daughter centrioles, showed that Ofd1 localized to the opposite, distal ends (Bahe et al., 2005; Keller et al., 2008) (Figure 2G, Figure S2H). To ascertain the localization of Ofd1 more precisely, we examined Ofd1 localization relative to Ninein, Odf2, and Cep164, which are parts of the subdistal and distal centriole appendages (Graser et al., 2007; Ishikawa et al., 2005; Mogensen et al., 2000; Nakagawa et al., 2001; Piel et al., 2000) (Figure 2H-L). Ofd1 was located at the very distal ends of centrioles, at a more central position than the subdistal and distal appendages.

Taken together, these data reveal that Ofd1 localizes to the distal ends of all centrioles (mother, daughter, and procentrioles), closely associated with the centriole microtubule barrel. This is consistent with immuno-electron microscopy studies that showed Ofd1 to be associated with centrioles (Romio et al., 2004).

Ofd1 mutant centrioles contain destabilized microtubules

As Ofd1 is in close proximity to centriolar microtubules, we examined whether Ofd1 associates with microtubule components. To determine what subcellular compartment Ofd1 associates with, we performed cellular fractionation and determined that Ofd1 was located in the cytoplasmic fraction (Figure 3A). We also found that Ofd1 was best solubulized in a modified RIPA buffer containing sodium deoxycholate and NP-

40 detergents (Figure 3B). Immunoprecipitation revealed that Ofd1 complexes contained γ-tubulin and acetylated tubulin, two forms of tubulin found in centriolar microtubules (Moudjou et al., 1996) (Figure 3C). Ofd1 complexes did not contain other proximal or distal centriolar proteins (Figure 3C, Figure S3A). Together with the above data that revealed Ofd1 localization at the centriole distal end, these data suggest that Ofd1 caps the distal ends of all centrioles in a complex intimately associated with centriolar microtubules.

Centriolar microtubules are extremely stable, as reflected by their resistance to microtubule depolymerizing drugs (Kochanski and Borisy, 1990). To assess whether abnormal centriole length reflects altered centriolar microtubule dynamics, we treated cells with nocodazole. Whereas nocodazole did not affect the length of wild type centrioles, it shrank *Ofd1* mutant centrioles (Figure 3D).

Stabilized microtubules are associated with PTMs such as acetylation and polyglutamylation (Bobinnec et al., 1998; Loktev et al., 2008). We therefore investigated whether microtubules of long *Ofd1* mutant centrioles have aberrant PTMs. Although the microtubules of long centrioles were normally acetylated, polyglutamyl groups were reduced or absent from approximately 50% of long centrioles (Figure 3E-F). Thus, Ofd1 may constrain centriole length in part by affecting the dynamics of centriolar microtubules.

Ofd1 controls elongation of the distal centriole in G2

Procentrioles first elongate during S phase, while daughter centrioles elongate and mature during G2. To investigate if cell cycle phase influenced whether loss of Ofd1 was

permissive for aberrant elongation, we blocked cells in G1, S, or G2 (Figure S3C). G1 arrested cells showed a lower proportion of long centrioles, while G2 arrested cells showed a higher proportion of long centrioles, indicating that elongation defects occurred predominantly during G2, the phase during which centriole maturation and daughter centriole elongation normally occurs (Figure 4A, Figure S3D).

To understand what part of the centriole was elongating abnormally, we examined the long centrioles for the presence of distal centriole components. Poc5 normally localizes to a small region in the centriole distal lumen (Azimzadeh et al., 2009). The *Ofd1* mutant long centrioles displayed an expanded Poc5 region that comprised most of their length (Figure 4B). The appendage proteins Ninein and Odf2 usually localize to a small domain at the centriole subdistal and distal end, respectively (Mogensen et al., 2000; Nakagawa et al., 2001; Piel et al., 2000). Though sometimes found in the middle of long centrioles, expanded domains of Ninein and Odf2 were seen on many *Ofd1* mutant long centrioles as well (Figure 4C, Figure S4C). The centriole distal end contains electron dense material within the lumen (Vorobjev and Chentsov, 1980). In TEM images, the electron dense distal end comprised most of the long *Ofd1* mutant centrioles, whereas the electron sparse proximal end was of comparatively normal size (Figure 4D, Figure S3B). Centrin, which is normally present in the centriole distal lumen (Paoletti et al., 1996), was often present in discrete foci within the abnormal long centriole, suggesting that the elongated distal domain was structurally abnormal (Figure 1C, Figure S3E). Together, these data suggest that Ofd1 acts during G2 to restrain elongation specifically of the distal centriole.

Ofd1 controls elongation of mother and daughter centrioles

Because Ofd1 localized to all centrioles, we were interested to know if the distal ends of mother, daughter, and procentrioles showed equivalent length abnormalities in the absence of Ofd1. To determine if procentrioles showed length abnormalities, we re-examined the data regarding localization of Odf2. Odf2 is a component of appendages specifically found only on mother centrioles in G1-S and on both mother and maturing daughter centrioles in G2 (Nakagawa et al., 2001). Odf2 is never found on procentrioles. In asynchronous cells, 95% of long centrioles were positive for Odf2, suggesting that the long centrioles were not procentrioles (Figure 4C). TEM of long centrioles supported this conclusion, as *Ofd1* mutant long centrioles showed appendages, procentriole nucleation, and microtubules anchored at the distal ends (Figure 4D-E, S1I, S3B, S4B), characteristics of mother and daughter centrioles not possessed by procentrioles (Piel et al., 2000).

As described above, during G1-S the mother centriole is the only Odf2-positive centriole in the cell. Therefore, the presence of a single long Odf2-positive centriole in *Ofd1* mutant cells indicated that the long centriole was the mother centriole (Figure 4C, last 3 columns). Thus, the mother centriole depends upon Ofd1 for length control.

Although most $Ofd1^{Gt}$ cells had only one long centriole, they occasionally had two (Figure 4F), suggesting that daughter centrioles could also elongate aberrantly in the absence of Ofd1. In order to determine if daughter centrioles show Ofd1-dependent length perturbations, we assayed for the presence of the daughter centriole component Centrobin (Zou et al., 2005). Some long centrioles also contained Centrobin, indicating that long centrioles present in $Ofd1^{Gt}$ cells can display characteristics of daughter

centrioles (Figure 4G). These experiments suggest that Ofd1 controls both mother and daughter centriole length.

Ofd1 is required for formation of distal, but not subdistal, appendages

As demonstrated above, Ofd1 localizes to a domain central to the distal appendages. We examined subdistal appendages in wild type and *Ofd1*^{Gt} cells by immunofluorescent localization of Ninein, a subdistal appendage component, as well as by TEM. Ninein showed the normal localization to the proximal mother and daughter, as well as the subdistal mother centriole in *Ofd1*^{Gt} cells (Figure 5A). The appendages are an important site of microtubule anchoring with characteristic TEM appearances depending on plane of section (Delgehyr et al., 2005; Paintrand et al., 1992) (Figure iB). Based on both longitudinal and transverse sections, loss of Ofd1 did not affect subdistal appendage structure or microtubule anchoring (Figure 5B, Figure S4A).

Subdistal appendages were also present on long *Ofd1* mutant centrioles, either in the middle of the long centriole or spread out along the elongated distal domain, as assayed by immunofluorescence localization or by TEM (Figure S1I, 4D-E, S4B-C). Though their proximal-distal position was sometimes abnormal, the structure of the subdistal appendages appeared normal on the long centrioles as well.

In contrast to the subdistal appendages, *Ofd1*^{Gt} cells showed severe defects in distal appendage formation (Figure 5C). Loss of Ofd1 caused complete loss of the distal appendage component Cep164 from all centrioles. As *Ofd1*^{Gt} cells expressed Cep164 (Figure 5D), but the distal appendages of *Ofd1*^{Gt} centrioles appeared less electron dense by TEM (Figure 5E, Figure S4B), the delocalization of Cep164 in *Ofd1*^{Gt} cells suggested

a failure to form normal distal appendages. Whereas wild type distal appendages showed the characteristic elongated triangular shape with increased density on one end, loss of Ofd1 caused the appendages to appear thin and uniform along the length, on both normal (Figure 5E) and abnormal length centrioles (Figure S4B). Cep164 was not associated with immunoprecipitated Ofd1 complexes, suggesting that Ofd1 does not directly recruit Cep164 (Figure S3A), but rather is more generally required to promote normal distal appendage formation.

To establish the extent of the distal appendage defects, we examined centriolar localization of Odf2 in asynchronous *Ofd1*^{Gt} cells. Odf2 is required for both subdistal and distal appendage formation and localizes at the base of the appendages (Ishikawa et al., 2005; Nakagawa et al., 2001). Unlike Cep164, Odf2 localized to the distal centriole in asynchronous *Ofd1* mutant cells (data not shown). To ascertain if the distal appendage defects might be temporally related to the centriole elongation defects, cells were synchronized and Odf2 localization followed as the cell cycle progressed. At 0 hr, cells were in G1, with one mother and one daughter centriole. As the cells progressed through G2/M at 8-10 hr, the daughter matured by gaining appendages and Odf2 localization (Figure iA, Figure S4D). This process was observed by monitoring the presence of cells with two Odf2 spots, indicating two mature centrioles. During G2, the same phase in which centriole elongation defects occur, *Ofd1*^{Gt} cells had significantly fewer cells with two Odf2-positive centrioles (Figure 5F-G). No differences in acquisition of the subdistal appendage marker Ninein was observed, suggesting that the maturation defect is confined to the distal appendages (data not shown). Restoring Ofd1 protein expression in

Ofd1^{Ofd1myc} cells restored normal localization of Cep164 and Odf2 to the mother centriole (Figure 2I, J).

To determine if Ofd1 required Odf2 or Cep164 to localize to centrioles, we transfected hTERT-RPE1 cells with short interfering RNAs (siRNA) directed against luciferase (control, GL2), Odf2, or Cep164 and assessed Ofd1 centrosomal localization (Figure S4E-F). Removing Cep164 or Odf2 from centrioles did not change Ofd1 localization, indicating that Ofd1 does not require these distal appendage proteins to localize to centrioles.

Together, these data indicated that Ofd1 is required for recruitment of distal appendage proteins. Odf2 is associated with both distal and subdistal appendage structures and participates in their formation (Ishikawa et al., 2005; Nakagawa et al., 2001). Cep164, on the other hand, is only associated with the distal appendages (Graser et al., 2007). It seems that some Odf2 protein, perhaps the pool associated with the subdistal appendages, is recruited normally in *Ofd1* mutant cells, whereas the distal appendage-specific protein Cep164 is not.

Ofd1 is required for the recruitment of Ift88 to the centrosome

As distal appendages may also be important for docking of intraflagellar transport (IFT) proteins during the process of ciliogenesis (Deane et al., 2001), we examined Ift recruitment. Two components of Ift complex B, Ift20 and Ift80, localized normally to centrosomes in *Ofd1*^{Gt} cells (Follit et al., 2006; Lucker et al., 2005) (Figure 6A-B). Similarly, Kif3a, part of the anterograde Ift motor, localized to centrosomes in both wild type and *Ofd1*^{Gt} cells (Figure 6C). Ift88, another Ift complex B component, is present at

the centrosome and along the cilium (Haycraft et al., 2007). Immunofluorescence staining and quantification revealed that, in contrast to Ift20, Ift80 and Kif3a, Ift88 failed to associate with centrosomes in *Ofd1*^{Gt} cells (Figure 6D-E). This defect is not due to differences in protein expression, as wild type and *Ofd1*^{Gt} cells expressed Ift88 at similar levels (Figure 6F). Restoring Ofd1 protein expression in *Ofd1*^{Ofd1myc} cells restored normal localization of Ift88 to the centrosome (Figure 6G-H). Together, these data suggest that loss of Ofd1 caused a specific loss of Ift88 from the centrosome.

To determine if loss of centrosomal Ift88 was due to a general disruption of trafficking to the centrosome, we investigated localization of three proteins known to be important for this function: Dynactin, Pericentrin, and Cep290 (Jurczyk et al., 2004; Kim et al., 2008; Quintyne and Schroer, 2002; Tsang et al., 2008). All localized normally in cells lacking Ofd1 (Figure S5), indicating that the requirement for Ofd1 in the recruitment of Ift88 does not reflect a general disruption of centrosomal trafficking.

As both Ofd1 and Ift88 localize to centrosomes, we were interested to determine if Ofd1 co-localized with Ift88 to the same regions of this organelle. In ciliated cells, Ift88 colocalized with Ofd1 at the base of the cilium (Figure 6G). When cells were not ciliated, Ift88 and Ofd1 colocalized at the distal end of the mother centriole (Jurczyk et al., 2004) (Figure 6H).

Both Ift88 and centriole appendages are required for ciliogenesis (Ishikawa et al., 2005; Pazour et al., 2000). An important step in ciliogenesis is docking to a vesicular membrane (Sorokin, 1962). In TEM images, *Ofd1*^{Gt} centrioles were never seen docked to a vesicle or at the plasma membrane. Consistent with this, and previous data showing that Ofd1 is required for ciliogenesis (Ferrante et al., 2006), *Ofd1*^{Gt} cells did not make

primary cilia (Figure 6I). Collectively these data revealed that Ofd1 is required for length control of the distal mother and daughter centriole, recruitment of distal appendages and Ift88, and ciliogenesis.

OFD1 syndrome-associated mutations cause centriole length defects and disrupt normal ciliogenesis

Ofd1 protein has an amino-terminal Lis1 homology (LisH) domain and five coiled-coil domains that are important for centrosomal localization (Romio et al., 2004). To identify how human mutations affected Ofd1 function, we generated ES cell lines expressing five disease-associated missense mutations (Figure S6A): S75F and A80T affect the LisH domain, S437R affects the second coiled-coil domain, and G139S and KDD359-361FSY affect intervening highly conserved residues (Ferrante et al., 2001; Rakkolainen et al., 2002; Romio et al., 2003; Thauvin-Robinet et al., 2006). Using the Floxin system, we inserted Myc-tagged murine *Ofd1* alleles containing the homologous mutations into the *Ofd1* locus. Because the cells are hemizygous for *Ofd1*, they express only the inserted mutant allele under control of the endogenous promoter.

Cells were examined for Ofd1 protein expression and centrosomal localization. All disease-associated alleles were expressed, though three (S75F, A80T and KDD359-361FSY) reduced protein levels (Figure 7A, Table 2). These finding are consistent with previous studies in HEK293 cells that found that the A80T mutation reduced protein half-life (Gerlitz et al., 2005). Because KDD359-361FSY mutates the region of the protein that the Ofd1 antibody is expected to recognize, protein levels were also compared by immunoprecipitating and blotting against the carboxy-terminal Myc tag. The same

decrease was seen by this method (Figure S6B). Low levels of the S75F and A80T mutant proteins prohibited accurate assessment of centriolar localization in ES cells. The S75F mutant protein has been shown previously to localize normally to centrioles in HEK293 cells, and deletion of the LisH domain does not affect Ofd1 localization (Romio et al., 2004). None of the other disease associated mutations altered centriolar localization (Figure 7B).

To assess how disease-associated mutations affected Ofd1 function, centrioles were examined for length defects, Cep164 and Ift88 recruitment. A quantitative summary of this data is presented in Table 2 and Figure S6C with all lines compared to wild type ES cells. However, the significance of these differences cannot be determined directly from this type of comparison, as Ofd1-Myc Floxin cells express reduced levels of Ofd1 (Singla et al., 2009). This reduction does not affect centriole length control or Cep164 recruitment, but does reduce Ift88 recruitment and ciliogenesis (Figure S6C). *Ofd1*^{Rev} cells (Singla et al., 2009) expressed wild type Ofd1 at still lower levels, lower than any of the disease allele lines (data not shown). This reduced level did not affect centriole size, but did affect recruitment of Cep164 and Ift88, as well as ciliogenesis. (Figure S6C).

To understand how disease mutations affect Ofd1 function independent of protein stability, disease-allele carrying cells were compared to a line that expressed similar levels of wild type Ofd1 (Figure 7C). The G139S and S437R *Ofd1* mutant lines expressed protein levels comparable to the Floxin Ofd1-Myc line. The S75F, A80T, and KDD359-361FSY mutant lines expressed protein levels comparable to *Ofd1*^{Rev}. Comparing these lines suggested that the deficits described below are not entirely attributable to decreased protein levels.

Four *Ofd1* mutations decreased the ability of Ofd1 to restrain centriole elongation, resulting in abnormally long centrioles (Figure 7D). Quantification of long centrioles indicated that the hypomorphic mutations affected Ofd1 function to different degrees, indicating that the mutations represent an allelic series (Figure S6C). Mutations in the LisH domain caused the most profound centriole elongation. In contrast, the KDD359-361FSY mutation decreased the number of long centrioles below that observed in cells expressing similar levels of wild type Ofd1, suggesting that this mutation may shorten centrioles (Figure 7C).

Cep164 recruitment was affected by A80T, one mutation affecting the LisH domain, but none of the other mutations (Figure S6D, Table 2).

The LisH mutations blocked Ift88 recruitment. Of the other mutations only S437R affected Ift88 recruitment, suggesting that the second coiled coil of Ofd1 is particularly important for recruiting Ift88 (Figure S6E, Table 2).

The LisH mutations also blocked ciliogenesis, whereas the carboxy-terminal mutations caused decreased ciliogenesis (Figure 7C, S6F).

Thus, phenotyping a variety of human disease mutations reveals that distinct Ofd1 domains contribute to genetically separable Ofd1 functions. Although the disease-associated missense mutations represented alleles with varying degrees of stability and function, all compromised the ability of Ofd1 to regulate centriole length and ciliogenesis.

DISCUSSION

Summary

Taken together, our results reveal that Ofd1 is a critical component of the distal centriole required for centriole length control, distal appendage formation and Ift88 recruitment. Ofd1 localizes to all centriole distal ends, and Ofd1 complexes with α- and γ-tubulin. *Ofd1* mutant cells show instability of centriolar microtubules, suggesting that Ofd1 functions as a cap to stabilize centriolar microtubules at a defined length.

Daughter centrioles normally elongate and gain subdistal and distal appendages during centriole maturation in G2 phase. Ofd1 regulation of centriolar size is most critical in G2, and only mother and daughter centriole distal ends show excessive elongation in the absence of Ofd1. Thus, Ofd1 capping may be specifically required for stabilization and length control of centrioles during centriole maturation (Figure 7E).

Loss of Ofd1 does not affect subdistal appendage structure or function. Distal appendage formation, on the other hand, is severely perturbed, suggesting that centriole stability may be a prerequisite for assembly of distal, but not subdistal, appendages.

Ofd1 control of centriole length and distal structure are separable functions

OFD1 patients do not show a tight genotype-phenotype correlation, making it difficult to assign a relationship between *OFD1* mutations and disease severity (Feather et al., 1997; Prattichizzo et al., 2008). Use of the Floxin system allowed us to create a panel of ES cell models that express alleles orthologous to human disease alleles. Expression of the disease alleles from the endogenous *Ofd1* locus allows for direct comparison of the effects of the mutation on gene function. The phenotyping of these cellular models indicated that the human disease-associated mutations form an allelic

series which, from weakest to strongest, are KDD359-361FSY, S347R, G139S, S75F and A80T.

We found that the LisH domain is essential for all Ofd1 functions. In contrast, mutations carboxy-terminal to the LisH domain and in the coiled-coil domain do not abolish Cep164 localization, Ift88 recruitment, or ciliogenesis, but do affect centriole length. Whereas it is likely that many manifestations of OFD1 are due to defective ciliogenesis, the additional Ofd1 roles discovered by modeling the disease in ES cells raise the possibility that some OFD1 phenotypes may be due to centriolar, not ciliary, dysfunction. Centrosomes have many important developmental functions, including roles in cell migration and fate determination (Higginbotham and Gleeson, 2007). It will be interesting to investigate if and how centriolar length dysfunction contributes to OFD1 pathogenesis.

As loss of Ofd1 also causes defects in distal appendage formation and centriolar recruitment of Ift88, it is possible that these phenotypes are secondary to abnormal centriole elongation. Alternatively, the requirement for Ofd1 in distal appendage formation and Ift88 recruitment may reflect separate function(s) from its role in centriole length control. In support of this possibility, neither Cep164 nor Ift88, proteins respectively critical for distal appendage formation and ciliogenesis, have been implicated in centriole length control (Graser et al., 2007; Pazour et al., 2000). Moreover, our finding that the G139S and KDD359-361FSY substitutions disrupted centriole length control without changing Ift88 or Cep164 localization indicates that length abnormalities do not necessarily result in the other *Ofd1* null phenotypes. These missense mutations also reveal that distinct domains of Ofd1 are involved in centriole length control and

recruitment of distal appendages and Ift88. Interestingly, cells expressing G139S and KDD359-361FSY mutant forms of Ofd1 also show decreased ciliogenesis, suggesting that control of centriole length itself may be essential for ciliogenesis.

CPAP, CP110 and Ofd1 have different roles in centriole length control

The proteins CPAP, Poc1, and CP110 also have functions in centriole length control (Keller et al., 2008; Kohlmaier et al., 2009; Schmidt et al., 2009; Tang et al., 2009), summarized in Table 3. CPAP is part of the proximal centriole and is required for procentriole formation (Kleylein-Sohn et al., 2007). In contrast, Ofd1 is part of the distal centriole and is not required for procentriole formation. Abnormal centrioles caused by CPAP overexpression can display procentriole characteristics and show incomplete centriolar walls. Loss of *Ofd1* affects mother and daughter centrioles, but not procentrioles, and does not affect the integrity of centriole walls.

Overexpression of CPAP induces long centrioles that do not display a normal proximal to distal polarity, as CPAP and other proximal centriole proteins are present along the length of the centriole (Kohlmaier et al., 2009; Schmidt et al., 2009; Tang et al., 2009). Also, the abnormal elongated portion of CPAP-associated centrioles can initiate procentriole formation, a function of the proximal centriole. Long CPAP-associated centrioles do not possess an elongated appendage domain, as appendages are located in the middle of the long centriole. These findings suggest that CPAP overexpression induces the formation of an elongated domain at the distal end of the centriole that possesses proximal characteristics.

In contrast to long CPAP-associated centrioles, long *Ofd1* mutant centrioles do not nucleate extra procentrioles and display expanded localization of distal centriole proteins. These findings suggest that loss of Ofd1 results in elongation of a distal centriole-like domain. The extensive differences between the CPAP overexpression phenotype and the Ofd1 loss-of-function phenotype argue that CPAP and Ofd1 may regulate the elongation of different domains within the centriole. CPAP may regulate the elongation of proximal domains, whereas Ofd1 is required to regulate the elongation of the distal domain.

The functions of CP110 and Ofd1 are similarly distinct. Although both proteins control centriole length, CP110 shows a complicated localization pattern and may be present on 1, 2, 3, or all 4 centrioles ((Spektor et al., 2007), our unpublished observations). Once centrioles are formed, the influences that control CP110 presence or absence from centrioles are not understood, although CP110 is never present when a centriole possesses a cilium. In contrast, Ofd1 is located on the distal ends of all centrioles throughout the cell cycle, regardless of ciliary status. This localization may reflect the role of Ofd1 in distal appendage formation, a role not shared by CP110.

Although not studied as extensively as CPAP overexpression, the elongated centrioles of CP110 depleted cells show morphological similarities to the abnormal CPAP centrioles. Depletion of CP110, like CPAP overexpression and unlike loss of Ofd1, affects procentriole length, suggesting distinct roles for CP110 and Ofd1 during the centrosome cycle.

Centrioles dramatically elongate at two times during the centrosome cycle: first during procentriole initiation and growth, and later during centriole maturation, the

process by which daughter centrioles obtain the length and appendages characteristic of mother centrioles (Chretien et al., 1997). What may not have been fully appreciated before our study is that building the proximal and distal centriole are two very different processes. Structural components required to make the proximal procentriole include Poc1, CPAP, Centrobin, and Cep135. As CP110 is required for centriole duplication and the regulation of both centriole and procentriole length, CP110 may function primarily in procentriole initiation and growth (Chen et al., 2002; Kleylein-Sohn et al., 2007; Tsang et al., 2006). Building the distal part of the centriole requires Poc5, and for subsequent elongation and maturation, appendage proteins like Odf2 and Cep164. We have found that Ofd1, on the other hand, specifically regulates mother and daughter centriole elongation at G2, suggesting that it functions in centriole maturation and coordinates elongation of this final, distal domain with the construction of centriolar appendages. (Figure 7E). The major differences in the complement of proteins that compose the proximal and distal centriole, and the lack of any other proteins similar to Ofd1, argues that different mechanisms control elongation of these domains. Thus, CP110 and Ofd1 may regulate centriole length at different points of the centrosome cycle. One could also imagine that dissimilar factors influence the cellular decision to initiate centrosome duplication (procentriole biogenesis) as compared to centriole maturation. It then follows that regulation of procentriole elongation might look distinct from maturation, though both processes ostensibly control centriolar microtubule elongation.

Ofd1, CP110, and centriole evolution

Ofd1 orthologs are present in the genomes of all organisms with canonical centriole structure and cilia, including single celled organisms such as *Chlamydomonas* (Figure S7A). "Canonical" centriole structure refers to the presence of the 9-triplet microtubule pattern and distinct appendages on the mother centriole (Figure S8A). The multiciliated organisms *Tetrahymena* and *Paramecium* also contain another Ofd1 paralog, Ofd1β. Ofd1 and Ofd1β are most similar in the N-terminal half, though Ofd1β does not contain the LisH domain (Figure S7B). Since we demonstrated the LisH domain to be essential for all Ofd1 functions, it is unclear if Ofd1β plays a similar role in centriole structure, or has additional functions. Perhaps Ofd1β is important for biogenesis of the many centrioles required to make multiple cilia, serving a strictly structural instead of regulatory role. Organisms with divergent centriole structure (singlet or doublet microtubules, no clear mother centriole appendages, Figure S8A) have an ortholog that is most closely related to Ofd1β (*Drosophila, Tribolium*). These organisms also only possess cilia on a specialized subset of cells, sensory neurons and sperm.

CP110 orthologs are absent from the genomes of many single celled eukaryotes such as *Tetrahymena,* but are possessed by animal lineages, including nematodes and insects (Figure S8B). This association of CP110 with multicellularity may reflect the complexity of integrating inputs such as growth factor signaling into the coordination of the centrosome cycle with the cell cycle (Figure S8C).

Centriole function, ciliogenesis and cell division

Phylogenetic analysis shows without exception that organisms without centrioles also do not have cilia (Marshall, 2009). Several authors postulate that ciliogenesis is the

original, ancestral function of centrioles, and that centriolar association with mitosis and cell division is a derived characteristic (Bornens and Azimzadeh, 2007; Marshall, 2009; Woodland and Fry, 2008). A number of lines of evidence support the hypothesis that centrioles are absolutely required for ciliogenesis, but are dispensable in mitosis. Centrioles and centrosomes are not required for mitosis, even in organisms that normally possess them. Mammalian oocytes progress through meiosis II without centrioles, and after fertilization in the mouse, early embryonic cleavages proceed in the absence of centrioles (Sun and Schatten, 2007). *Drosophila* larvae that lose all centrioles by the third-instar larval stage develop into an almost morphologically normal adult fly (Basto et al., 2006). Indeed, the major phenotype of these "centrosome-less" flies is inability to move, caused by lack of neuronal cilia. Sensory neurons are the only ciliated population of cells in flies, besides sperm. Finally, as described here, the severe structural abnormalities in centrioles caused by loss of Ofd1 only disturbs ciliogenesis, while other functions associated with centrioles (mitosis, microtubule nucleation and organization), remain normal.

On the other hand, some evidence suggests that centrioles and centrosomes have a role in asymmetric cell divisions, independent of their role in ciliogenesis. Disrupting centrioles in *C. elegans* embryos arrests embryos at the 1 or 2-cell stage, and *Drosophila* without centrioles show defects in asymmetric neuroblast divisions (Basto et al., 2006). Asymmetric cell division also contributes to neurogenesis in the mammalian neocortex, with neural progenitor cells preferentially inheriting the oldest centriole after division. This asymmetric centrosome inheritance is functionally important, as removing Ninein function causes both cells to leave the progenitor niche and differentiate, depleting the

stem cell population (Wang et al., 2009). Ninein is required for both centriolar microtubule anchoring and ciliogenesis, so it is unclear which function is important for maintaining progenitor fate. To answer this question, it would be interesting to study neurogenesis in an OFD1 mouse model, as loss of Ofd1 specifically causes ciliary loss without perturbing Ninein function and microtubule organization. Evidence from an *in vitro* model using embryoid body differentiation suggests that loss of Ofd1 causes increased neurogenesis, consistent with a role for cilia and/ or centrioles in maintaining progenitor fate (Hunkapiller et al., 2010).

Mutations in several centrosomal and centriolar genes cause primary microcephaly, suggested to be due to mitotic abnormalities in neural progenitors (Cox et al., 2006). It is not known if these mutations also affect ciliogenesis, and thus whether effects are due directly to centrosomal dysfunction during mitosis, or if abnormal ciliary signaling precedes these defects. However, ciliopathy patients do not show microcephaly, indicating that there may a specific centrosomal contribution besides ciliogenesis to the proper regulation of neurogenesis.

Does *OFD1* have an independent ciliary function?

The human *OFD1* gene undergoes alternative splicing, producing two transcripts (de Conciliis et al., 1998). The first, designated *OFD1a*, produces the longer protein, approximately 1011 amino acids long. The second, *OFD1b*, produces a protein that contains the first 353 amino acids of OFD1a with 13 alternative C-terminal amino acids (Figure S9). Both isoforms are ubiquitously expressed, but the expression level of *OFD1b* is lower in many tissues (de Conciliis et al., 1998; Romio et al., 2003). The

function of *OFD1b* is completely unknown. Comparison to *OFD1a* shows that *OFD1b* contains the LisH domain and the first coiled-coil domain. Based on previous localization studies, *OFD1b* would be predicted to only partially localize to the centrosome (Romio et al., 2004). It would be interesting to create a Floxin cell line expressing the *OFD1b* isoform to determine localization, and if this protein had a role in stabilizing other types of microtubules, perhaps ciliary or cytoplasmic.

As mentioned in the introduction, *OFD1* mutations can cause different ciliopathies, depending on the location of the mutation. OFD1 syndrome (OFD1S) shows an X-linked dominant pattern with lethality in males, and is associated with mutations in exons 1-17 of *OFD1*. Simpson-Golabi-Behmel syndrome type 2 (SGBS2) and X-linked Joubert syndrome (XL-JS) have an X-linked recessive pattern with males affected exclusively. SGBS2 and XL-JS are caused by mutations in exon 16 and exon 21 of *OFD1*, respectively. Both SGBS2 and XL-JS patients have recurrent respiratory infections caused by dysfunctional motile cilia in respiratory epithelial cells, suggesting that in addition to its role in primary ciliogenesis, *OFD1* is also required for proper formation and/ or function of motile cilia (Budny et al., 2006; Coene et al., 2009). Consistent with this hypothesis, morpholino knockdown of *ofd1* in zebrafish embryos results in abnormal cilia in Kupffer's vesicle that are short and do not move properly (Ferrante et al., 2009). Intriguingly, TEM of these cilia revealed misplaced axonemal microtubules and abnormal ciliary vesicular bulges. Are these ciliary defects secondary to centriolar defects, or does *OFD1* have an independent function in controlling ciliary microtubule length, patterning, or stability? Investigating ciliary structure in the previously described Floxin cell lines expressing human *OFD1* alleles, as well as creating

new Floxin lines expressing SGBS2 and XL-JS alleles could provide insight into this question.

Human mutations define functionally important *OFD1* domains

The large majority of mutations from OFD1S, SGBS2, and XL-JS patients are frameshift, splice site, and nonsense mutations (81% of all described mutations) (Macca and Franco, 2009). Many of these are likely to cause nonsense-mediated decay of the resulting transcript. Of the 14 known missense mutations, 9 are located within the LisH domain, emphasizing the importance of this domain for *OFD1* function. The portion of the protein between the LisH and first coiled-coil domain may also be important for regulating microtubule stability, as the G139S mutation located here causes elongated centrioles without affecting Cep164 or Ift88 localization.

All the coiled-coil (cc) domains are important for mediating centrosomal localization, as well as for specific protein-protein interactions. The second cc is of particular significance for Ift88 recruitment, while the fourth and fifth cc are critical for interaction with Lebercilin (*LCA5*, mutated in a form of Leber Congenital Amaurosis retinal degeneration) (Coene et al., 2009).

The region between the first and second cc domains is well conserved amongst vertebrate orthologs of *Ofd1*, and two different missense mutations from OFD1S patients affect this region. One of these mutations (KDD359-361FSY) caused a hypermorphic allele of *Ofd1* that shortened centriolar microtubules without affected Cep164 or Ift88 localization, suggesting that this domain is also central to Ofd1 control of microtubule stability. We propose to define this region as a third type of functional domain in *Ofd1*,

the intercoil domain (Figure S9). Further investigation into the mechanism of Ofd1 function as discussed below could elucidate how the intercoil domain is important for regulating microtubule dynamics.

Ofd1 controls elongation of a distinct centriole distal domain

The microtubule pattern of centrioles shows a change from a triplet arrangement at the proximal end to a doublet arrangement at the distal end. This shift in microtubule pattern occurs approximately where the subdistal appendages attach to the centriole (Paintrand et al., 1992). Perhaps Ofd1 controls elongation specifically of distal centriole doublet microtubules, while other proteins like CP110 regulate triplet microtubule length. It would be interesting to study *Ofd1*^{Gt} centrioles with a technique such as EM tomography that allows better visualization of microtubule pattern to determine whether the abnormally elongated portion of the centriole contained doublet microtubules only.

The LisH domain may be involved in the regulation of microtubule dynamics (Emes and Ponting, 2001). We favor a model for Ofd1 function in which the coiled-coil domains mediate Ofd1 centrosomal localization, and the LisH domain then stabilizes centriole doublet microtubules during elongation, allowing posttranslational modification of centriolar microtubules and construction of distal appendages. After centriole maturation, Ofd1 remains at the centriole distal end, where the second coiled-coil domain is important for recruitment of Ift88.

Defining the mechanism of *Ofd1* function

Though the current study helps define the cellular role of *Ofd1* in centrosome structure and function, many questions remain about the detailed mechanism of how Ofd1 works. To investigate whether Ofd1 binds directly to microtubules, it would be interesting to perform a microtubule binding assay with *in vitro* translated Ofd1. Finding other interacting proteins would also give insight into mechanism, as so far only one interactor, Lebercilin, is known (Coene et al., 2009). Purification of Ofd1 complexes followed by mass spectrometry would be an unbiased approach to identify new interactors.

Another open question is the role of phosphorylation in Ofd1 function. Mass spectrometry studies identified phosphorylation, possibly cell cycle related, at three different residues in Ofd1: serines 173, 672, and 689 (Dephoure et al., 2008; Sui et al., 2008). Ofd1 localization at the centrosome diminishes during mitosis; perhaps phosphorylation is important in controlling centriolar localization. Further analysis of Ofd1 localization, centriole length, and ciliogenesis needs to be carried out on the Floxin cell lines carrying phospho-dead and phospho-mimetic substitutions at these residues.

Conclusion

Centrioles have long fascinated scientists because of their extremely complex but ordered pattern. Yet, the components, biogenesis and function of centrioles remained mysterious until recently because of the technical challenges inherent in working with these tiny organelles. When I began graduate school, centriole composition and regulation of biogenesis was mostly a black box, with few structural or regulatory components known. Much more was known about the pericentriolar matrix, especially in

regards to mitotic spindle organization, which was seen as the main function of the centrosome. In the past seven years, proteomic and genetic studies have finally allowed us to peek inside the microtubule barrels that had been recalcitrant to investigation for so long, giving us a new understanding of the how, what and why of the centriole.

The picture that is coming into focus reveals that the idea of "THE centriole" is an incorrect conception of the true nature of this organelle. Centrioles are dynamic, changing in composition and function over time as they progress from procentriole, to daughter, to mother. Some components, such as α-tubulin, are a stable part of all centrioles. Other proteins are only found in a particular type of centriole, for example the distal appendage protein Cep164 on mother centrioles. Still other proteins are required for centriole formation, but have only a transient association with the centrioles themselves, such as Sas-6. Changes in function accompany changes in centriole composition. Each type of centriole has very different microtubule organizing abilities, with the mother capable of anchoring cytoplasmic microtubules and nucleating a cilium.

It is this centriole-cilium connection that we share with our humblest unicellular relatives, that has persisted throughout evolutionary time. Conservation of *Ofd1* suggests that Ofd1 is part of an ancient mechanism for regulating centriole structure and length and reveals the importance of centriole length control in centrosome function.

EXPERIMENTAL PROCEDURES

Cell Lines and Cell Culture

Ofd1^{Gt} (RRF427) E14 ES cell line was obtained from BayGenomics. *Ofd1*^{Rev}, *Ofd1*^{Ofd1myc}, and cell lines with human mutations were created as described previously (Singla et al.,

2009). Official allele names are listed in Table 4. Cells were cultured on 0.1% gelatin in GMEM supplemented with 10% FBS, glutamine, pyruvate, NEAA, βME, and LIF. 3T3 (ATCC) and POC1-GFP U2OS (gift of Dr. Wallace Marshall) cells were cultured in DMEM supplemented with 10% FBS and antibiotics. IMCD3 (ATCC) and hTERT-RPE1 (gift of Dr. Wallace Marshall) were cultured in DMEM:F12 supplemented with 10% FBS and antibiotics.

cDNA constructs and cloning

Ofd1 cDNA was cloned as described previously (Singla et al., 2009). Missense mutations were created using Quik Change II XL site directed mutagenesis kit (Stratagene). Final products were confirmed by sequencing.

Creation of Floxin cell lines

Missense mutations S75F and A80T occur in exon 1 of Ofd1, while G139S occurs in exon 3. The gene trap insertion in $Ofd1^{Gt}$ cells is in intron 3 of the *Ofd1* genomic locus. Full length cDNA for Ofd1-Myc-S75F, Ofd1-Myc-A80T, and Ofd1-Myc-G139S, alleles in which the mutation occurs in exons upstream of the gene trap insertion site, was cloned into the vector pFloxin-IRES (Genbank EU916835). Missense mutations S437R and KDD359-361FSY occur in exons downstream of the gene trap insertion site. cDNA for exons 4-23 of Ofd1-Myc-S437R and Ofd1-Myc-KDD359-361FSY was cloned into the vector pFloxin (Genbank EU916834). pFloxin and pFloxin-IRES constructs were electroporated into $Ofd1^{Rev}$ cells as previously described. Cells were selected with 300

μg/mL G418 (Invitrogen) and colonies were transferred to 48 well plates after 6 days. Correct integration was verified by genomic PCR.

Antibodies

Antibodies to Ofd1 were generated by Covance, Inc. Rabbits were immunized with the peptide [H]-CDTYDQKLKTELLKYQLELKDDYI–[NH2] corresponding to amino acids 340-362 of murine Ofd1. Antibody was used at 1:5000 for Western blotting and for immunofluorescence, 1:2000 in murine cells, 1:1000 in human cells. Acetylated tubulin antibody (Sigma T6793) was used at 1:1000, γ–Tubulin (Santa Cruz sc-7396) 1:200, γ–Tubulin (Abcam ab11316) 1:500, Kif3A (Sigma K3515) 1:200, Centrin (Abcam ab11257) 1:200, alpha Tubulin (Sigma T9026) 1:1000, Pericentrin (Covance PRB-432C) 1:500, Myc (Novus Biologicals NB600-335) 1:200 for IF and 3 μg for IP, GFP (Roche 11814460001) 1:250, Sas-6 (Santa Cruz sc-81431) 1:300 for IF, 1:200 for western. Rabbit anti-Ift88 (gift of Dr. Bradley Yoder) was used at 1:5000 for Western and 1:500 for IF, rabbit anti-Ift20 (gift of Dr. Gregory Pazour) 1:1000, rabbit anti-Ift80 (gift of Dr. Suzanne Nix) 1:200, rabbit anti-Rootletin (Root6, gift of Dr. Tiansen Li) 1:5000, rabbit anti-Ninein (gift of Dr. James Sillibourne) 1:20000, rabbit anti-Odf2 (gift of Dr. Sachiko Tsukita) 1:200, rabbit anti-Centrobin (gift of Dr. Qingsen Gao) 1:750, rabbit anti-Poc5 (gift of Dr. Juliette Azimzadeh) 1:500, rabbit anti-Cep164 (gift of Dr. Erich Nigg) 1:5000 for Western and 1:1000 for IF, rabbit anti-CP110 or Cep97 (gifts of Dr. Brian Dynlacht) at 1:500 and 1:200, respectively. Rabbit anti-p150 (gift of Dr. Erika Holzbauer) 1:100, rabbit anti-Cep290 (gift of Dr. Chengchao Shou) 1:500, Mouse anti-polyglutamylated tubulin (GT335) (gift of Dr. Carsten Janke) 1:500 or 1:3000. Secondary antibodies

donkey anti- mouse, rabbit, or goat conjugated with Alexa Fluor 488 or 555 (Invitrogen) or Cy5 (Jackson Labs), or bovine anti-goat FITC (Jackson Labs), were used at 1:400. Secondary antibodies donkey anti-mouse, rabbit, or goat biotin (Jackson Labs), and streptavidin 488, 555 (Invitrogen) or Cy5 (Jackson Labs) were used at 1:300.

Immunofluorescence and Microscopy

For ES cell ciliation studies: ES cells were plated on coverslips coated with 1% matrigel (BD) and treated with 0.5 mM mimosine (Sigma) overnight to arrest cells. Cells were fixed 5' in 4% PFA, washed in PBS, and fixed 2-3' in -20° 100% methanol. The cells were washed in PBS with 0.1% Triton-X100 (PBST), blocked in 2% BSA in PBST, and incubated with primary antibodies in block for 1 hr at RT. The cells were washed in PBST, incubated with secondary antibodies in block for 30' at RT, and mounted with Vectashield hardset with DAPI (Vector labs).

POC1-GFP U2OS S-phase arrest: Cells were plated on coverslips and treated with 3.2 μg/mL aphidocolin (Sigma) for 72 hr, then fixed in 100% methanol and washed and processed as above.

For cell synchronization studies: Cells were synchronized using thymidine-mimosine block(Fujii-Yamamoto et al., 2005). Briefly, cells were plated on coated coverslips in 2.5 mM thymidine, incubated for 12 hr, released into regular media for 6 hr, then blocked in 0.5 mM mimosine for 6 hr. Timepoints were taken after release from mimosine block. Cells for FACS were collected as described below. For IF, cells were fixed in 100% methanol, then washed and processed as above.

For all other experiments, cells were plated on coverslips and fixed in 100% methanol, then washed and processed as above.

Slides were viewed on a Deltavision microscope (Applied Precision) and image processing was completed with Deltavision and Metamorph (Molecular Devices) software. Images are maximum projections of Z-stacks.

Immunoblots, Cell Fractionation and Quantification

Cells were grown in flasks, trypsinized, collected, and washed once in PBS. Cell pellets were lysed in buffer (50 mM Tris-HCl, pH 7.4, 150 mM NaCl, 1 mM EDTA, 1:200 dilution protease inhibitor cocktail (Calbiochem)) containing 1% NP-40, 1%Triton-X-100, 0.25% sodium deoxycholate, or 1%NP-40 and 0.25% sodium deoxycholate (modified RIPA) for 30 minutes at 4 degrees. Lysates were centrifuged for 15 minutes, 16,000 rcf, at 4 degrees. Cleared supernatants were transferred to a new tube and 6X reducing sample buffer was added to the pellet.

For cell fractionation, 2E6 cells were collected and fractionated using the NE-PER kit (Pierce) according to manufacturer's protocol.

Ofd1 protein expression was quantified by densitometry and normalized to actin.

Immunoprecipitations

Cells were grown in flasks, trypsinized, collected, and washed once in PBS. Cell pellets were lysed in modified RIPA buffer for 30 minutes at 4 degrees. Lysates were centrifuged for 15 minutes, 16,000 rcf, at 4 degrees. Protein concentration of the cleared supernatant was determined by Bradford assay. Supernatants were standardized to 1.6

mg/ mL concentration, 3 mg total protein, and pre-cleared with protein G agarose beads (Invitrogen) for 2 hours. Beads were removed and supernatants were incubated overnight with 1.6 μg Ofd1 antibody. Next day, complexes were captured with protein G beads for 1 hr. Beads were washed 4 times with modified RIPA and proteins eluted with 6X reducing sample buffer.

Population Doubling Studies, FACS, and Microtubule Regrowth Assays

Population doubling: Cell lines were grown in T25 flasks, counted and replated every 3 days.

FACS: Cells from a confluent T75 flask were collected and stained with propidium iodide. Samples were analyzed on a BD FACsort (Beckton Dickinson), 40,000 events collected per sample. FlowJo software (TreeStar) was used to perform cell cycle analysis.

Microtubule regrowth assays: Cells were plated on coated coverslips and treated with 1 μM nocodazole for 1 hr in culture to depolymerize microtubules. Cells were fixed with 100% methanol at 0", 30", 1', 2', 10', and 15' after nocodazole washout, and processed for IF as described above.

Electron Microscopy

Cells were plated on 8 well Permanox slides (Nunc), fixed in 3% glutaraldehyde in 0.1M phosphate buffer (PB) for 30' at room temperature, then washed 3 times in 0.1M PB. Cells were postfixed in 2% osmium for 2 hr, dehydrated and embedded in Araldite (Durcupan, Fluka). Serial ultrathin sections (70nm) were cut with a diamond knife, stained with lead citrate and examined under a FEI Tecnai Spirit electron microscope.

Percent of *Ofd1*^{Gt} cells with long centrioles was determined using information from centrioles in both longitudinal and transverse sections. Quantitative centriole length measurements were performed on longitudinal sections only using ImageTool software.

Centriole Dynamics and Cell Cycle Studies

Cells were plated on coated coverslips, then treated with 10 μg/mL nocodazole for 1 hr in culture, or 0.5 mM mimosine, 3.2 μg/ mL aphidocolin, or 2 μM camptothecin (Sigma) overnight. Cells were fixed in 100% methanol and processed for IF as described above.

siRNA transfections

hTERT-RPE1 cells were plated at 2E4 cells/ well on glass coverslips in a 24 well plate. Next day, wells were changed to 0.5 mL Opti-MEM (Invitrogen) and transfected with siRNA against GL2, Cep164, or Odf2 using HiPerfect transfection reagent (Qiagen) with the following conditions: 3 μL siRNA (stock is 20 μM), 3 μL HiPerfect, 100 μL Opti-MEM per well. Two days later, wells were changed to DMEM/F12 media, no serum, 1 mL per well. After another two days, cells were fixed with 100% methanol and processed for immunofluorescence as described above.

siRNAs were generated by Qiagen against the following target DNA sequences:

GL2: AACGTACGCGGAATACTTCGA

Cep164: CAGGTGACATTTACTATTTCA

Odf2: AGACTAATGGAGCAACAAG

Statistics

All error bars represent one standard deviation. For immunofluorescence quantifications, at least 200 cells were counted on each of duplicate coverslips in at least two separate experiments. Student's unpaired t-test was used to determine statistical significance with a p value of less than 0.05.

ACKNOWLEDGEMENTS

The authors thank Wallace Marshall and Elizabeth Blackburn for use of Deltavision microscopes, Lani Keller, Juliette Azimzadeh, Hiroaki Ishikawa and the members of the Reiter lab for critical discussions and reading of this manuscript. We also thank the centrosome and cilia communities for generously sharing antibodies. This work was funded by grants from the National Science Foundation (V.S.), NIH (RO1AR054396), CIRM (RN2-00919), the Burroughs Wellcome Fund, the Packard Foundation, the Leona M. and Harry B. Helmsley Charitable Trust, and the Sandler Family Supporting Foundation (J.F.R.).

AUTHOR CONTRIBUTIONS

V.S. and J.R. conceived and designed the experiments. V.S., M.R.R., and J.M.G.V. performed the experiments. V.S. and J.R. wrote the paper.

REFERENCES

Anderson, R.G. (1972). The three-dimensional structure of the basal body from the rhesus monkey oviduct. J Cell Biol *54*, 246-265.

Azimzadeh, J., and Bornens, M. (2007). Structure and duplication of the centrosome. J Cell Sci *120*, 2139-2142.

Azimzadeh, J., Hergert, P., Delouvee, A., Euteneuer, U., Formstecher, E., Khodjakov, A., and Bornens, M. (2009). hPOC5 is a centrin-binding protein required for assembly of full-length centrioles. J Cell Biol *185*, 101-114.

Badano, J.L., Mitsuma, N., Beales, P.L., and Katsanis, N. (2006). The ciliopathies: an emerging class of human genetic disorders. Annu Rev Genomics Hum Genet *7*, 125-148.

Badano, J.L., Teslovich, T.M., and Katsanis, N. (2005). The centrosome in human genetic disease. Nat Rev Genet *6*, 194-205.

Bahe, S., Stierhof, Y.D., Wilkinson, C.J., Leiss, F., and Nigg, E.A. (2005). Rootletin forms centriole-associated filaments and functions in centrosome cohesion. J Cell Biol *171*, 27-33.

Basto, R., Lau, J., Vinogradova, T., Gardiol, A., Woods, C.G., Khodjakov, A., and Raff, J.W. (2006). Flies without centrioles. Cell *125*, 1375-1386.

Benton, R., Sachse, S., Michnick, S.W., and Vosshall, L.B. (2006). Atypical membrane topology and heteromeric function of Drosophila odorant receptors in vivo. PLoS Biol *4*, e20.

Bettencourt-Dias, M., and Glover, D.M. (2009). SnapShot: centriole biogenesis. Cell *136*, 188-188 e181.

Bisceglia, M., Galliani, C.A., Senger, C., Stallone, C., and Sessa, A. (2006). Renal cystic diseases: a review. Adv Anat Pathol *13*, 26-56.

Bobinnec, Y., Khodjakov, A., Mir, L.M., Rieder, C.L., Edde, B., and Bornens, M. (1998). Centriole disassembly in vivo and its effect on centrosome structure and function in vertebrate cells. J Cell Biol *143*, 1575-1589.

Bornens, M. (2002). Centrosome composition and microtubule anchoring mechanisms. Curr Opin Cell Biol *14*, 25-34.

Bornens, M., and Azimzadeh, J. (2007). Origin and evolution of the centrosome. Adv Exp Med Biol *607*, 119-129.

Budny, B., Chen, W., Omran, H., Fliegauf, M., Tzschach, A., Wisniewska, M., Jensen, L.R., Raynaud, M., Shoichet, S.A., Badura, M.*, et al.* (2006). A novel X-linked recessive mental retardation syndrome comprising macrocephaly and ciliary dysfunction is allelic to oral-facial-digital type I syndrome. Hum Genet *120*, 171-178.

Cardenas-Rodriguez, M., and Badano, J.L. (2009). Ciliary biology: understanding the cellular and genetic basis of human ciliopathies. Am J Med Genet C Semin Med Genet *151C*, 263-280.

Chen, Z., Indjeian, V.B., McManus, M., Wang, L., and Dynlacht, B.D. (2002). CP110, a cell cycle-dependent CDK substrate, regulates centrosome duplication in human cells. Dev Cell *3*, 339-350.

Chretien, D., Buendia, B., Fuller, S.D., and Karsenti, E. (1997). Reconstruction of the centrosome cycle from cryoelectron micrographs. J Struct Biol *120*, 117-133.

Christensen, S.T., Pedersen, L.B., Schneider, L., and Satir, P. (2007). Sensory cilia and integration of signal transduction in human health and disease. Traffic *8*, 97-109.

Coene, K.L., Roepman, R., Doherty, D., Afroze, B., Kroes, H.Y., Letteboer, S.J., Ngu, L.H., Budny, B., van Wijk, E., Gorden, N.T.*, et al.* (2009). OFD1 is mutated in X-linked

Joubert syndrome and interacts with LCA5-encoded lebercilin. Am J Hum Genet *85*, 465-481.

Corbit, K.C., Shyer, A.E., Dowdle, W.E., Gaulden, J., Singla, V., Chen, M.H., Chuang, P.T., and Reiter, J.F. (2008). Kif3a constrains beta-catenin-dependent Wnt signalling through dual ciliary and non-ciliary mechanisms. Nat Cell Biol *10*, 70-76.

Cox, J., Jackson, A.P., Bond, J., and Woods, C.G. (2006). What primary microcephaly can tell us about brain growth. Trends Mol Med *12*, 358-366.

de Conciliis, L., Marchitiello, A., Wapenaar, M.C., Borsani, G., Giglio, S., Mariani, M., Consalez, G.G., Zuffardi, O., Franco, B., Ballabio, A.*, et al.* (1998). Characterization of Cxorf5 (71-7A), a novel human cDNA mapping to Xp22 and encoding a protein containing coiled-coil alpha-helical domains. Genomics *51*, 243-250.

Deane, J.A., Cole, D.G., Seeley, E.S., Diener, D.R., and Rosenbaum, J.L. (2001). Localization of intraflagellar transport protein IFT52 identifies basal body transitional fibers as the docking site for IFT particles. Curr Biol *11*, 1586-1590.

Delgehyr, N., Sillibourne, J., and Bornens, M. (2005). Microtubule nucleation and anchoring at the centrosome are independent processes linked by ninein function. J Cell Sci *118*, 1565-1575.

Dephoure, N., Zhou, C., Villen, J., Beausoleil, S.A., Bakalarski, C.E., Elledge, S.J., and Gygi, S.P. (2008). A quantitative atlas of mitotic phosphorylation. Proc Natl Acad Sci U S A *105*, 10762-10767.

Emes, R.D., and Ponting, C.P. (2001). A new sequence motif linking lissencephaly, Treacher Collins and oral-facial-digital type 1 syndromes, microtubule dynamics and cell migration. Hum Mol Genet *10*, 2813-2820.

Feather, S.A., Winyard, P.J., Dodd, S., and Woolf, A.S. (1997). Oral-facial-digital syndrome type 1 is another dominant polycystic kidney disease: clinical, radiological and histopathological features of a new kindred. Nephrol Dial Transplant *12*, 1354-1361.

Ferrante, M.I., Giorgio, G., Feather, S.A., Bulfone, A., Wright, V., Ghiani, M., Selicorni, A., Gammaro, L., Scolari, F., Woolf, A.S.*, et al.* (2001). Identification of the gene for oral-facial-digital type I syndrome. Am J Hum Genet *68*, 569-576.

Ferrante, M.I., Romio, L., Castro, S., Collins, J.E., Goulding, D.A., Stemple, D.L., Woolf, A.S., and Wilson, S.W. (2009). Convergent extension movements and ciliary function are mediated by ofd1, a zebrafish orthologue of the human oral-facial-digital type 1 syndrome gene. Hum Mol Genet *18*, 289-303.

Ferrante, M.I., Zullo, A., Barra, A., Bimonte, S., Messaddeq, N., Studer, M., Dolle, P., and Franco, B. (2006). Oral-facial-digital type I protein is required for primary cilia formation and left-right axis specification. Nat Genet *38*, 112-117.

Follit, J.A., Tuft, R.A., Fogarty, K.E., and Pazour, G.J. (2006). The intraflagellar transport protein IFT20 is associated with the Golgi complex and is required for cilia assembly. Mol Biol Cell *17*, 3781-3792.

Fujii-Yamamoto, H., Kim, J.M., Arai, K., and Masai, H. (2005). Cell cycle and developmental regulations of replication factors in mouse embryonic stem cells. J Biol Chem *280*, 12976-12987.

Gerlitz, G., Darhin, E., Giorgio, G., Franco, B., and Reiner, O. (2005). Novel functional features of the Lis-H domain: role in protein dimerization, half-life and cellular localization. Cell Cycle *4*, 1632-1640.

Graser, S., Stierhof, Y.D., Lavoie, S.B., Gassner, O.S., Lamla, S., Le Clech, M., and Nigg, E.A. (2007). Cep164, a novel centriole appendage protein required for primary cilium formation. J Cell Biol *179*, 321-330.

Habedanck, R., Stierhof, Y.D., Wilkinson, C.J., and Nigg, E.A. (2005). The Polo kinase Plk4 functions in centriole duplication. Nat Cell Biol *7*, 1140-1146.

Haycraft, C.J., Zhang, Q., Song, B., Jackson, W.S., Detloff, P.J., Serra, R., and Yoder, B.K. (2007). Intraflagellar transport is essential for endochondral bone formation. Development *134*, 307-316.

Higginbotham, H.R., and Gleeson, J.G. (2007). The centrosome in neuronal development. Trends Neurosci *30*, 276-283.

Huangfu, D., Liu, A., Rakeman, A.S., Murcia, N.S., Niswander, L., and Anderson, K.V. (2003). Hedgehog signalling in the mouse requires intraflagellar transport proteins. Nature *426*, 83-87.

Hunkapiller, J., Singla, V., Seol, A.D., and Reiter, J.F. (2010). The ciliogenic protein Ofd1 restrains embryonic stem cell differentiation into neurons. (in preparation)

Ishikawa, H., Kubo, A., Tsukita, S., and Tsukita, S. (2005). Odf2-deficient mother centrioles lack distal/subdistal appendages and the ability to generate primary cilia. Nat Cell Biol *7*, 517-524.

Jurczyk, A., Gromley, A., Redick, S., San Agustin, J., Witman, G., Pazour, G.J., Peters, D.J., and Doxsey, S. (2004). Pericentrin forms a complex with intraflagellar transport proteins and polycystin-2 and is required for primary cilia assembly. J Cell Biol *166*, 637-643.

Keller, L.C., Geimer, S., Romijn, E., Yates, J., 3rd, Zamora, I., and Marshall, W.F. (2008). Molecular Architecture of the Centriole Proteome: The Conserved WD40 Domain Protein POC1 Is Required for Centriole Duplication and Length Control. Mol Biol Cell.

Keller, L.C., Romijn, E.P., Zamora, I., Yates, J.R., 3rd, and Marshall, W.F. (2005). Proteomic analysis of isolated chlamydomonas centrioles reveals orthologs of ciliary-disease genes. Curr Biol *15*, 1090-1098.

Kim, J., Krishnaswami, S.R., and Gleeson, J.G. (2008). CEP290 interacts with the centriolar satellite component PCM-1 and is required for Rab8 localization to the primary cilium. Hum Mol Genet *17*, 3796-3805.

Kleylein-Sohn, J., Westendorf, J., Le Clech, M., Habedanck, R., Stierhof, Y.D., and Nigg, E.A. (2007). Plk4-induced centriole biogenesis in human cells. Dev Cell *13*, 190-202.

Kochanski, R.S., and Borisy, G.G. (1990). Mode of centriole duplication and distribution. J Cell Biol *110*, 1599-1605.

Kohlmaier, G., Loncarek, J., Meng, X., McEwen, B.F., Mogensen, M.M., Spektor, A., Dynlacht, B.D., Khodjakov, A., and Gonczy, P. (2009). Overly long centrioles and defective cell division upon excess of the SAS-4-related protein CPAP. Curr Biol *19*, 1012-1018.

Kozminski, K.G., Beech, P.L., and Rosenbaum, J.L. (1995). The Chlamydomonas kinesin-like protein FLA10 is involved in motility associated with the flagellar membrane. J Cell Biol *131*, 1517-1527.

Loktev, A.V., Zhang, Q., Beck, J.S., Searby, C.C., Scheetz, T.E., Bazan, J.F., Slusarski, D.C., Sheffield, V.C., Jackson, P.K., and Nachury, M.V. (2008). A BBSome subunit links ciliogenesis, microtubule stability, and acetylation. Dev Cell *15*, 854-865.

Lucker, B.F., Behal, R.H., Qin, H., Siron, L.C., Taggart, W.D., Rosenbaum, J.L., and Cole, D.G. (2005). Characterization of the intraflagellar transport complex B core: direct interaction of the IFT81 and IFT74/72 subunits. J Biol Chem *280*, 27688-27696.

Lum, L., and Beachy, P.A. (2004). The Hedgehog response network: sensors, switches, and routers. Science *304*, 1755-1759.

Macca, M., and Franco, B. (2009). The molecular basis of oral-facial-digital syndrome, type 1. Am J Med Genet C Semin Med Genet *151C*, 318-325.

Marshall, W.F. (2009). Centriole evolution. Curr Opin Cell Biol *21*, 14-19.

Marszalek, J.R., Liu, X., Roberts, E.A., Chui, D., Marth, J.D., Williams, D.S., and Goldstein, L.S. (2000). Genetic evidence for selective transport of opsin and arrestin by kinesin-II in mammalian photoreceptors. Cell *102*, 175-187.

Mikule, K., Delaval, B., Kaldis, P., Jurcyzk, A., Hergert, P., and Doxsey, S. (2007). Loss of centrosome integrity induces p38-p53-p21-dependent G1-S arrest. Nat Cell Biol *9*, 160-170.

Mogensen, M.M., Malik, A., Piel, M., Bouckson-Castaing, V., and Bornens, M. (2000). Microtubule minus-end anchorage at centrosomal and non-centrosomal sites: the role of ninein. J Cell Sci *113 (Pt 17)*, 3013-3023.

Morisawa, T., Yagi, M., Surono, A., Yokoyama, N., Ohmori, M., Terashi, H., and Matsuo, M. (2004). Novel double-deletion mutations of the OFD1 gene creating multiple novel transcripts. Hum Genet *115*, 97-103.

Moudjou, M., Bordes, N., Paintrand, M., and Bornens, M. (1996). gamma-Tubulin in mammalian cells: the centrosomal and the cytosolic forms. J Cell Sci *109 (Pt 4)*, 875-887.

Nakagawa, Y., Yamane, Y., Okanoue, T., Tsukita, S., and Tsukita, S. (2001). Outer dense fiber 2 is a widespread centrosome scaffold component preferentially associated with mother centrioles: its identification from isolated centrosomes. Mol Biol Cell *12*, 1687-1697.

Nauli, S.M., Alenghat, F.J., Luo, Y., Williams, E., Vassilev, P., Li, X., Elia, A.E., Lu, W., Brown, E.M., Quinn, S.J.*, et al.* (2003). Polycystins 1 and 2 mediate mechanosensation in the primary cilium of kidney cells. Nat Genet *33*, 129-137.

Nigg, E.A., and Raff, J.W. (2009). Centrioles, centrosomes, and cilia in health and disease. Cell *139*, 663-678.

Nigg, E.A.e. (2004). Centrosomes in Development and Disease (Wiley-VCH).

Nonaka, S., Tanaka, Y., Okada, Y., Takeda, S., Harada, A., Kanai, Y., Kido, M., and Hirokawa, N. (1998). Randomization of left-right asymmetry due to loss of nodal cilia generating leftward flow of extraembryonic fluid in mice lacking KIF3B motor protein. Cell *95*, 829-837.

Paintrand, M., Moudjou, M., Delacroix, H., and Bornens, M. (1992). Centrosome organization and centriole architecture: their sensitivity to divalent cations. J Struct Biol *108*, 107-128.

Pan, J., and Snell, W.J. (2003). Kinesin II and regulated intraflagellar transport of Chlamydomonas aurora protein kinase. J Cell Sci *116*, 2179-2186.

Paoletti, A., Moudjou, M., Paintrand, M., Salisbury, J.L., and Bornens, M. (1996). Most of centrin in animal cells is not centrosome-associated and centrosomal centrin is confined to the distal lumen of centrioles. J Cell Sci *109 (Pt 13)*, 3089-3102.

Pazour, G.J., Dickert, B.L., Vucica, Y., Seeley, E.S., Rosenbaum, J.L., Witman, G.B., and Cole, D.G. (2000). Chlamydomonas IFT88 and its mouse homologue, polycystic kidney disease gene tg737, are required for assembly of cilia and flagella. J Cell Biol *151*, 709-718.

Pazour, G.J., Wilkerson, C.G., and Witman, G.B. (1998). A dynein light chain is essential for the retrograde particle movement of intraflagellar transport (IFT). J Cell Biol *141*, 979-992.

Piel, M., Meyer, P., Khodjakov, A., Rieder, C.L., and Bornens, M. (2000). The respective contributions of the mother and daughter centrioles to centrosome activity and behavior in vertebrate cells. J Cell Biol *149*, 317-330.

Prattichizzo, C., Macca, M., Novelli, V., Giorgio, G., Barra, A., and Franco, B. (2008). Mutational spectrum of the oral-facial-digital type I syndrome: a study on a large collection of patients. Hum Mutat *29*, 1237-1246.

Quintyne, N.J., and Schroer, T.A. (2002). Distinct cell cycle-dependent roles for dynactin and dynein at centrosomes. J Cell Biol *159*, 245-254.

Rakkolainen, A., Ala-Mello, S., Kristo, P., Orpana, A., and Jarvela, I. (2002). Four novel mutations in the OFD1 (Cxorf5) gene in Finnish patients with oral-facial-digital syndrome 1. J Med Genet *39*, 292-296.

Romio, L., Fry, A.M., Winyard, P.J., Malcolm, S., Woolf, A.S., and Feather, S.A. (2004). OFD1 is a centrosomal/basal body protein expressed during mesenchymal-epithelial transition in human nephrogenesis. J Am Soc Nephrol *15*, 2556-2568.

Romio, L., Wright, V., Price, K., Winyard, P.J., Donnai, D., Porteous, M.E., Franco, B., Giorgio, G., Malcolm, S., Woolf, A.S.*, et al.* (2003). OFD1, the gene mutated in oral-facial-digital syndrome type 1, is expressed in the metanephros and in human embryonic renal mesenchymal cells. J Am Soc Nephrol *14*, 680-689.

Rosenbaum, J.L., and Witman, G.B. (2002). Intraflagellar transport. Nat Rev Mol Cell Biol *3*, 813-825.

Schmidt, T.I., Kleylein-Sohn, J., Westendorf, J., Le Clech, M., Lavoie, S.B., Stierhof, Y.D., and Nigg, E.A. (2009). Control of centriole length by CPAP and CP110. Curr Biol *19*, 1005-1011.

Schneider, L., Clement, C.A., Teilmann, S.C., Pazour, G.J., Hoffmann, E.K., Satir, P., and Christensen, S.T. (2005). PDGFRalphaalpha signaling is regulated through the primary cilium in fibroblasts. Curr Biol *15*, 1861-1866.

Sharma, N., Berbari, N.F., and Yoder, B.K. (2008). Ciliary dysfunction in developmental abnormalities and diseases. Curr Top Dev Biol *85*, 371-427.

Singla, V., Hunkapiller, J., Santos, N., Seol, A.D., Norman, A.R., Wakenight, P., Skarnes, W.C., and Reiter, J.F. (2009). Floxin, a resource for genetically engineering mouse ESCs. Nature Methods.

Snow, J.J., Ou, G., Gunnarson, A.L., Walker, M.R., Zhou, H.M., Brust-Mascher, I., and Scholey, J.M. (2004). Two anterograde intraflagellar transport motors cooperate to build sensory cilia on C. elegans neurons. Nat Cell Biol *6*, 1109-1113.

Sorokin, S. (1962). Centrioles and the formation of rudimentary cilia by fibroblasts and smooth muscle cells. J Cell Biol *15*, 363-377.

Spektor, A., Tsang, W.Y., Khoo, D., and Dynlacht, B.D. (2007). Cep97 and CP110 suppress a cilia assembly program. Cell *130*, 678-690.

Strnad, P., Leidel, S., Vinogradova, T., Euteneuer, U., Khodjakov, A., and Gonczy, P. (2007). Regulated HsSAS-6 levels ensure formation of a single procentriole per centriole during the centrosome duplication cycle. Dev Cell *13*, 203-213.

Sui, S., Wang, J., Yang, B., Song, L., Zhang, J., Chen, M., Liu, J., Lu, Z., Cai, Y., Chen, S.*, et al.* (2008). Phosphoproteome analysis of the human Chang liver cells using SCX and a complementary mass spectrometric strategy. Proteomics *8*, 2024-2034.

Sun, Q.Y., and Schatten, H. (2007). Centrosome inheritance after fertilization and nuclear transfer in mammals. Adv Exp Med Biol *591*, 58-71.

Tang, C.J., Fu, R.H., Wu, K.S., Hsu, W.B., and Tang, T.K. (2009). CPAP is a cell-cycle regulated protein that controls centriole length. Nat Cell Biol *11*, 825-831.

Thauvin-Robinet, C., Cossee, M., Cormier-Daire, V., Van Maldergem, L., Toutain, A., Alembik, Y., Bieth, E., Layet, V., Parent, P., David, A.*, et al.* (2006). Clinical, molecular, and genotype-phenotype correlation studies from 25 cases of oral-facial-digital syndrome type 1: a French and Belgian collaborative study. J Med Genet *43*, 54-61.

Tsang, W.Y., Bossard, C., Khanna, H., Peranen, J., Swaroop, A., Malhotra, V., and Dynlacht, B.D. (2008). CP110 suppresses primary cilia formation through its interaction with CEP290, a protein deficient in human ciliary disease. Dev Cell *15*, 187-197.

Tsang, W.Y., Spektor, A., Luciano, D.J., Indjeian, V.B., Chen, Z., Salisbury, J.L., Sanchez, I., and Dynlacht, B.D. (2006). CP110 cooperates with two calcium-binding proteins to regulate cytokinesis and genome stability. Mol Biol Cell *17*, 3423-3434.

Vorobjev, I.A., and Chentsov, Y.S. (1980). The ultrastructure of centriole in mammalian tissue culture cells. Cell Biol Int Rep *4*, 1037-1044.

Wang, X., Tsai, J.W., Imai, J.H., Lian, W.N., Vallee, R.B., and Shi, S.H. (2009). Asymmetric centrosome inheritance maintains neural progenitors in the neocortex. Nature *461*, 947-955.

Wong, S.Y., and Reiter, J.F. (2008). The primary cilium at the crossroads of mammalian hedgehog signaling. Curr Top Dev Biol *85*, 225-260.

Wong, S.Y., Seol, A.D., So, P.L., Ermilov, A.N., Bichakjian, C.K., Epstein, E.H., Jr., Dlugosz, A.A., and Reiter, J.F. (2009). Primary cilia can both mediate and suppress Hedgehog pathway-dependent tumorigenesis. Nat Med *15*, 1055-1061.

Woodland, H.R., and Fry, A.M. (2008). Pix proteins and the evolution of centrioles. PLoS ONE *3*, e3778.

Zou, C., Li, J., Bai, Y., Gunning, W.T., Wazer, D.E., Band, V., and Gao, Q. (2005). Centrobin: a novel daughter centriole-associated protein that is required for centriole duplication. J Cell Biol *171*, 437-445.

Figure i. Coordination of the centrosome and cell division cycles.

(**A**) Diagram showing centriole duplication and maturation in coordination with the cell cycle. MC, mother centriole. DC, daughter centriole. (**B**) Diagram depicting the TEM appearance of a mother centriole in transverse and longitudinal views.

Figure i

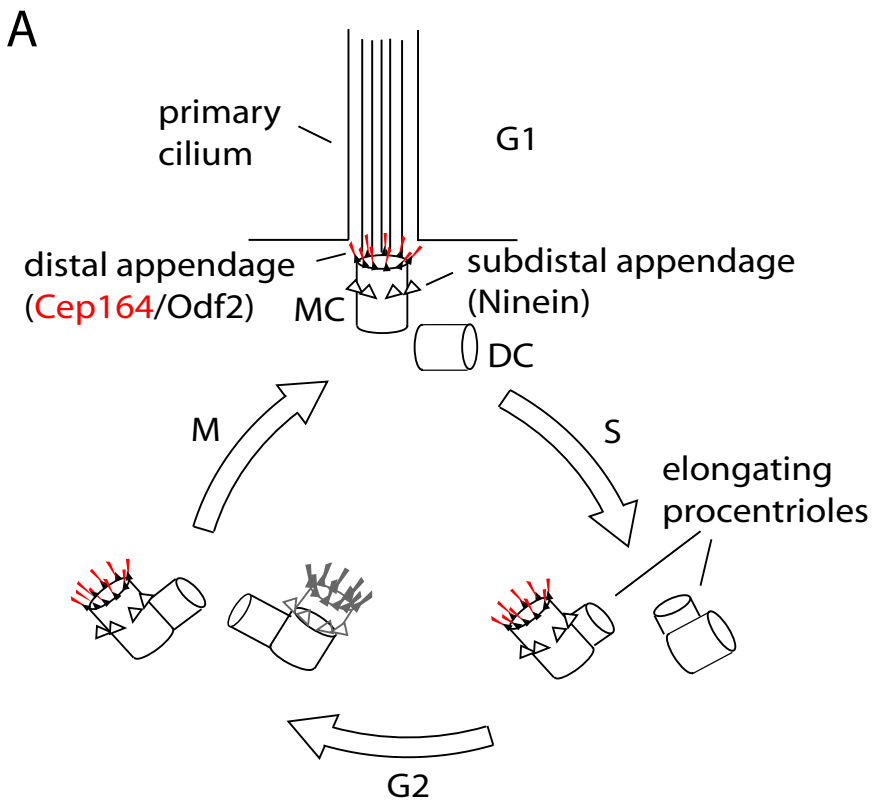
A
primary cilium
G1
distal appendage (Cep164/Odf2)
MC
subdistal appendage (Ninein)
DC
M
S
elongating procentrioles
G2
B
Longitudinal section
Transverse section
distal
distal appendage
subdistal appendage
proximal
distal appendages
subdistal appendages
proximal

Figure ii. Primary cilia are highly structured and are found in many organisms and on many cell types.

(**A**) Electron micrograph of the primary cilium of a canary brain radial glia (Alvarez-Buylla et al., 1998). (**B**) Schematic showing structure of the basal body and primary cilium [modified from (Anderson, 1972; O'Toole et al., 2003)]. (**C**) The green alga *Chlamydomonas* showing flagella (green, arrow) and basal body (red). Nuclei are blue. [(**D**) to (**L**)] Scanning electron and immunohistological images of primary cilia (arrows) of (**D**) the mouse node, (**E**) the mouse neural tube, emanating from basal bodies (red), (**F**) the Xenopus neural tube, (**G**) the zebrafish neural tube, (**H**) a mouse neurogenic astrocyte, (**I**) a mouse embryonic epidermal cell, (**J**) a mouse somite, (**K**) mouse embryonic stem cells, and (**L**) mouse astrocytes expressing glial fibrillary acidic protein (red). Also shown in (H) are motile ependymal cell cilia (arrowhead). Scale bars, 1 μm [(A), (C), and (D)] and 10 μm [(E) to (L)].

Alvarez-Buylla, A., Garcia-Verdugo, J.M., Mateo, A.S., and Merchant-Larios, H. (1998). Primary neural precursors and intermitotic nuclear migration in the ventricular zone of adult canaries. J Neurosci *18*, 1020-1037.

Anderson, R.G. (1972). The three-dimensional structure of the basal body from the rhesus monkey oviduct. J Cell Biol *54*, 246-265.

O'Toole, E.T., Giddings, T.H., McIntosh, J.R., and Dutcher, S.K. (2003). Three-dimensional organization of basal bodies from wild-type and delta-tubulin deletion strains of Chlamydomonas reinhardtii. Mol Biol Cell *14*, 2999-3012.

Figure ii

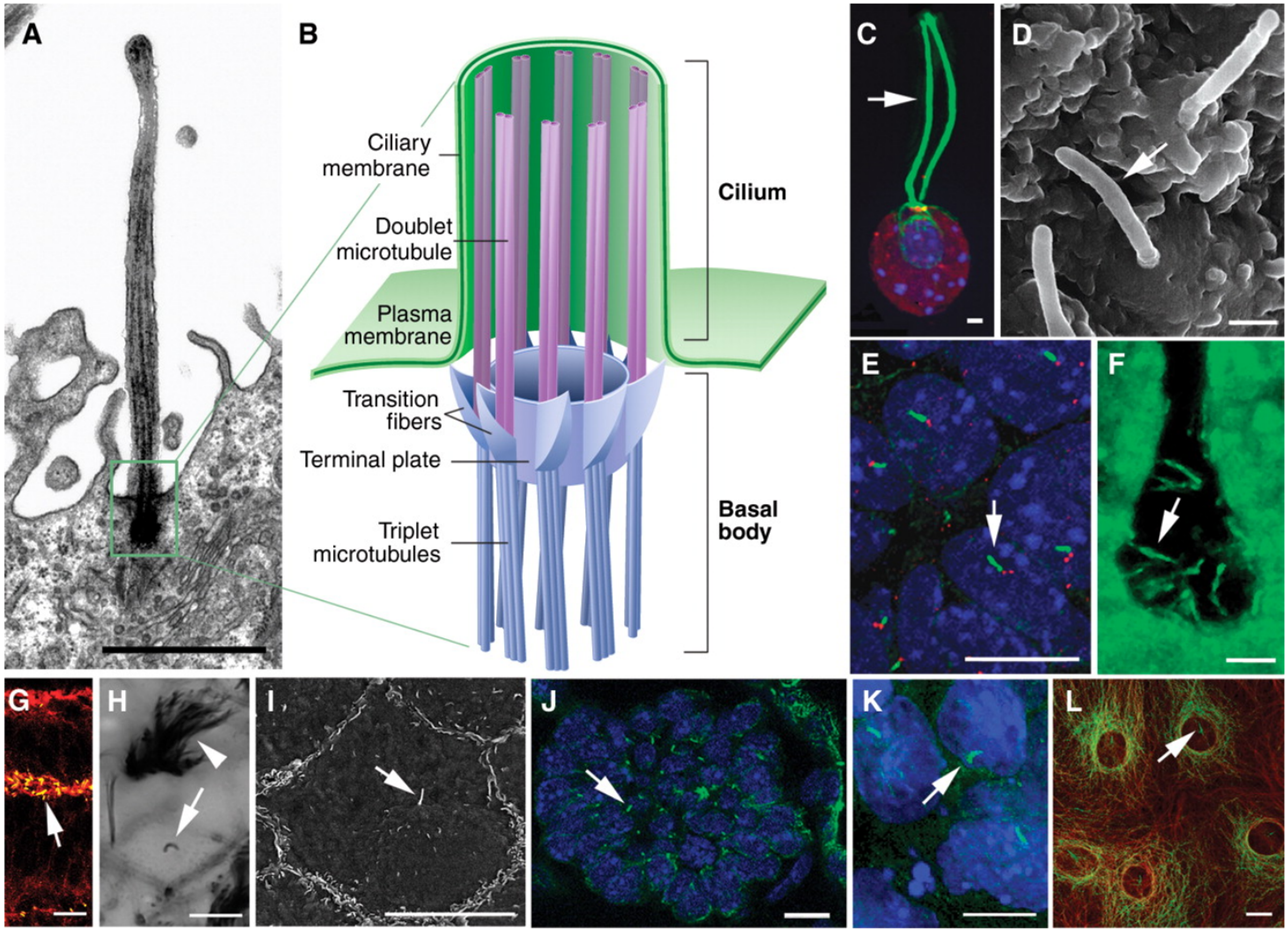
A
B
Ciliary membrane
Doublet microtubule
Plasma membrane
Transition fibers
Terminal plate
Triplet microtubules
Cilium
Basal body
C
D
E
F
G
H
I
J
K
L

Figure 1. Ofd1 is essential for centriole length control.

(**A**) Immunoblot of cell lysate supernatants from wild type (WT) and *Ofd1*^{Gt} cells. 15 μg protein loaded per lane. (**B**) Longitudinal TEM sections of WT and *Ofd1*^{Gt} cell centrioles. Long centrioles (defined as > 600 nm) are seen in 35% of *Ofd1*^{Gt} cells. P, proximal end and D, distal end of centriole. Graph shows centriole length data, collected from 9 WT and 23 *Ofd1*^{Gt} centrioles. Each measured centriole was from a distinct cell. (**C**) Representative fluorescence micrographs of WT and *Ofd1*^{Gt} cells showing centrosomes (Pericentrin and γ-tubulin), centrioles (Centrin and acetylated tubulin), and DNA (DAPI). (**D**) Transverse TEM sections of WT and *Ofd1*^{Gt} cell centrioles. White arrows indicate triplet microtubules. Normal length centrioles are contained within a maximum of 8-10 transverse sections, whereas long centrioles span more than 10 sections. Scale bars indicate 200 nm (TEM), 5 μm, and 1 μm (inset).

Figure 1

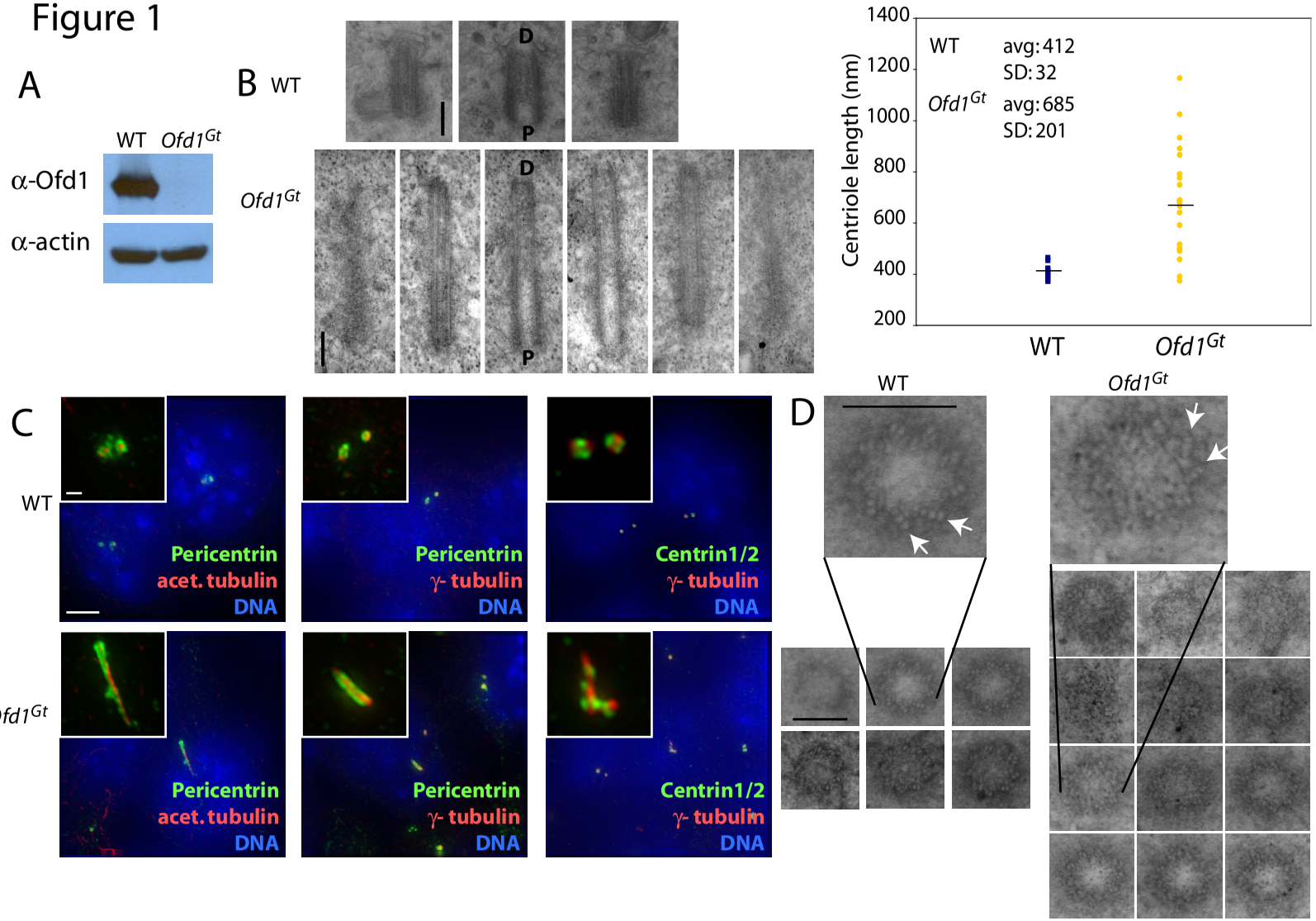
A
WT
Ofd1Gt
α-Ofd1
α-actin
B
WT
Ofd1Gt
D
P
Centriole length (nm)
1400
1200
1000
800
600
400
200
WT
avg: 412
SD: 32
Ofd1Gt
avg: 685
SD: 201
C
WT
Ofd1Gt
Pericentrin
acet. tubulin
DNA
Pericentrin
γ- tubulin
DNA
Centrin1/2
γ- tubulin
DNA
D
WT
Ofd1Gt

Figure 2. Ofd1 localizes to the distal ends of mother, daughter, and procentrioles. (**A-C**) Representative micrographs of WT and *Ofd1*^{Gt} cells showing centrosomes (γ-tubulin), centrioles and cilia (acetylated tubulin), DNA (DAPI), and other indicated antibodies. (**D**) WT cells showing centrosomes (γ-tubulin), Ofd1, and the proximal procentriole (Sas-6). (**E**) *Ofd1*^{Ofd1myc} cells showing centrosomes (γ-tubulin), Myc (Ofd1-Myc), and the distal procentriole (Poc5). Poc5 localizes more strongly to mother or daughter centrioles than to procentrioles. (**F**) *Ofd1*^{Ofd1myc} cells showing centrosomes (γ-tubulin), Myc (Ofd1-Myc), and the distal centriole and procentriole (CP110). (**G**) *Ofd1*^{Ofd1myc} cells showing centrosomes (γ-tubulin), Myc (Ofd1-Myc), and the proximal centriole (Rootletin). (**H**) *Ofd1*^{Ofd1myc} cells showing centrosomes (γ-tubulin), Myc (Ofd1-Myc), and mother centriole subdistal appendages (Ninein). The mother centriole is marked by 3 Ninein foci (2 on the subdistal appendages and one on the proximal end) whereas the daughter centriole is marked by one Ninein focus (on the proximal end). (**I**) *Ofd1*^{Ofd1myc} cells showing centrosomes (γ-tubulin), Myc (Ofd1-Myc), and mother centriole appendages (Odf2). (J) *Ofd1*^{Ofd1myc} cells showing Myc (Ofd1-Myc), mother centriole distal appendages (Cep164), and centrosomes (γ-tubulin). (**K**) - (**L**) Schematics showing *Ofd1*^{Ofd1myc} cells stained for Myc (Ofd1-Myc), mother centriole subdistal (Ninein) or distal (Cep164) appendages, and centrosomes (γ-tubulin). MC, mother centriole. DC, daughter centriole. PC, procentriole. Scale bars (A)-(B) indicate 5 μm and 1 μm (inset), and 1 μm for (C)-(L).

Figure 2, A-F

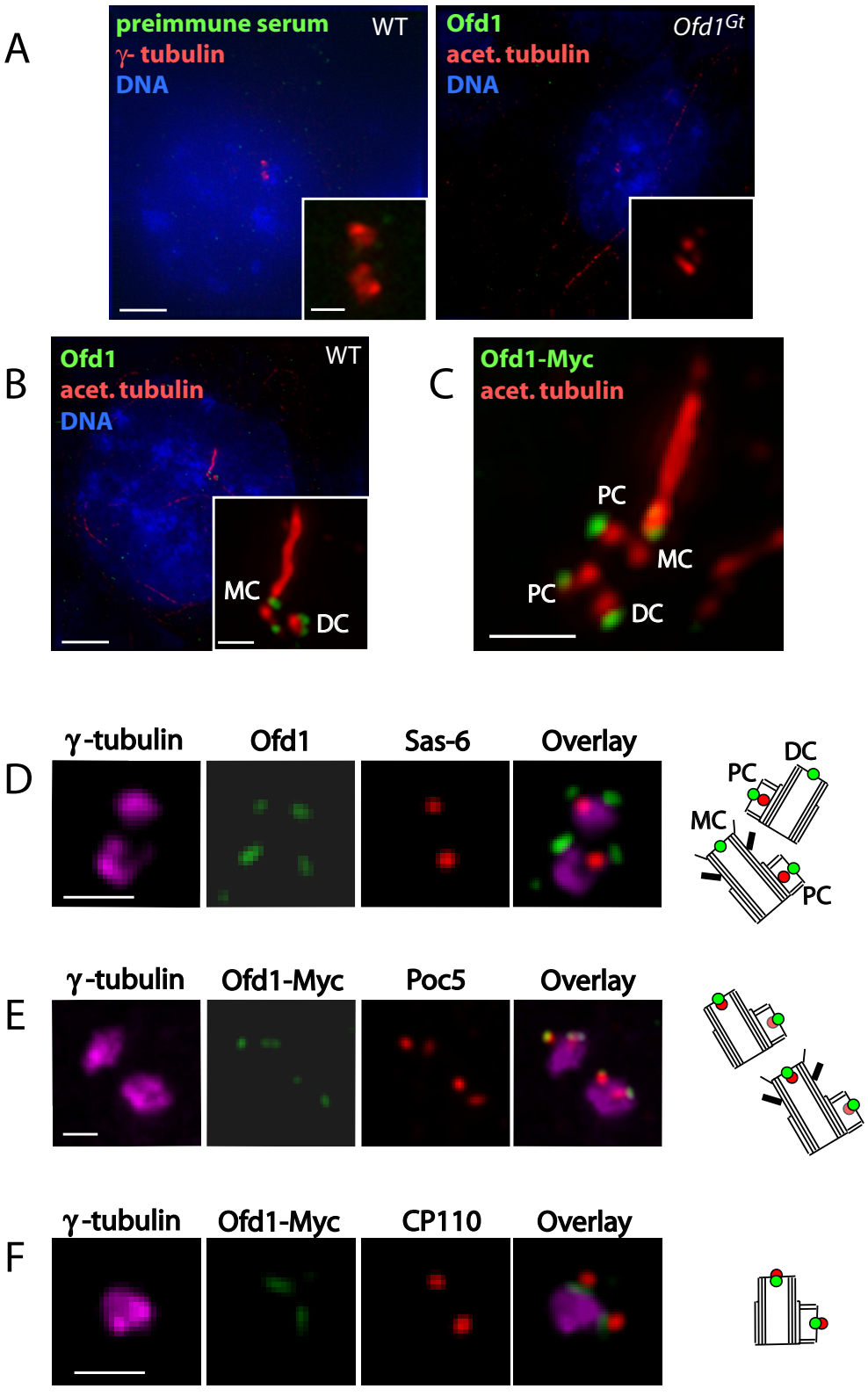
A
preimmune serum
γ- tubulin
DNA
WT
Ofd1
acet. tubulin
DNA
Ofd1Gt
B
Ofd1
acet. tubulin
DNA
WT
MC
DC
C
Ofd1-Myc
acet. tubulin
PC
MC
PC
DC
D
γ-tubulin
Ofd1
Sas-6
Overlay
DC
PC
MC
PC
E
γ-tubulin
Ofd1-Myc
Poc5
Overlay
F
γ-tubulin
Ofd1-Myc
CP110
Overlay

Figure 2, G-L

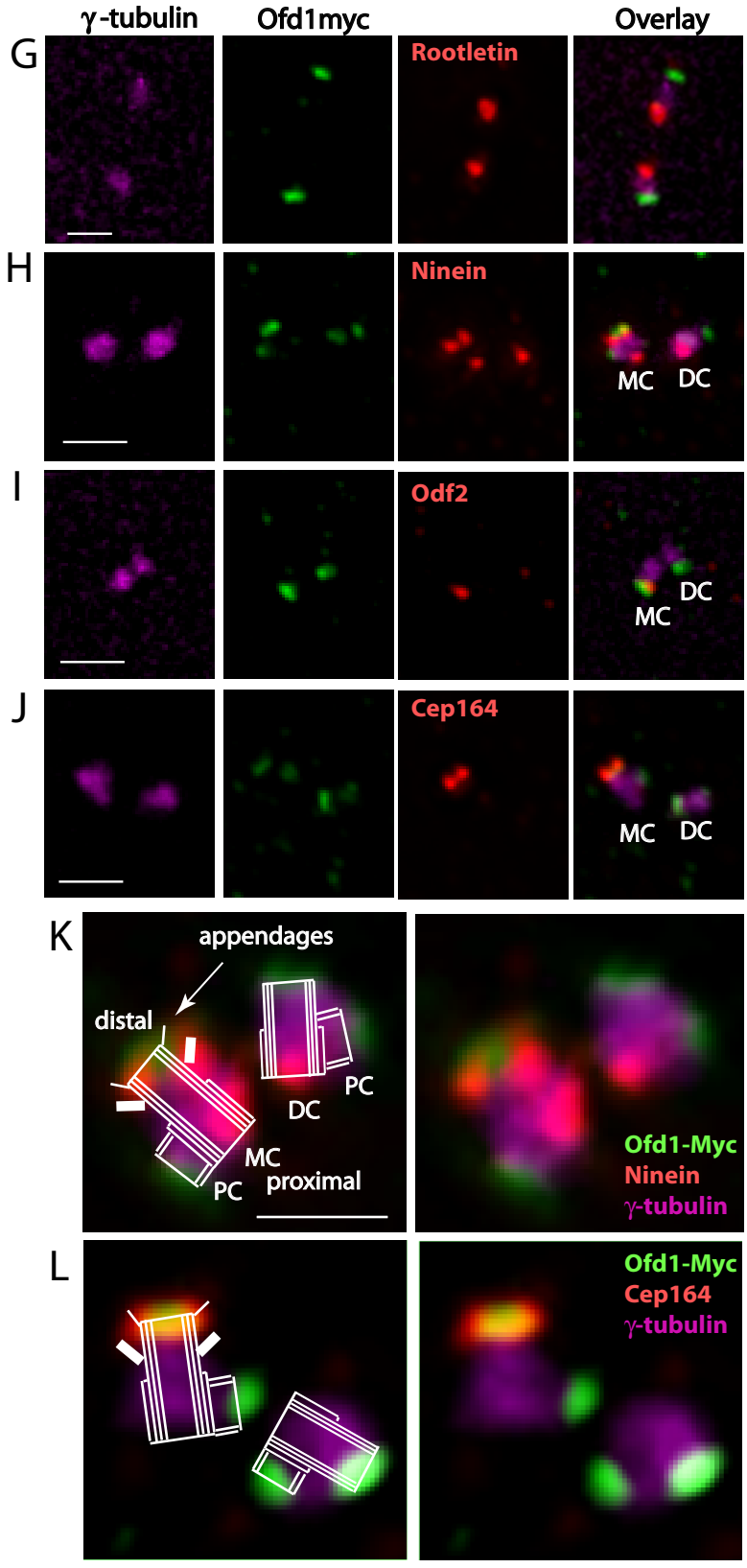
γ-tubulin
Ofd1myc
Overlay
G
Rootletin
H
Ninein
MC
DC
I
Odf2
DC
MC
J
Cep164
MC
DC
K
appendages
distal
PC
DC
MC
PC
proximal
Ofd1-Myc
Ninein
γ-tubulin
L
Ofd1-Myc
Cep164
γ-tubulin

Figure 3. Ofd1 complexes contain centriolar microtubule components and control centriole microtubule stability.

(**A**) Immunoblot showing Ofd1 (detected with an Ofd1 antibody) in cytoplasmic, nuclear, and insoluble fractions of WT or *Ofd1*^{Gt} cell lysate. (**B**) Immunoblot showing Ofd1 (detected with an Ofd1 antibody) in the supernatant (S) and pellet (P) of WT cells lysed with various detergents. (**C**) Immunoblots of Ofd1 complexes immunoprecipitated from WT or *Ofd1*^{Gt} cell supernatant with an Ofd1 antibody. (**D**) Graph indicating percent of long centrioles in WT and *Ofd1*^{Gt} cells. Cells were treated with nocodazole, fixed and stained for α- and γ-tubulin. γ-tubulin foci more than twice as long as they were wide were counted as long centrioles. Because immunofluorescent (IF) microscopy has lower resolution than TEM, a smaller percent of *Ofd1*^{Gt} centrioles appeared long when assessed by IF (6-10% by IF versus 35% by TEM). (**E**) WT and *Ofd1*^{Gt} cells stained for centrosomes (γ-tubulin) and acetylated tubulin. (**F**) WT and *Ofd1*^{Gt} cells stained for centrosomes (γ-tubulin) and polyglutamylated tubulin (GT335). Arrows indicate areas of reduced or absent polyglutamylation. Scale bars indicate 1μm.

Figure 3

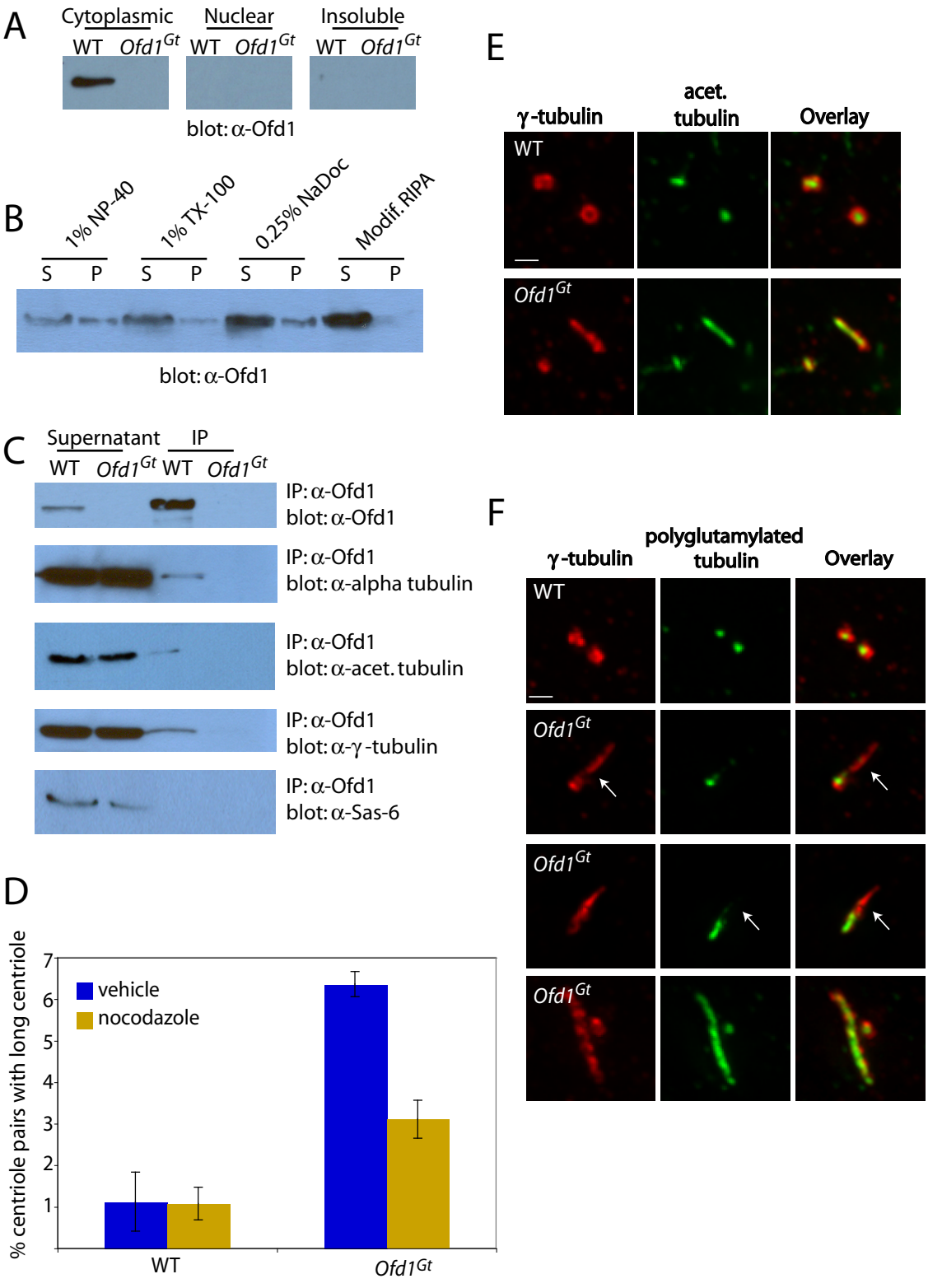
A
Cytoplasmic
Nuclear
Insoluble
WT
Ofd1Gt
blot: α-Ofd1
B
1% NP-40
1% TX-100
0.25% NaDoc
Modif. RIPA
S
P
blot: α-Ofd1
C
Supernatant
IP
IP: α-Ofd1
blot: α-Ofd1
blot: α-alpha tubulin
blot: α-acet. tubulin
blot: α-γ-tubulin
blot: α-Sas-6
D
% centriole pairs with long centriole
vehicle
nocodazole
E
γ-tubulin
acet. tubulin
Overlay
F
polyglutamylated tubulin

Figure 4. Ofd1 restrains growth of the distal domain of both mother and daughter centrioles in G2.

(**A**) Graph indicating the percent of long centrioles in WT and *Ofd1*^{Gt} cells in different cell cycle phases. Asterisks indicate statistically significant differences compared to the asynchronous population ($p < 0.01$). (**B**) The distal centriole (Poc5), centrosomes (γ-tubulin), and DNA (DAPI) of WT and *Ofd1*^{Gt} cells. Poc5 localizes more strongly to mother or daughter centrioles than to procentrioles. PC, procentriole. C, centriole. (**C**) Centriole appendages (Odf2) and centrosomes (γ-tubulin) of WT and *Ofd1*^{Gt} cells. (**D**) Longitudinal and (**E**) transverse TEM sections of a WT and long *Ofd1*^{Gt} centriole. Centriole proximal domain (P), distal domain (D), subdistal appendages (white arrows), procentrioles (black arrows). Arrowheads indicate centrioles in low magnification TEM images. Brown arrows show direction of section sequence. Normal length centrioles are contained within 8-10 sequential transverse sections, whereas long centrioles span more than 10 sections. (**F**) *Ofd1*^{Gt} cells showing centrosomes (Pericentrin and γ-tubulin) and DNA (DAPI). (**G**) Daughter centrioles and procentrioles (Centrobin), centrosomes (γ-tubulin), and DNA (DAPI) of WT and *Ofd1*^{Gt} cells. In S-G2 phase, Centrobin localizes more strongly to the procentrioles than to the daughter centriole. Arrows indicate daughter centrioles. Scale bars indicate 2 μm (TEM, low magnification), 200 nm (TEM, high magnification), 5 μm and 1 μm (inset).

Figure 4, A-C

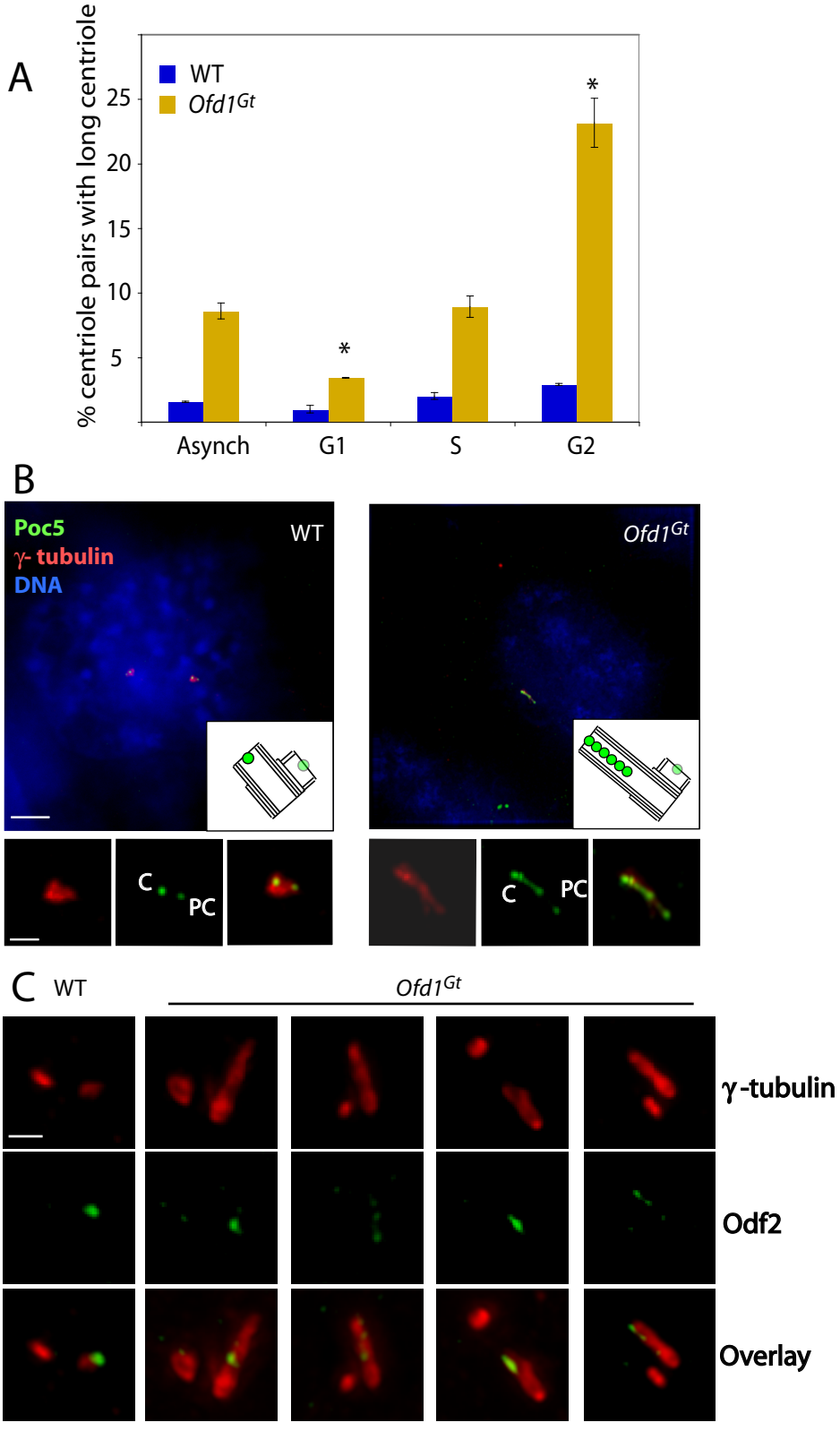
A
% centriole pairs with long centriole
WT
Ofd1Gt
25
20
15
10
5
*
*
Asynch
G1
S
G2
B
Poc5
γ- tubulin
DNA
WT
Ofd1Gt
C
PC
C
PC
C WT
Ofd1Gt
γ-tubulin
Odf2
Overlay

Figure 4, D-G

D

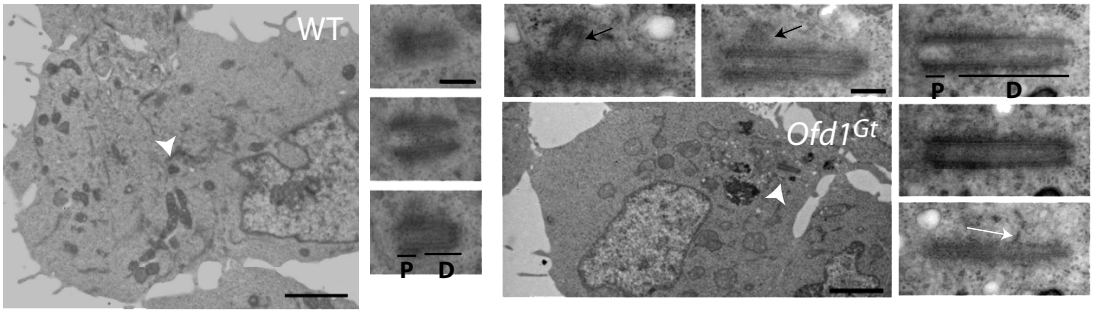

E

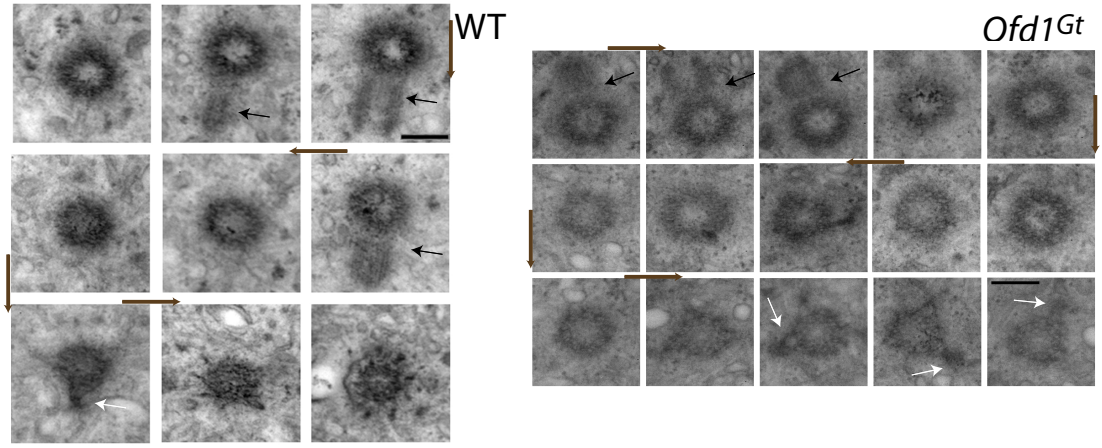

F

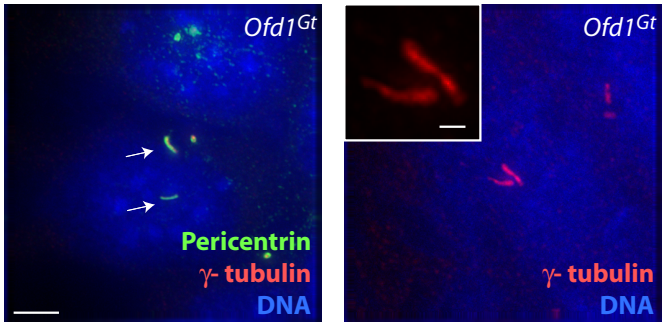

G

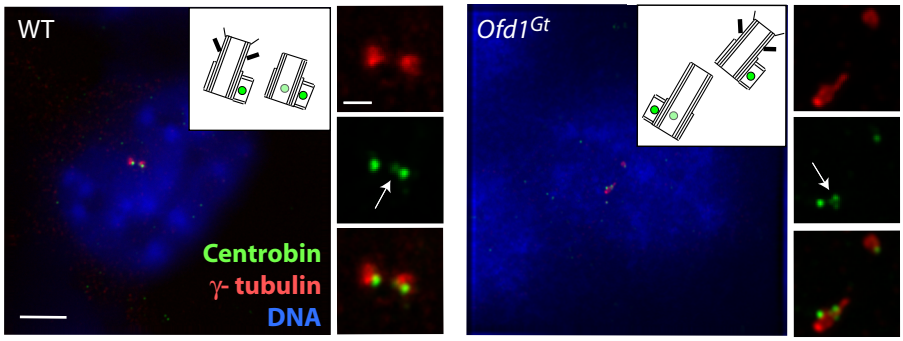

Figure 5. Ofd1 is essential for distal appendage formation.

(**A**) Centrioles (acetylated tubulin) and mother centriole subdistal appendages (Ninein) of WT and *Ofd1*^{Gt} cells. (**B**) TEM longitudinal views of WT and *Ofd1*^{Gt} centrioles. Arrows indicate subdistal appendages. (**C**) Centrioles (acetylated tubulin) and mother centriole distal appendages (Cep164) of WT and *Ofd1*^{Gt} cells. Graph shows percent of centrosome pairs showing Cep164 localization in WT and *Ofd1*^{Gt} cells. (**D**) Immunblot showing Cep164 in the supernatants of WT and *Ofd1*^{Gt} cell lysates. 20 μg protein loaded per lane. (**E**) TEM transverse views of WT and *Ofd1*^{Gt} centrioles. Arrows indicate distal appendages. (Full serial reconstructions are included in Figure S4). (**F**) Centrioles and cilia (acetylated tubulin), centriole appendages (Odf2), centrosomes (γ-tubulin), and DNA (DAPI) of WT and *Ofd1*^{Gt} cells at the indicated time after release from cell synchronization block. Arrowheads indicate centrioles positive for Odf2. (**G**) Quantification of Odf2 foci per cell in WT and *Ofd1*^{Gt} cells at the indicated time after release from cell synchronization block. Asterisks indicate $p < 0.05$. Scale bar indicates 200 nm (TEM) and 1 μm.

Figure 5, A-E

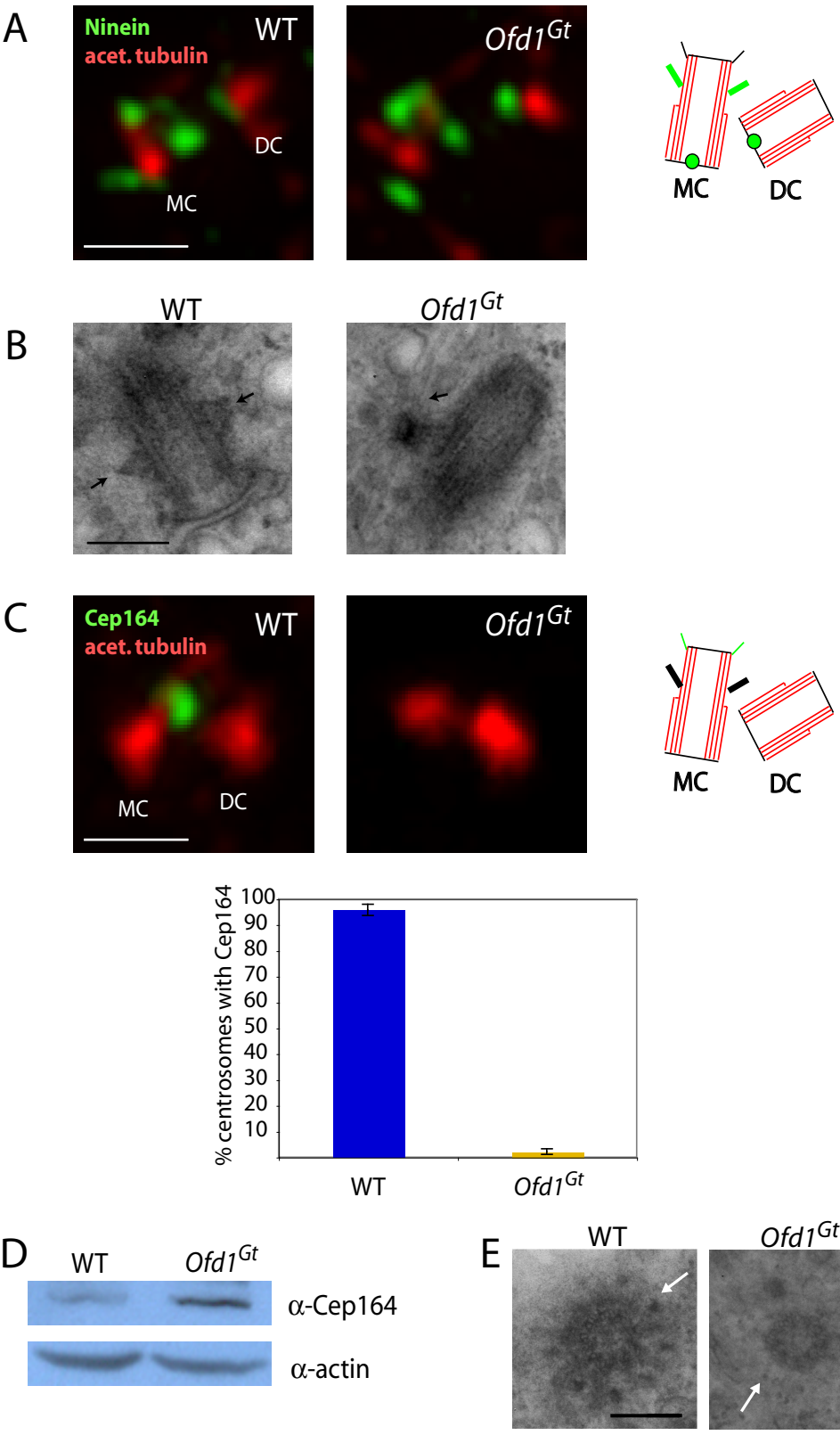
A
Ninein
acet. tubulin
WT
DC
MC
Ofd1Gt
MC
DC
B
WT
Ofd1Gt
C
Cep164
acet. tubulin
WT
MC
DC
Ofd1Gt
MC
DC
% centrosomes with Cep164
100
90
80
70
60
50
40
30
20
10
WT
Ofd1Gt
D
WT
Ofd1Gt
α-Cep164
α-actin
E
WT
Ofd1Gt

Figure 5, F-G

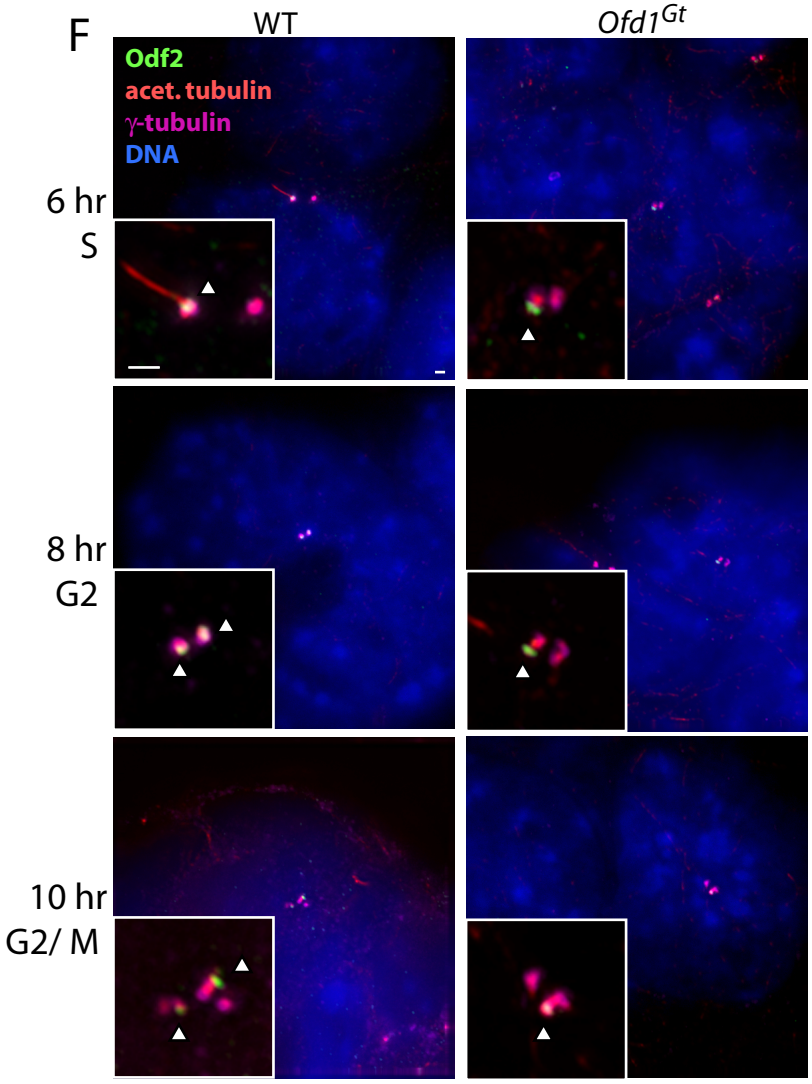
F
WT
Ofd1Gt
Odf2
acet. tubulin
γ-tubulin
DNA
6 hr
S
8 hr
G2
10 hr
G2/ M

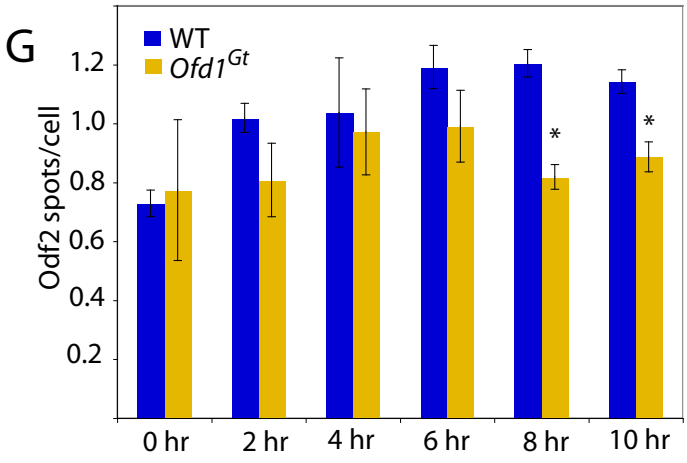
G
WT
Ofd1Gt
Odf2 spots/cell
1.2
1.0
0.8
0.6
0.4
0.2
*
*
0 hr
2 hr
4 hr
6 hr
8 hr
10 hr

Figure 6. Ofd1 is required for centrosomal recruitment of Ift88, but not Ift20, Ift80, or Kif3a.

(**A**) The intraflagellar transport protein Ift20, centrosomes (γ–tubulin), and DNA (DAPI) of WT and *Ofd1*^{Gt} cells. IFT20 localizes to the Golgi and near the centrosome (Follit et al., 2006). (**B**) Ift80, centrosomes (γ–tubulin), and DNA (DAPI) of WT and *Ofd1*^{Gt} cells. (**C**) Anterograde kinesin motor component Kif3A, centrosomes (γ–tubulin), and DNA (DAPI) of WT and *Ofd1*^{Gt} cells. (**D**) Ift88, centrosomes (γ–tubulin), and DNA (DAPI) of WT and *Ofd1*^{Gt} cells. (**E**) Graph showing percent of centrosome pairs with Ift88 localization in WT and *Ofd1*^{Gt} cells. (**F**) Immunblot showing Ift88 in the supernatants of WT and *Ofd1*^{Gt} cell lysates. 20 μg protein loaded per lane. (**G**) Ift88, Ofd1-Myc (Myc), and centrioles and cilia (acetylated tubulin) of *Ofd1*^{Ofd1myc} cells. (**H**) Ift88, Ofd1-Myc (Myc), and centrosomes (γ-tubulin) of *Ofd1*^{Ofd1myc} cells. (**I**) Centrioles and cilia (acetylated tubulin), centrosomes (γ-tubulin), and DNA (DAPI) of WT, *Ofd1*^{Gt} and *Ofd1*^{Ofd1myc} cells. Arrows indicate cilia. Scale bar indicates 5 μm or 1 μm (inset, (G)-(H)).

Follit, J.A., Tuft, R.A., Fogarty, K.E., and Pazour, G.J. (2006). The intraflagellar transport protein IFT20 is associated with the Golgi complex and is required for cilia assembly. Mol Biol Cell *17*, 3781-3792.

Figure 6, A-D

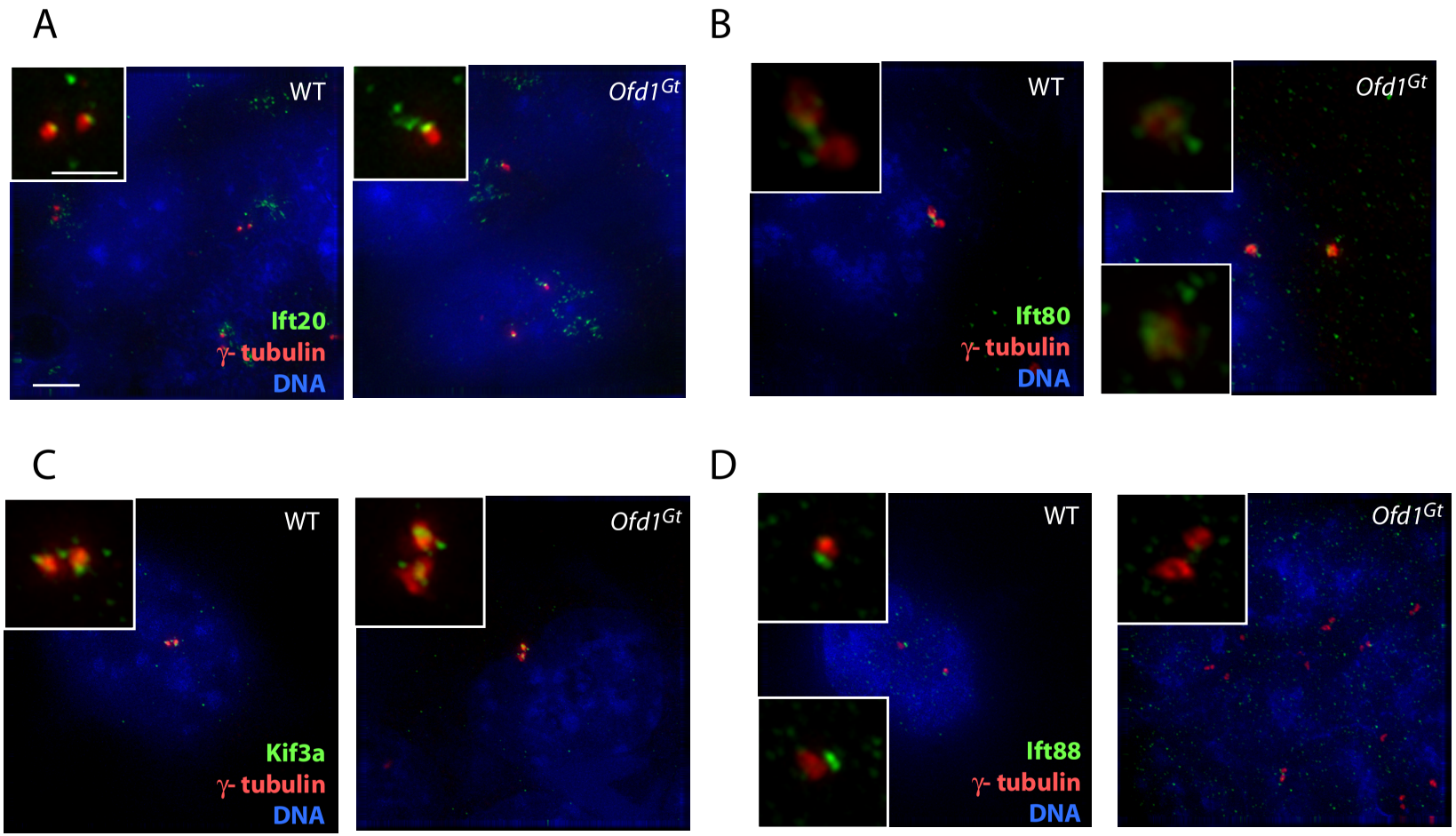
A
WT
Ofd1Gt
Ift20
γ- tubulin
DNA
B
WT
Ofd1Gt
Ift80
γ- tubulin
DNA
C
WT
Ofd1Gt
Kif3a
γ- tubulin
DNA
D
WT
Ofd1Gt
Ift88
γ- tubulin
DNA

Figure 6, E-I

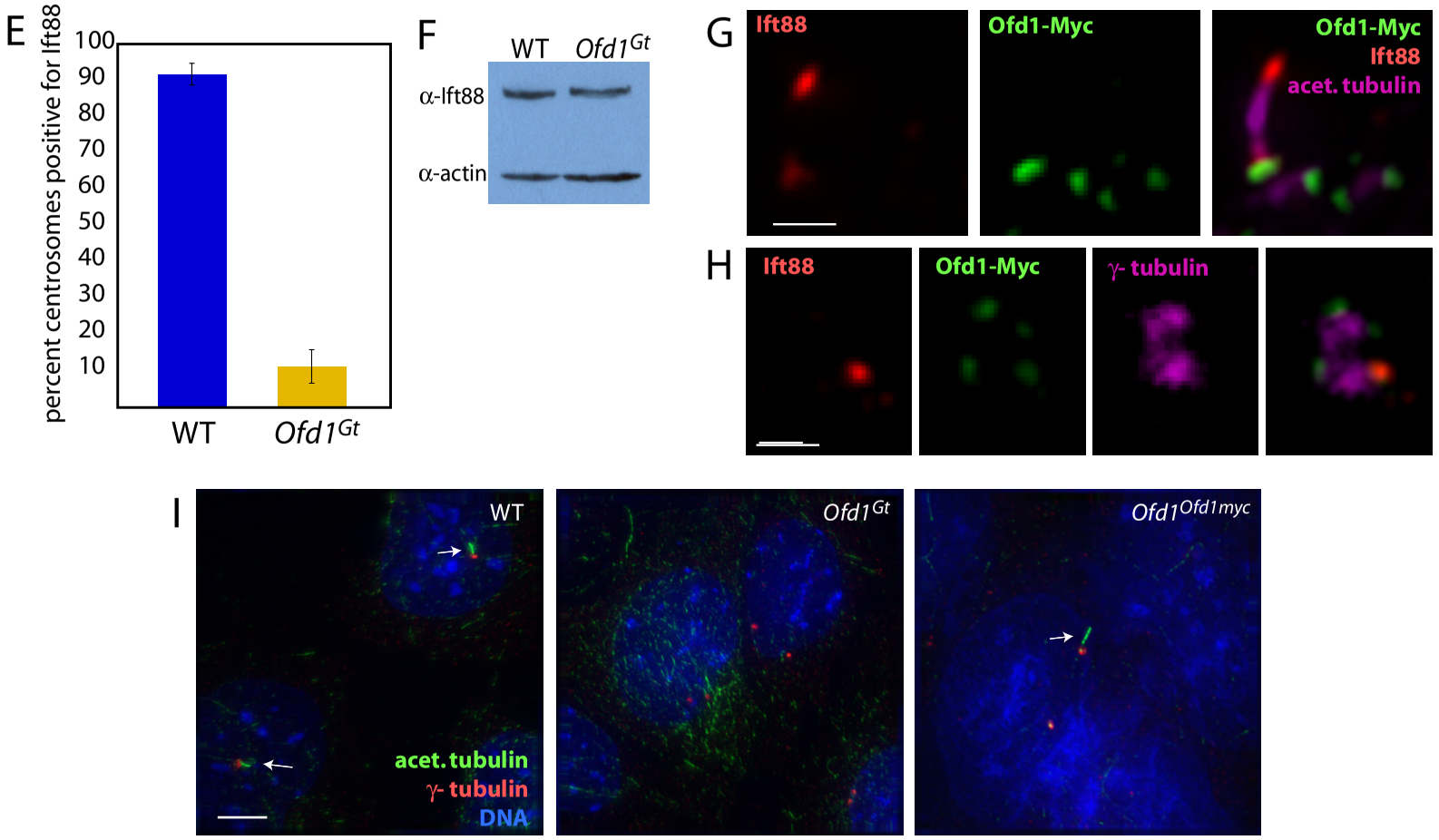
E
percent centrosomes positive for Ift88
100
90
80
70
60
50
40
30
20
10
WT
Ofd1Gt
F
WT
Ofd1Gt
α-Ift88
α-actin
G
Ift88
Ofd1-Myc
Ofd1-Myc
Ift88
acet. tubulin
H
Ift88
Ofd1-Myc
γ- tubulin
I
WT
Ofd1Gt
Ofd1Ofd1myc
acet. tubulin
γ- tubulin
DNA

Figure 7. Missense *Ofd1* mutations found in human patients affect centriole length control and ciliogenesis.

(**A**) Immunoblots showing Ofd1 (detected with an Ofd1 antibody) in the supernatants of lysates from cells of the indicated genotypes. 20 μg protein loaded per lane. (**B**) Cells of the indicated genotypes stained for Ofd1-Myc (Myc), centrosomes (γ-tubulin), and DNA (DAPI). (**C**) Graphs comparing the frequencies of long centriole formation, centriolar localization of Cep164 and Ift88, and ciliogenesis of cells with *Ofd1* alleles to $Ofd1^{Rev}$, $Ofd1^{IRESOfd1myc}$, or $Ofd1^{Ofd1myc}$ cells. Asterisks indicate statistically significant differences ($p < 0.05$). (**D**) Cells of the indicated genotypes showing centrosomes (γ-tubulin) and DNA (DAPI). (**E**) In wild type cells, the mother centriole distal appendages contain Odf2 and Cep164, and Ift88 is recruited at the transition zone into the primary cilium. Ofd1 binds to the distal ends of centriolar microtubules, stabilizes centrioles at the proper length during maturation and recruits Ift88 and distal appendage proteins. In the absence of Ofd1, both mother and daughter centrioles show microtubule destabilization and unrestrained elongation of the distal domain during G2, the phase during which centriole maturation occurs. Without Ofd1, subdistal and distal appendages may be present in the middle of the long centriole, or distributed along the elongated portion. The inability to make primary cilia may be due to centriole elongation defects, distal appendage defects, Ift88 recruitment defects, inability to dock to a vesicular membrane (Sorokin, 1962), or a combination of these.

Sorokin, S. (1962). Centrioles and the formation of rudimentary cilia by fibroblasts and smooth muscle cells. J Cell Biol *15*, 363-377.

Figure 7, A-D

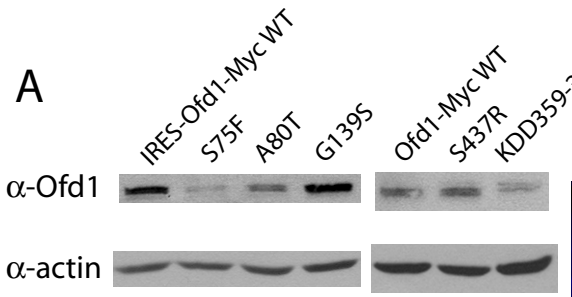
A
IRES-Ofd1-Myc WT
S75F
A80T
G139S
Ofd1-Myc WT
S437R
KDD359-361FSY
α-Ofd1
α-actin

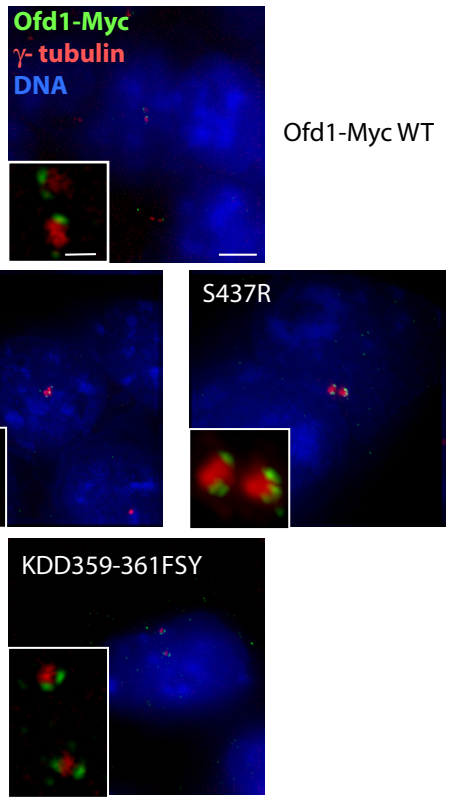
B
Ofd1-Myc
γ- tubulin
DNA
Ofd1-Myc WT
G139S
S437R
KDD359-361FSY

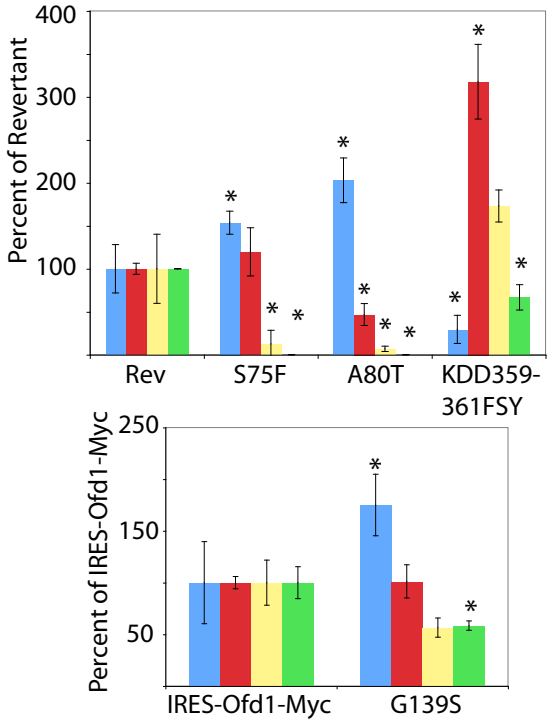
C
Percent of Revertant
400
300
200
100
Rev
S75F
A80T
KDD359-361FSY
Percent of IRES-Ofd1-Myc
250
150
50
IRES-Ofd1-Myc
G139S
Long centrioles
Cep164 localization
Ift88 localization
Cilia

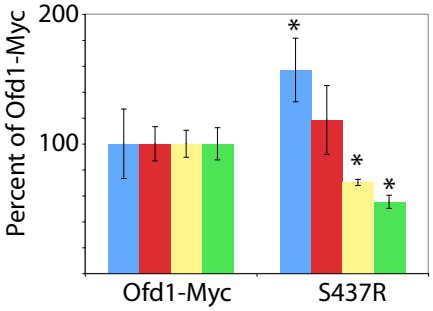
Percent of Ofd1-Myc
200
100
Ofd1-Myc
S437R

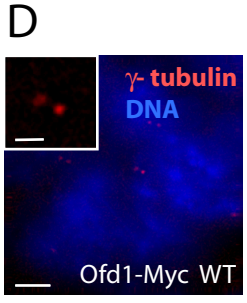
D
γ- tubulin
DNA
Ofd1-Myc WT

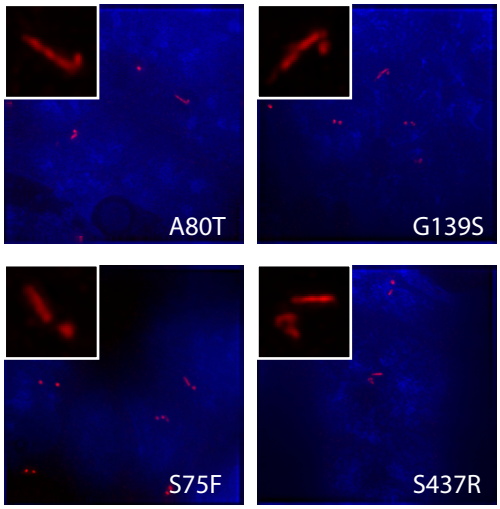
A80T
G139S
S75F
S437R

Figure 7, E

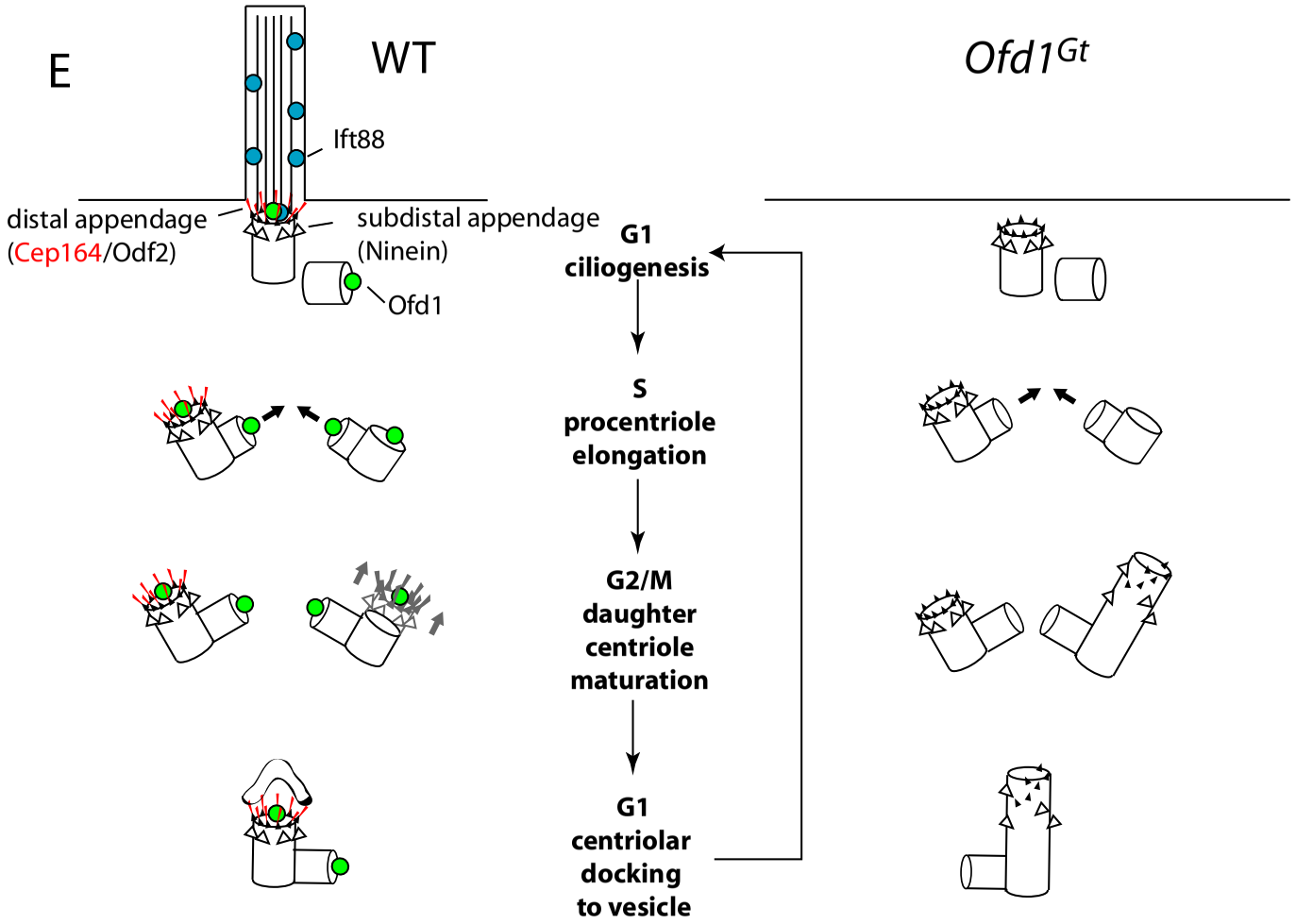
E
WT
Ofd1Gt
Ift88
distal appendage
(Cep164/Odf2)
subdistal appendage
(Ninein)
Ofd1
G1
ciliogenesis
S
procentriole
elongation
G2/M
daughter
centriole
maturation
G1
centriolar
docking
to vesicle

Figure S1. Ofd1 is not required for the mitotic or microtubule organizing functions of centrioles.

(A) Subdistal appendages (Ninein), centrosomes (γ-tubulin) and DNA (DAPI) of WT and *Ofd1*^{Gt} cells. **(B-C)** CP110 or Cep97, centrosomes or centrioles (γ-tubulin or acetylated tubulin) and DNA (DAPI) of WT and *Ofd1*^{Gt} cells. (**D)** Transverse TEM sections of normal length centrioles from *Ofd1*^{Gt} cells. Arrows indicate triplet microtubules. **(E)** Graph indicating the population doubling times of WT and *Ofd1*^{Gt} cells. (**F)** FACS analysis of DNA content and cell cycle phase distribution of asynchronous WT and *Ofd1*^{Gt} cells. Samples analyzed in duplicate in 2 separate experiments. (**G)** Microtubules (α-tubulin), centrosomes (γ-tubulin), and DNA (DAPI) of interphase and mitotic WT and *Ofd1*^{Gt} cells. (**H)** Procentrioles (Sas-6), centrosomes (γ-tubulin), and DNA (DAPI) of WT and *Ofd1*^{Gt} cells. Sas-6 is present in newly forming procentrioles. **(I)** Transverse TEM sections of a long *Ofd1*^{Gt} centriole. Procentriole (black arrow), subdistal appendages (white arrows). (**J)** Microtubules (α-tubulin) and centrosomes (γ-tubulin) of WT and *Ofd1*^{Gt} cells. Cells were incubated with nocodazole to depolymerize microtubules, drug was washed out, and microtubules were allowed to regrow from 0-15 minutes. Regrowth after 2 minutes is shown. Scale bar indicates 2 μm (TEM, low magnification), 200 nm (TEM, high magnification), 15 μm (panel G), 5 μm, or 1 μm (inset).

Supplementary 1, A-E

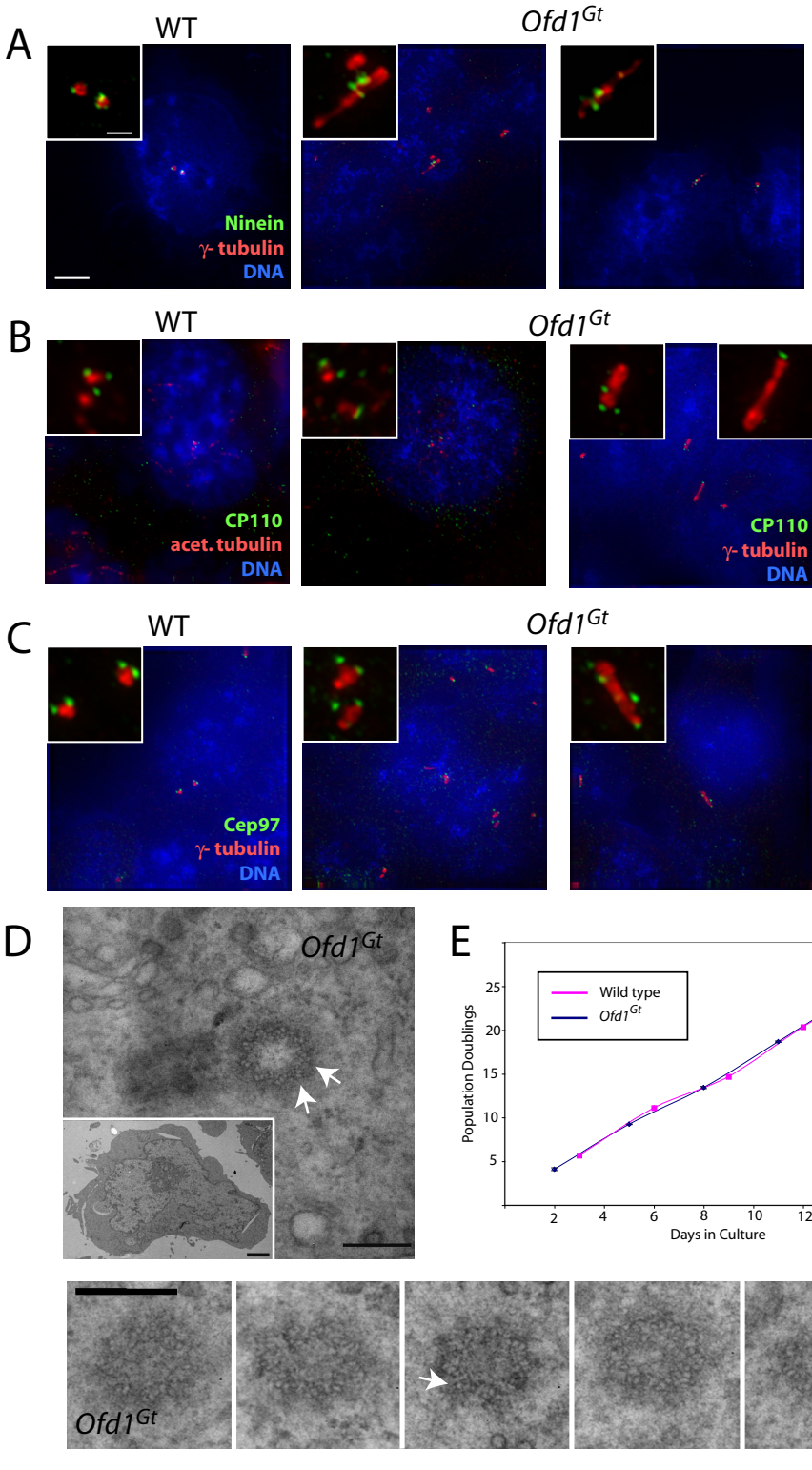

Supplementary 1, F-J

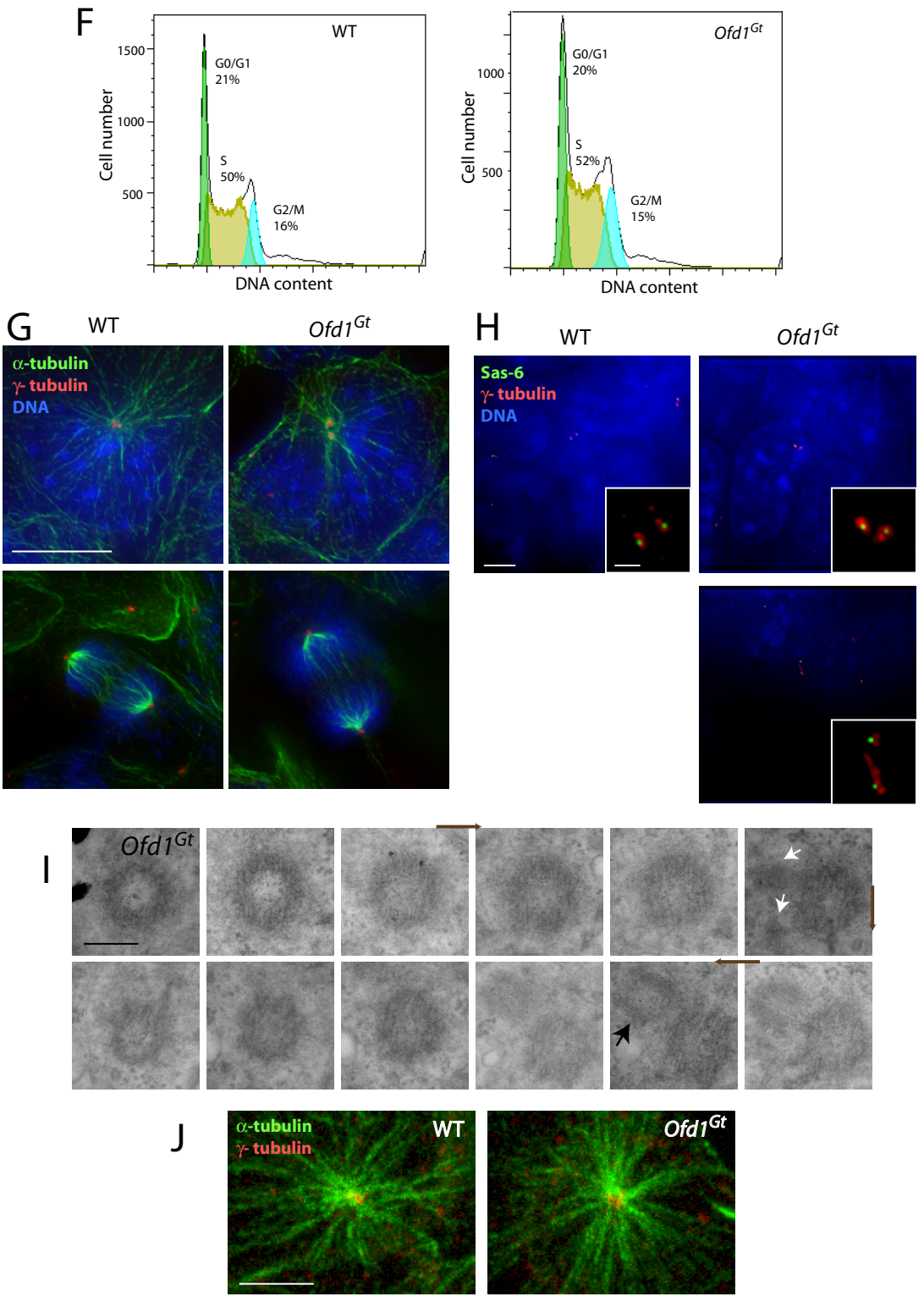

Figure S2. Ofd1 localizes to the distal ends of centrioles in diverse types of cells.

(**A)** Ofd1 and centrioles (acetylated tubulin and γ-tubulin) in synchronized WT ES cells at the indicated cell cycle phase. (**B)** Ofd1, centrioles and cilia (acetylated tubulin) in WT ES cells. MC, mother centriole. DC, daughter centriole. PC, procentriole. **(C)** Murine fibroblasts (NIH-3T3), intermedullary collecting duct (IMCD3), and human retinal pigmented epithelial cells (hTERT-RPE1) showing Ofd1, centrioles and cilia (acetylated tubulin), centrosomes (γ-tubulin), and DNA (DAPI). (**D)** S-phase arrested Poc1-GFP expressing U2OS (human osteosarcoma) cells showing Ofd1, Poc1-GFP (GFP), and DNA (DAPI). Poc1 marks all centrioles. (**E)** Immunoblot showing Ofd1 (detected with an Ofd1 antibody) in supernatant from cell lysate of $Ofd1^{Ofd1myc}$ cells. 15 μg protein loaded per lane. **(F)** Graph showing percent of cells with long centrioles in cells of the indicated genotypes. **(G)** Ofd1-Myc, centrioles (Centrin) and cilia (acetylated tubulin) in $Ofd1^{Ofd1myc}$ cells**. (H)** Poc1-GFP expressing U2OS cells showing Ofd1, Poc1-GFP (GFP), and DNA (DAPI). Scale bar indicates 5 μm or 1 μm (A-B, G and inset).

Supplementary 2

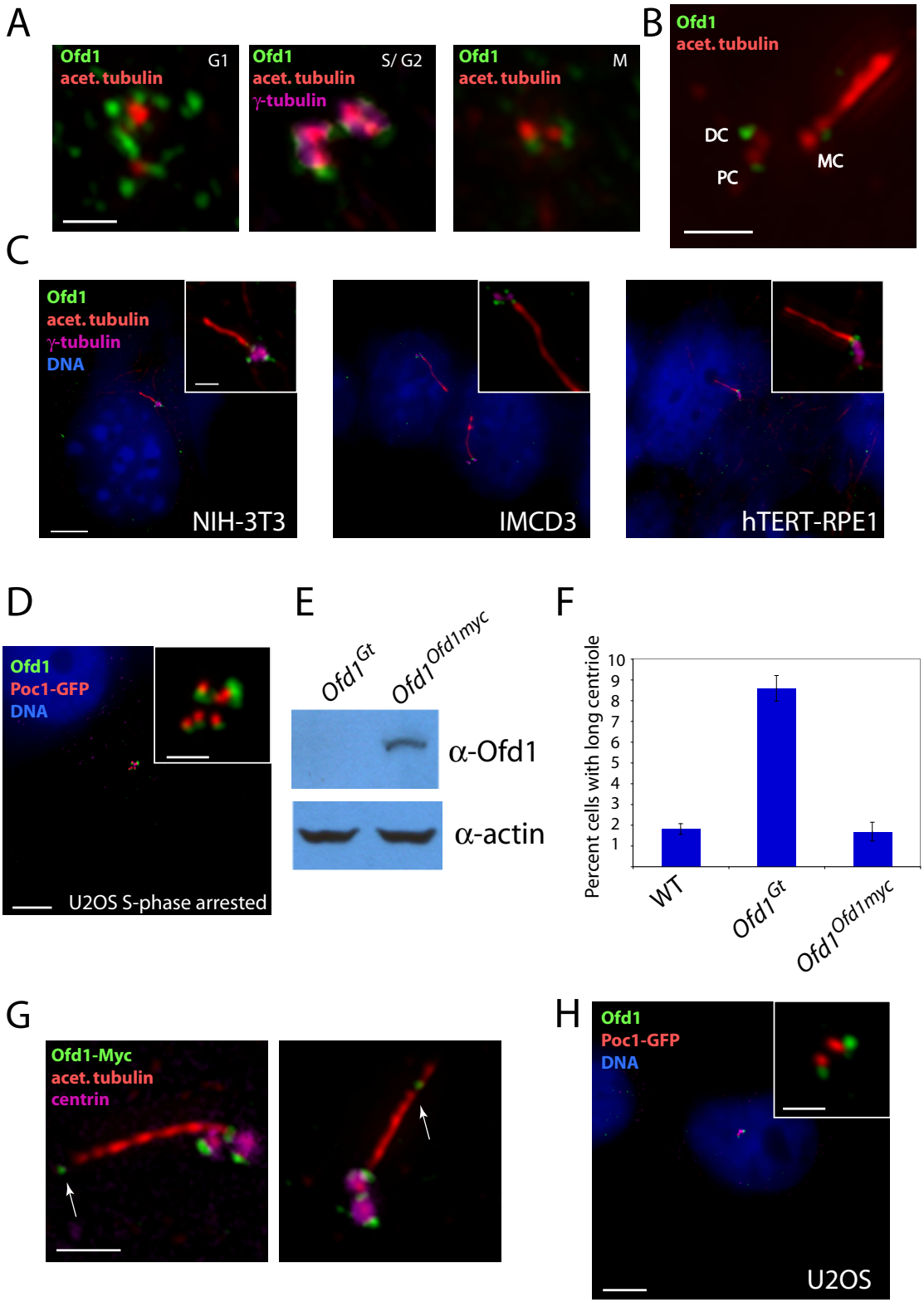

Figure S3. Loss of Ofd1 causes abnormal elongation of the centriole distal domain in G2.

(A) Immunoblot of Ofd1 complexes immunoprecipitated from WT cell supernatant with an Ofd1 antibody and detected with a Cep164 antibody. **(B)** Longitudinal TEM views of WT and *Ofd1*^{Gt} centrioles. White arrow indicates an elongated centriole. Black arrows point to microtubule anchoring at long centriole distal end. D, distal domain. P, proximal domain. (**C)** Different drugs arrest cells in distinct phases of the cell cycle. (**D)** Asynchronous or G2 arrested (+ camptothecin) WT and *Ofd1*^{Gt} cells showing centrosomes (γ-tubulin) and DNA (DAPI). Magnified region indicated by box. White arrows indicate elongated centrioles. **(E)** WT and *Ofd1*^{Gt} cells showing the centriole distal lumen (Centrin), centrosomes (γ-tubulin), and DNA (DAPI). Scale bar indicates 200 nm (TEM), 5 μm or 1 μm (inset).

Supplementary 3

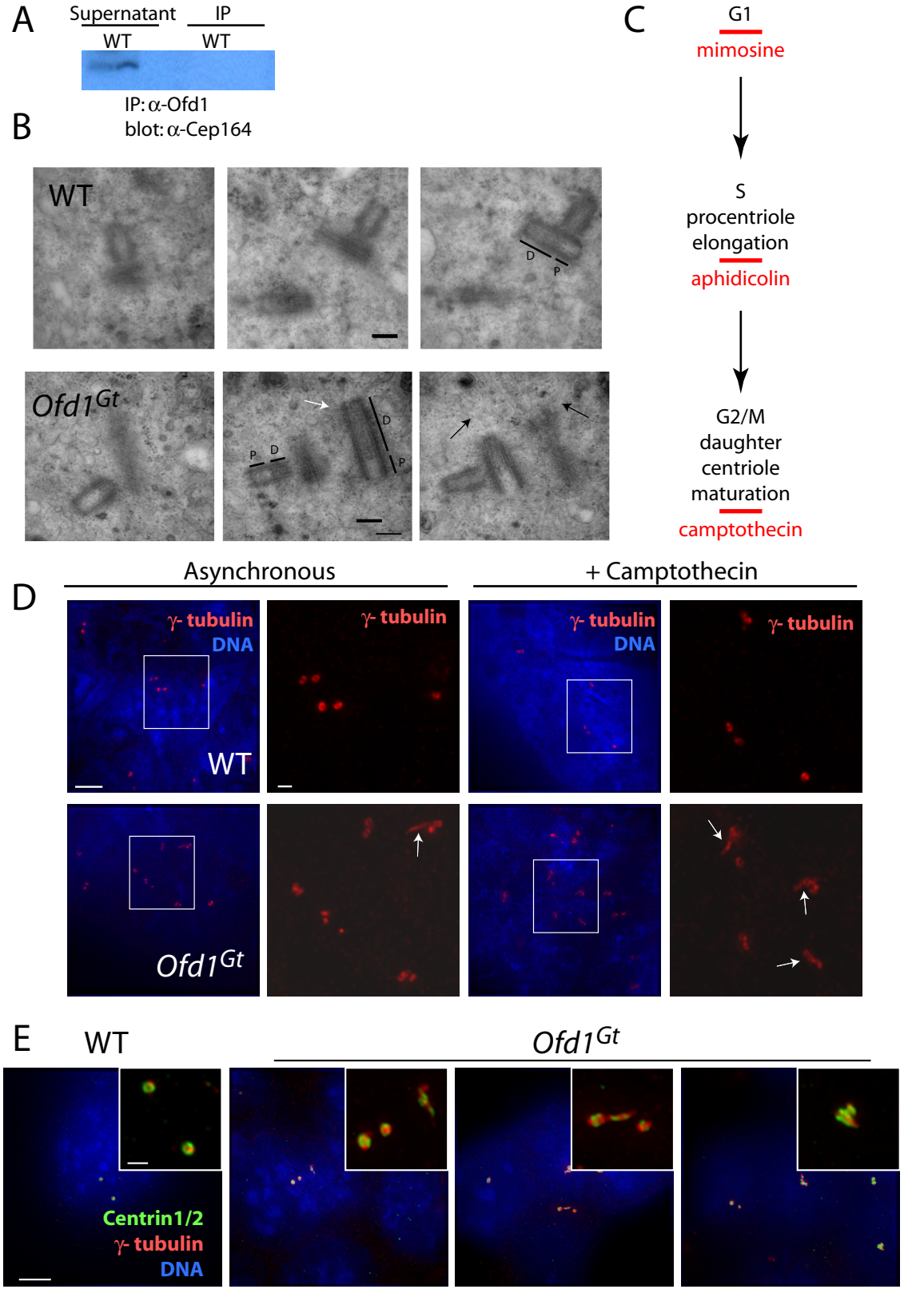

Figure S4. Ofd1 is essential for distal appendage formation.

(**A)** Transverse TEM serial reconstructions of the WT and *Ofd1*^{Gt} centrioles depicted in Figure 5F. White arrows indicate subdistal appendages. (**B)** Longitudinal and transverse TEM views of *Ofd1*^{Gt} long centrioles. White arrows indicate subdistal appendages, black arrow distal appendages. **(C)** Subdistal appendages (Ninein), centrosomes (γ-tubulin), and DNA (DAPI) of WT and *Ofd1*^{Gt} cells. (**D)** FACS analysis of DNA content and cell cycle phase of WT cells at the indicated time after release from thymidine-mimosine block. (**E**) Graph showing percent of centrosomes with Cep164 after treatment with the indicated siRNA, determined by immunofluorescence in hTERT-RPE1 cells. (**F**) Graph showing percent of centrosomes with Ofd1 after treatment with the indicated siRNA, determined by immunofluorescence in hTERT-RPE1 cells. Scale bar indicates 200 nm (TEM), 5 μm or 1 μm (inset).

Supplementary 4, A-B

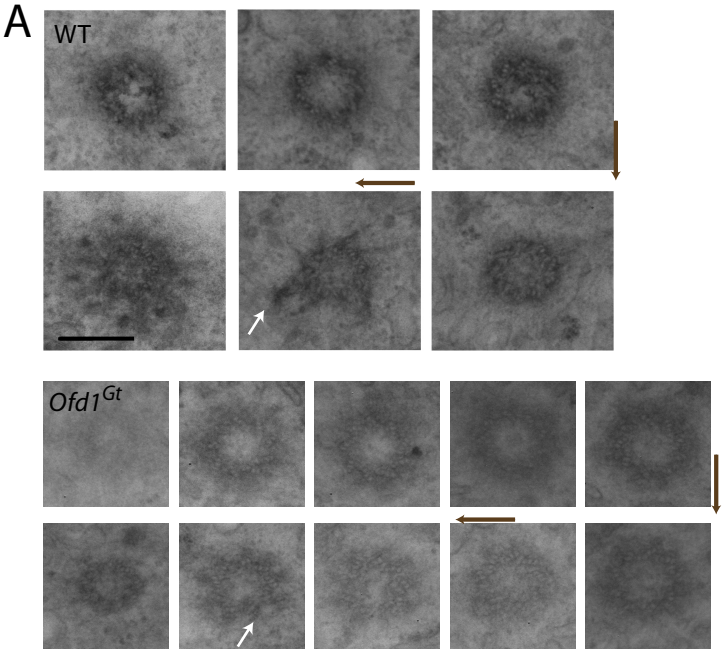

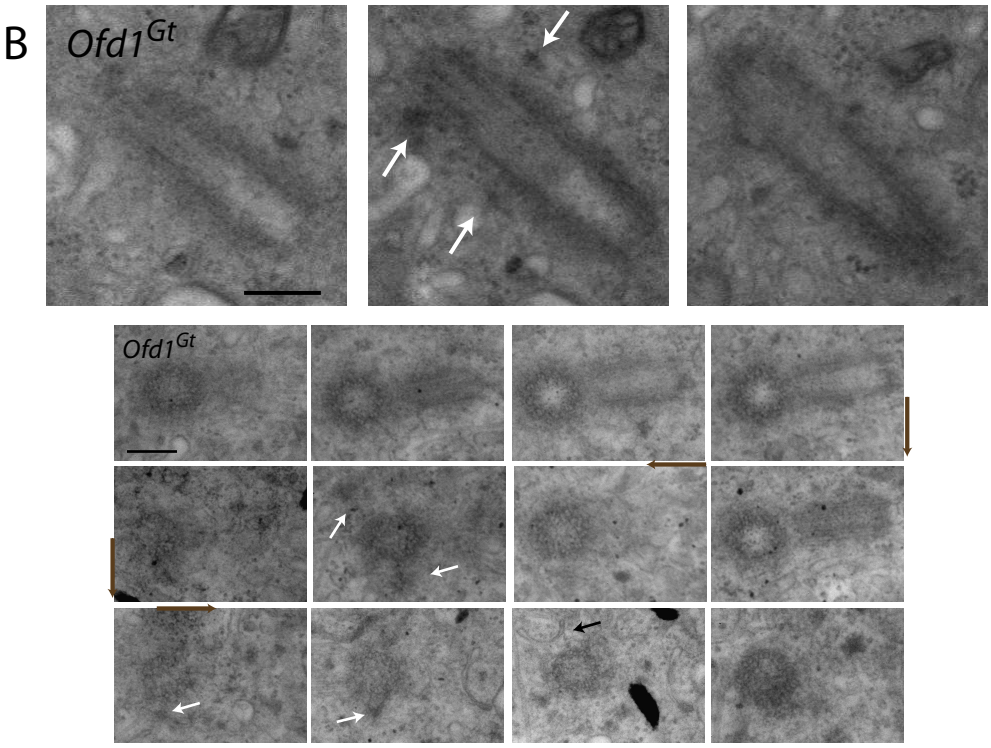

Supplementary 4, C-F

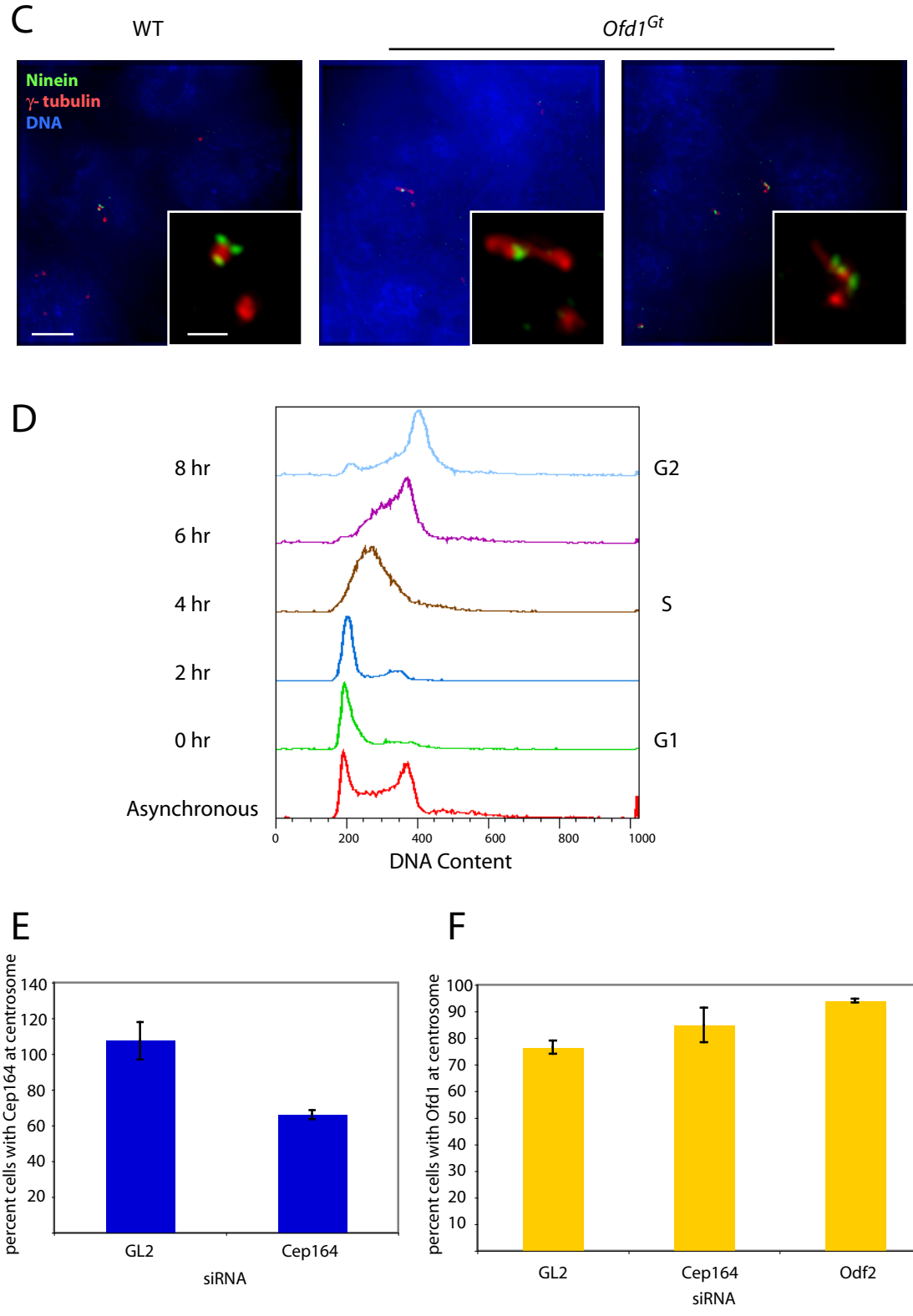

Figure S5. Ofd1 is not required for the centrosomal localization of trafficking proteins p150, Pericentrin or Cep290.

(A) p150, centrioles (acetylated tubulin), and DNA (DAPI) of WT and *Ofd1*^{Gt} cells. **(B)** Pericentrin, centrosomes (γ-tubulin) and DNA (DAPI) of WT and *Ofd1*^{Gt} cells. (**C)** Cep290, centrosomes (γ-tubulin), and DNA (DAPI) of WT and *Ofd1*^{Gt} cells. Scale bar indicates 5 μm or 1 μm (inset).

Supplementary 5

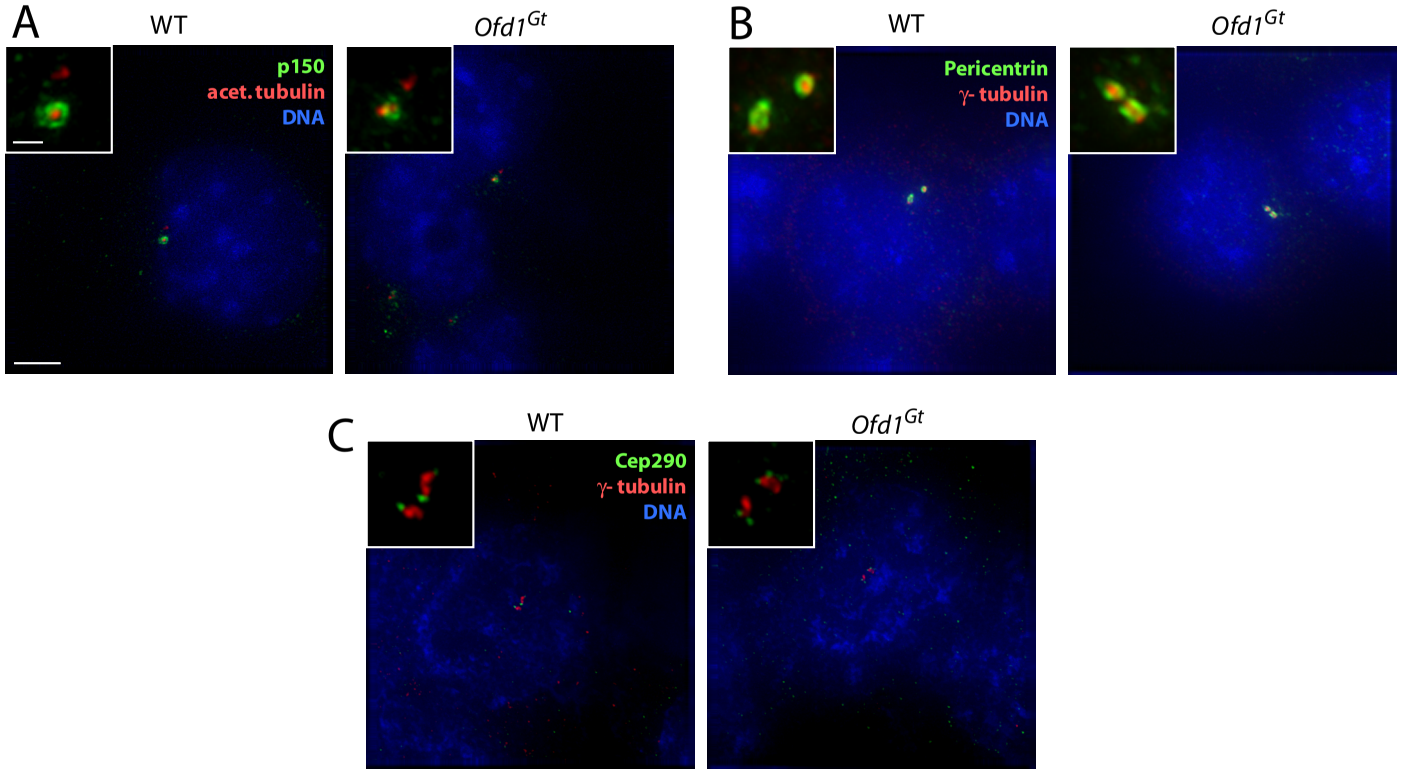

Figure S6. Disease-associated missense mutations in *Ofd1* affect centriole length, Cep164 and Ift88 recruitment, and ciliogenesis.

(A) Alignment of the N-terminal half of human and mouse Ofd1, depicting protein domains, peptide used to raise antibody, and locations of missense mutations (numbers given are for mouse Ofd1). (**B)** Immunoblot of Ofd1-Myc immunoprecipitated with a Myc antibody from cell lysate supernatants and detected with a Myc antibody. **(C)** Graph comparing the frequencies of long centriole formation, centriolar localization of Cep164 and Ift88, and ciliogenesis of cells with *Ofd1* alleles to WT cells. (**D**) Cells of the indicated genotypes showing mother centriole distal appendages (Cep164), centrosomes (γ-tubulin), and DNA (DAPI, blue). (**E**) Cells of the indicated genotypes showing Ift88, centrosomes (γ-tubulin), and DNA (DAPI). (**F**) Cells of the indicated genotypes showing cilia (acetylated tubulin) and DNA (DAPI). Scale bar indicates 5 μm or 1 μm (inset).

Supplementary 6, A-C

A

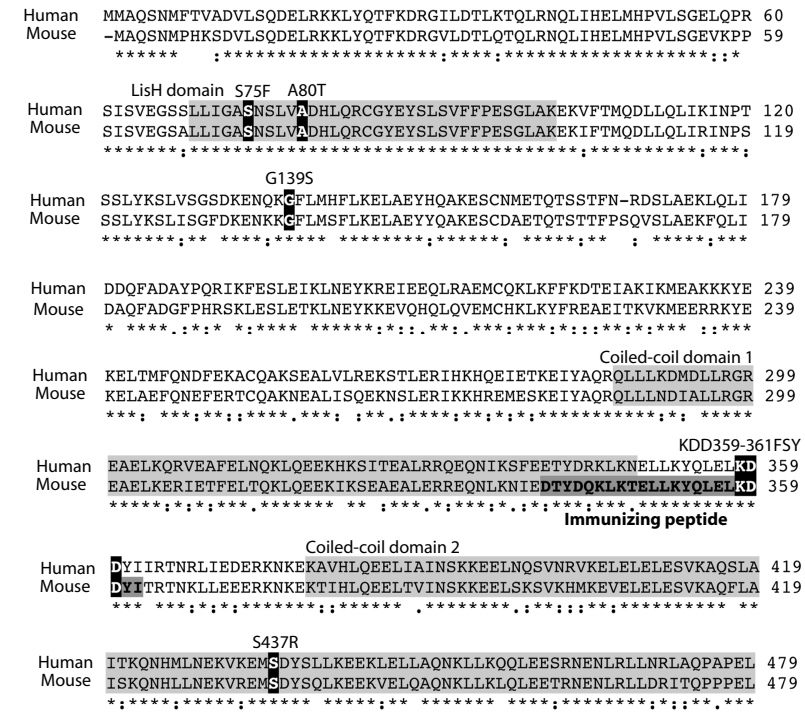

B

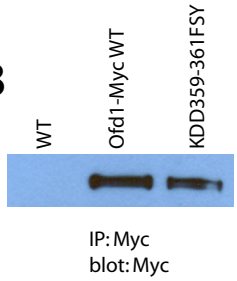

C

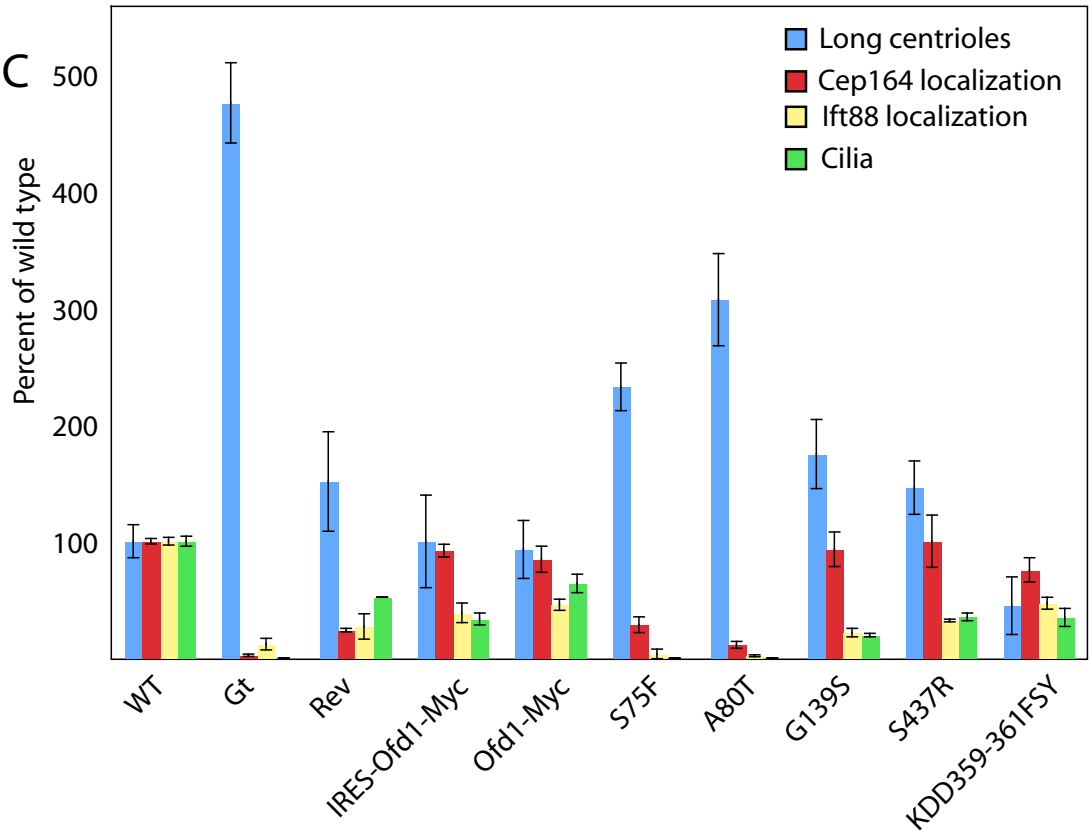

Supplementary 6, D-F

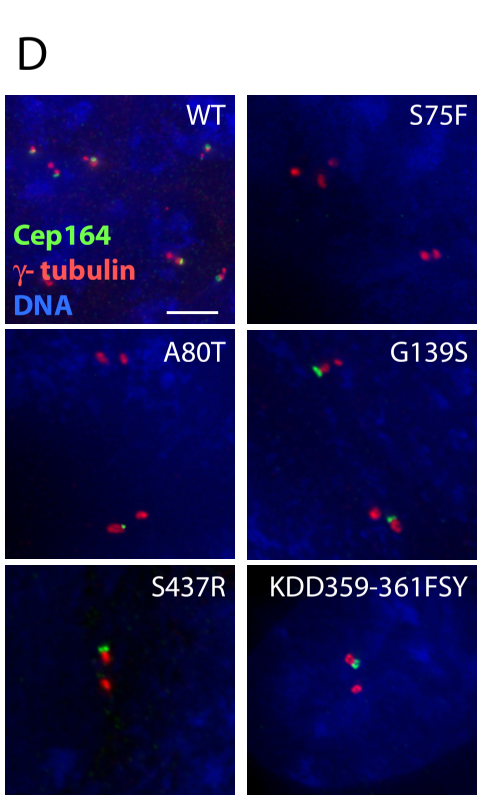

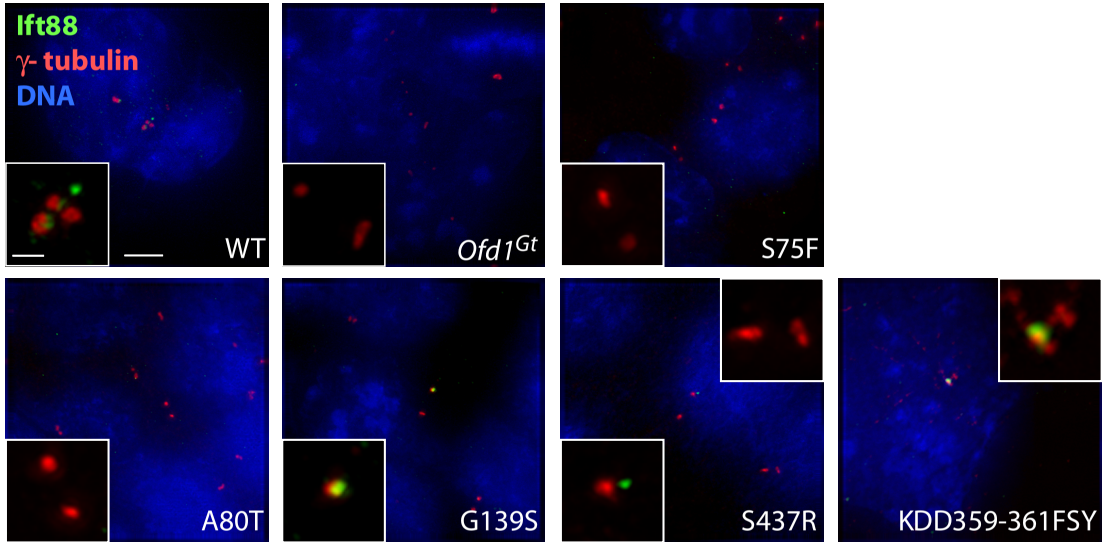

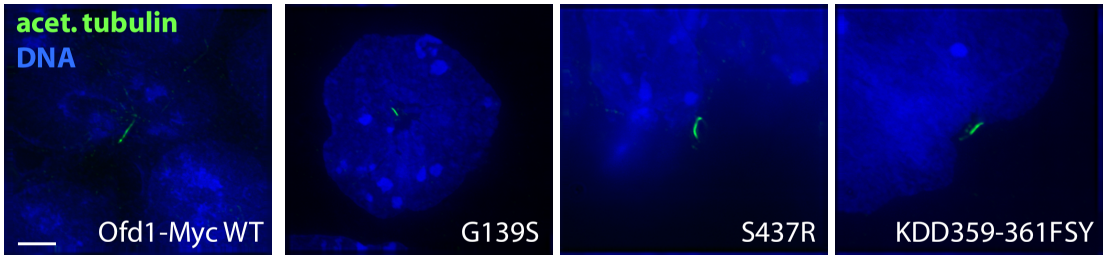

Figure S7. *Ofd1* phylogeny.

(**A**) Phylogram of *Ofd1*. Organisms with canonical centriole structure have *Ofd1* orthologs. (**B**) Alignment of *Tetrahymena* Ofd1 and Ofd1β protein sequences. Ofd1 LisH domain is highlighted in blue.

Supplementary 7

A

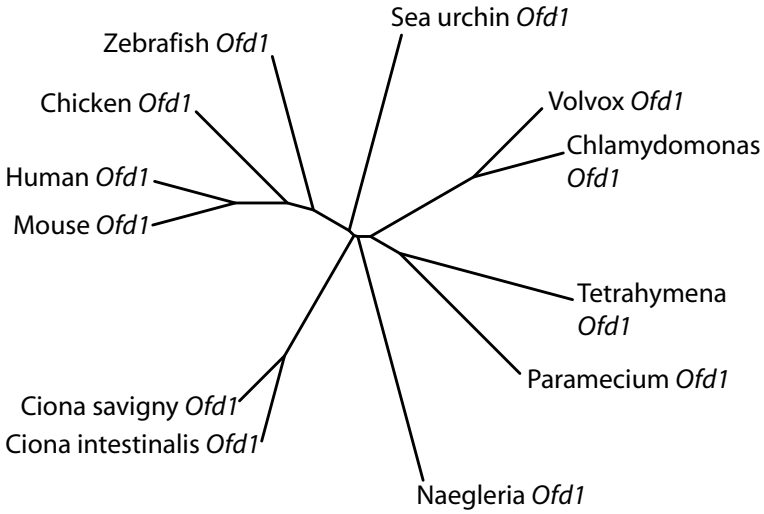

B

```
Tetra_Ofd1          -----MEQGEDNNDQYKEKLFHLFSDTGMLNSVKAQMRHKMIEKLVKSQKVQQVQQKIHD 55
Tetra-Ofd1beta      MFTEADLARQNEDLEFKKQLFESFKQTGIMDGMKVNLRKQIVDKLQQQTQTEKELKAAQT 60
                           :::: ::*::**. *.:**:::.:*.::*:::::** :. :.::  :  :

Tetra_Ofd1          EKNQHKALLMR------------LMASIVSEYFDKNDYSYSNSIFQPES-GYANKILQRF 102
Tetra-Ofd1beta      AINQSKKEEIESLRQKEFYRNQRIYAHLIADYLRTYDINYAYSIFLPEMRVNSNQILMRD 120
                      ** *   :.            : * ::::*: . * .*: *** **    :*:** *

Tetra_Ofd1          EILDIMNCKNIDNPKIS------ILETMVETYLNNVKNVPKTNCATQTEHADAIFNLEQR 156
Tetra-Ofd1beta      EICEAFLIEKDEYKQLDDQREKLSAIEIIVEMIKKFKKTKKVNREVQTESYEKSATMSMR 180
                    ** : :  :: :  ::.          ::   :::.*:. *.*  .***  :   .:. *

Tetra_Ofd1          LNTVDHKYREKVQEINTP-AHEIEERLQRFKREFENRIKAEMNAEVVRIREFEMAAVRME 215
Tetra-Ofd1beta      MDDINYEYGQKLDYFKLVSNKNVEESLAKYRKECEAKYKADLEMELQRFRDYELIEMRAL 240
                    :: ::::* :*:: ::    :::** * ::::* * : **::: *: *:*::*:  :*

Tetra_Ofd1          EQEKYRKLMSEYREELEKGYMDRLTKLREREKDTLEKCTNKMKEIESINHDHRQRILKDF 275
Tetra-Ofd1beta      EAERYQEKLTFHRKELDKVYNEKLQKLQEREKNAIELCKRRLEDLEKIQQENRQKHLNDI 300
                    * *:*:: :: :*:**:* * ::* **:****:::* *..:::::*.*::::**: *:*:

Tetra_Ofd1          ELLRMREDEIDKQRILNDETLKIQKQKLENLEQELKEKIKKAEESALIIEKKYQNDLAYT 335
Tetra-Ofd1beta      EAMNKKELEFRRHSCLDHIEVKEQREKLDKLEKDLKLKMREYESAKQLINTRIEEDISYR 360
                    * :. :* *: ::  *:.  :* *::**::**::** *::: *.:  :*:.: ::*::*

Tetra_Ofd1          KLEAHRDLEAEKLEIIEKKRILDEDMYKIKQVKVGEFIFKKLVDELNELRRQKKEQEFEL 395
Tetra-Ofd1beta      R---------------------------------------------NVLRQEQKYQELQK 375
                    :                                            * **:::* **::

Tetra_Ofd1          VQLRDNIRTVSDSYKRDQDSSRNLEQKLKIKDEEVNFFKNALEEQKKLVDQYKQSQVDNL 455
Tetra-Ofd1beta      KDVENQIKEEQAYINQQKQHLRNLEMQLQYLRDEN----DHLKKDVKELDYIKSEQYKEI 431
                     ::.::*:  .   :::::  **** :*:   :*     : *::: * :*  *..* .::

Tetra_Ofd1          KKFNNEIQVYQNQIEVLEEKIKELRKINKENEDLLDEARKQRYEMNYRQPLEFNHYHLNA 515
Tetra-Ofd1beta      QALRDQVRKHKESIEANEE---RLQHANKQMEILQDQIK---------------------- 467
                    : :.:::: :::.**. **   .*:: **: * * *: :

Tetra_Ofd1          PASYTAGPTSLKPQFQKELDDLREKRRQEILQYQRETEVVEKKNHSFKFENIWDISNASI 575
Tetra-Ofd1beta      ---------ILKSEVDQKAHSLEQRQSDQLNLHS-------------------------- 492
                             **.:.::: ..*.::: :::  :.

Tetra_Ofd1          DFTQFKGHKPSQDRDRQILEKAELTKSQMYQDFGLDKKAFTGIGGTNIIEESFREELDFA 635
Tetra-Ofd1beta      ------------------------------------------------------------

Tetra_Ofd1          KYEAKLKESYDKIDQNNSSRLRVMSEVERSRKDSFNVNKGKSEELQNQNFTIKKTTNQSP 695
Tetra-Ofd1beta      VYTMDMERNYNKLVETEKAYSLKLENLRQQSINDNLFLKNENKELSDINLRLEDEVSN-- 550
                     *  .::..*:*: :.:.:    :.::.:.  :.  . *.:.:**.: *: ::. ..:

Tetra_Ofd1          TKNTIEQQQSQEKIQTKSTFSKQTLNQISGLQDNPSLEQHQKYKKEDSQSLISKDAMLSI 755
Tetra-Ofd1beta      -------------LRRELRFIRKKLQEKEGENIDP--------------NTLNYSNTLKL 583
                                :: :  * ::.*:: .* : :*              . :. .  *.:

Tetra_Ofd1          PQTFTQQAEKKHSLKDSPLDTKKQTTLQPLIDLTKKDQKSSNLNYLPPPITQKQPQQSDF 815
Tetra-Ofd1beta      SPTHTQKISRGEKLMEEDLQNQDYRKNLDDIFQEMKSLKEKALFEFNNSLS--------- 634
                    . *.**: .: ..* :. *:.:.  .    *    *. *.. *  :  .::

Tetra_Ofd1          NYLDDFDDLDDFSDKNKKSNQPQPLKDDKKDLWSLPKDSDLNKKSVSNPFSKKKEDPFSS 875
Tetra-Ofd1beta      ------------------------------------------------------------

Tetra_Ofd1          KNEDIYGKKFDPFGKKDDKFGSKDDPFSSKKNDFSLPSTQNKQQKFEQKPAPYKQDKSTI 935
Tetra-Ofd1beta      ------------------------------------------------------------

Tetra_Ofd1          DNKEDDKTISEEIEEIVDYNEEIVEDLEYF 965
Tetra-Ofd1beta      -------------------------------
```

Figure S8. Ofd1 is associated with canonical centriole structure and cilia.

(**A**) Diagram of centriole structure and microtubule pattern in organisms considered to have "canonical" and "divergent" centriole structure. (**B**) Phylogram of *CP110*. Single-celled organisms do not contain *CP110* orthologs. (**C**) Hypothetical progression for gain of *CP110* function in centriole length control and ciliogenesis upon acquisition of multicellularity. Organisms that lost ciliation from most cells also lost the requirement for *Ofd1* in controlling centriole structure.

Supplementary 8

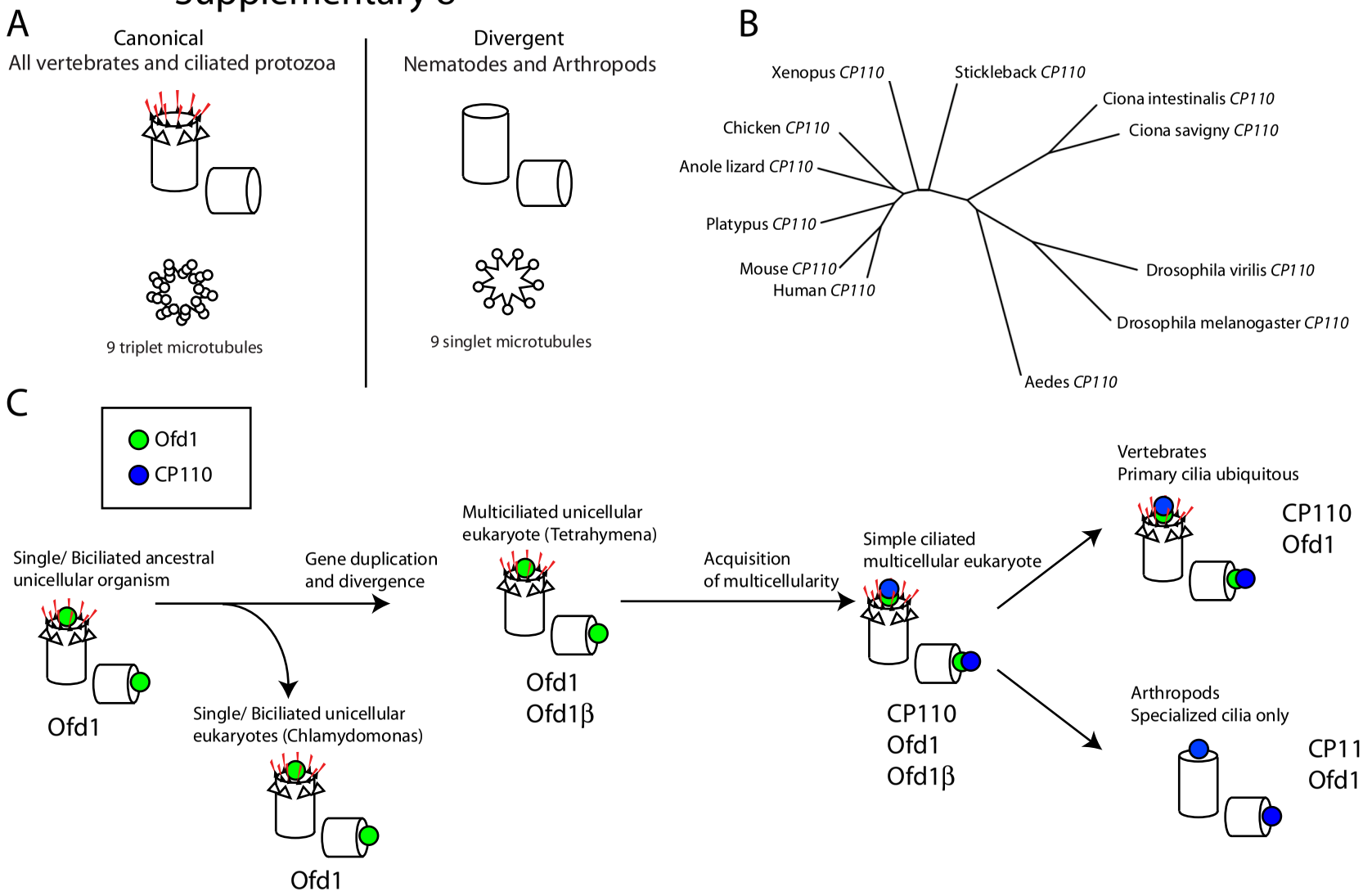

Figure S9. Domains of *OFD1* isoforms.

Alignment of protein sequences from human OFD1a and OFD1b showing domain locations.

Supplementary 9

```
OFD1a           MMAQSNMFTVADVLSQDELRKKLYQTFKDRGILDTLKTQLRNQLIHELMHPVLSGELQPR 60
OFD1b           MMAQSNMFTVADVLSQDELRKKLYQTFKDRGILDTLKTQLRNQLIHELMHPVLSGELQPR 60
                ************************************************************

                        LisH domain
OFD1a           SISVEGSSLLIGASNSLVADHLQRCGYEYSLSVFFPESGLAKEKVFTMQDLLQLIKINPT 120
OFD1b           SISVEGSSLLIGASNSLVADHLQRCGYEYSLSVFFPESGLAKEKVFTMQDLLQLIKINPT 120
                ************************************************************

OFD1a           SSLYKSLVSGSDKENQKGFLMHFLKELAEYHQAKESCNMETQTSSTFNRDSLAEKLQLID 180
OFD1b           SSLYKSLVSGSDKENQKGFLMHFLKELAEYHQAKESCNMETQTSSTFNRDSLAEKLQLID 180
                ************************************************************

OFD1a           DQFADAYPQRIKFESLEIKLNEYKREIEEQLRAEMCQKLKFFKDTEIAKIKMEAKKKYEK 240
OFD1b           DQFADAYPQRIKFESLEIKLNEYKREIEEQLRAEMCQKLKFFKDTEIAKIKMEAKKKYEK 240
                ************************************************************
                                                        Coiled-coil 1
OFD1a           ELTMFQNDFEKACQAKSEALVLREKSTLERIHKHQEIETKEIYAQRQLLLKDMDLLRGRE 300
OFD1b           ELTMFQNDFEKACQAKSEALVLREKSTLERIHKHQEIETKEIYAQRQLLLKDMDLLRGRE 300
                ************************************************************
                                                      Intercoil domain
OFD1a           AELKQRVEAFELNQKLQEEKHKSITEALRRQEQNIKSFEETYDRKLKNELLKYQLELKDD 360
OFD1b           AELKQRVEAFELNQKLQEEKHKSITEALRRQEQNIKSFEETYDRKLKNELLNFH------ 354
                ************************************************:::
                                  Coiled-coil 2
OFD1a           YIIRTNRLIEDERKNKEKAVHLQEELIAINSKKEELNQSVNRVKELELELESVKAQSLAI 420
OFD1b           ---------------RLHGVCLALGILI------------------------------- 367
                               : :.* *   ::

OFD1a           TKQNHMLNEKVKEMSDYSLLKEEKLELLAQNKLLKQQLEESRNENLRLLNRLAQPAPELA 480
OFD1b           ------------------------------------------------------------
```

Table 1. **Defects in ciliary functions cause several human diseases.**

Heterotaxia (Nonaka et al., 1998; Yost, 2003), retinal degeneration (Li et al., 1996; Liu et al., 2004), anosmia (Kulaga et al., 2004), polycystic kidney disease (Barr et al., 2001; Bisceglia et al., 2006; Chauvet et al., 2004; Hanaoka et al., 2000; Lin et al., 2003; Low et al., 2006; Nauli et al., 2003; Praetorius and Spring, 2001), polydactyly and neural patterning defects (Liu et al., 2005), neural patterning defects (Corbit et al., 2005; Huangfu et al., 2003; Liu et al., 2005), neural tube closure defects (Kyttala et al., 2006; Park et al., 2006; Ross et al., 2005; Simons et al., 2005; Smith et al., 2006).

Barr, M.M., DeModena, J., Braun, D., Nguyen, C.Q., Hall, D.H., and Sternberg, P.W. (2001). The Caenorhabditis elegans autosomal dominant polycystic kidney disease gene homologs lov-1 and pkd-2 act in the same pathway. Curr Biol *11*, 1341-1346.

Bisceglia, M., Galliani, C.A., Senger, C., Stallone, C., and Sessa, A. (2006). Renal cystic diseases: a review. Adv Anat Pathol *13*, 26-56.

Chauvet, V., Tian, X., Husson, H., Grimm, D.H., Wang, T., Hiesberger, T., Igarashi, P., Bennett, A.M., Ibraghimov-Beskrovnaya, O., Somlo, S.*, et al.* (2004). Mechanical stimuli induce cleavage and nuclear translocation of the polycystin-1 C terminus. J Clin Invest *114*, 1433-1443.

Corbit, K.C., Aanstad, P., Singla, V., Norman, A.R., Stainier, D.Y., and Reiter, J.F. (2005). Vertebrate Smoothened functions at the primary cilium. Nature *437*, 1018-1021.

Hanaoka, K., Qian, F., Boletta, A., Bhunia, A.K., Piontek, K., Tsiokas, L., Sukhatme, V.P., Guggino, W.B., and Germino, G.G. (2000). Co-assembly of polycystin-1 and -2 produces unique cation-permeable currents. Nature *408*, 990-994.

Huangfu, D., Liu, A., Rakeman, A.S., Murcia, N.S., Niswander, L., and Anderson, K.V. (2003). Hedgehog signalling in the mouse requires intraflagellar transport proteins. Nature *426*, 83-87.

Kulaga, H.M., Leitch, C.C., Eichers, E.R., Badano, J.L., Lesemann, A., Hoskins, B.E., Lupski, J.R., Beales, P.L., Reed, R.R., and Katsanis, N. (2004). Loss of BBS proteins causes anosmia in humans and defects in olfactory cilia structure and function in the mouse. Nat Genet *36*, 994-998.

Kyttala, M., Tallila, J., Salonen, R., Kopra, O., Kohlschmidt, N., Paavola-Sakki, P., Peltonen, L., and Kestila, M. (2006). MKS1, encoding a component of the flagellar apparatus basal body proteome, is mutated in Meckel syndrome. Nat Genet *38*, 155-157.

Li, T., Snyder, W.K., Olsson, J.E., and Dryja, T.P. (1996). Transgenic mice carrying the dominant rhodopsin mutation P347S: evidence for defective vectorial transport of rhodopsin to the outer segments. Proc Natl Acad Sci U S A *93*, 14176-14181.

Lin, F., Hiesberger, T., Cordes, K., Sinclair, A.M., Goldstein, L.S., Somlo, S., and Igarashi, P. (2003). Kidney-specific inactivation of the KIF3A subunit of kinesin-II inhibits renal ciliogenesis and produces polycystic kidney disease. Proc Natl Acad Sci U S A *100*, 5286-5291.

Liu, A., Wang, B., and Niswander, L.A. (2005). Mouse intraflagellar transport proteins regulate both the activator and repressor functions of Gli transcription factors. Development *132*, 3103-3111.

Liu, Q., Zuo, J., and Pierce, E.A. (2004). The retinitis pigmentosa 1 protein is a photoreceptor microtubule-associated protein. J Neurosci *24*, 6427-6436.

Low, S.H., Vasanth, S., Larson, C.H., Mukherjee, S., Sharma, N., Kinter, M.T., Kane, M.E., Obara, T., and Weimbs, T. (2006). Polycystin-1, STAT6, and P100 function in a pathway that transduces ciliary mechanosensation and is activated in polycystic kidney disease. Dev Cell *10*, 57-69.

Nauli, S.M., Alenghat, F.J., Luo, Y., Williams, E., Vassilev, P., Li, X., Elia, A.E., Lu, W., Brown, E.M., Quinn, S.J.*, et al.* (2003). Polycystins 1 and 2 mediate mechanosensation in the primary cilium of kidney cells. Nat Genet *33*, 129-137.

Nonaka, S., Tanaka, Y., Okada, Y., Takeda, S., Harada, A., Kanai, Y., Kido, M., and Hirokawa, N. (1998). Randomization of left-right asymmetry due to loss of nodal cilia generating leftward flow of extraembryonic fluid in mice lacking KIF3B motor protein. Cell *95*, 829-837.

Park, T.J., Haigo, S.L., and Wallingford, J.B. (2006). Ciliogenesis defects in embryos lacking inturned or fuzzy function are associated with failure of planar cell polarity and Hedgehog signaling. Nat Genet *38*, 303-311.

Praetorius, H.A., and Spring, K.R. (2001). Bending the MDCK cell primary cilium increases intracellular calcium. J Membr Biol *184*, 71-79.

Ross, A.J., May-Simera, H., Eichers, E.R., Kai, M., Hill, J., Jagger, D.J., Leitch, C.C., Chapple, J.P., Munro, P.M., Fisher, S.*, et al.* (2005). Disruption of Bardet-Biedl syndrome ciliary proteins perturbs planar cell polarity in vertebrates. Nat Genet *37*, 1135-1140.

Simons, M., Gloy, J., Ganner, A., Bullerkotte, A., Bashkurov, M., Kronig, C., Schermer, B., Benzing, T., Cabello, O.A., Jenny, A.*, et al.* (2005). Inversin, the gene product

mutated in nephronophthisis type II, functions as a molecular switch between Wnt signaling pathways. Nat Genet *37*, 537-543.

Smith, U.M., Consugar, M., Tee, L.J., McKee, B.M., Maina, E.N., Whelan, S., Morgan, N.V., Goranson, E., Gissen, P., Lilliquist, S.*, et al.* (2006). The transmembrane protein meckelin (MKS3) is mutated in Meckel-Gruber syndrome and the wpk rat. Nat Genet *38*, 191-196.

Yost, H.J. (2003). Left-right asymmetry: nodal cilia make and catch a wave. Curr Biol *13*, R808-809.

Table 1

Ciliary Function	Disease Phenotype
Nodal Flow	Heterotaxia
Photoreception	Retinal degeneration
Odorant reception	Anosmia
Mechanosensation	Polycystic kidney disease
Gli repressor formation	Polydactyly, neural patterning defects
Gli activator formation	Neural patterning defects
Convergent extension	Neural tube closure defects

Table 2. **Summary of phenotypes caused by OFD1 syndrome-associated mutations.** (**A**) Ofd1 protein expression quantified by immunoblot. Percentages reflect comparison to wild type (for the Gene trap line), *Ofd1*^{IRESOfd1myc} cells (for the S75F, A80T, G139S mutants) or *Ofd1*^{Ofd1myc} cells (for the S437R, KDD359-361FSYmutants), as appropriate. (**B**) Ofd1 centrosomal localization, as assessed by immunofluorescence. NA, not assessed. (**C-F**) Percent of cells showing long centrioles, centrosomal Cep164 and Ift88 localization, and cilia, as assessed by immunofluorescent staining and normalized to wild type cells. Asterisks indicate a statistically significant difference ($p < 0.05$) when compared to *Ofd1*^{IRESOfd1myc} or *Ofd1*^{Ofd1myc} cells (for G139S and S437R mutants, respectively), or *Ofd1*^{Rev} cells (for S75F, A80T, and KDD359-361FSY mutants). Errors are standard deviations.

Table 2

Cell Line	A Percent of Ofd1 protein expression, compared to control line	B Does Ofd1 localize to the centrosome?	C Percent of long centrioles, compared to wild type cells	D Percent of centrosomes with Cep164 localization, compared to wild type cells	E Percent of centrosomes with Ift88 localization, compared to wild type cells	F Percent of cells with cilia, compared to wild type cells
Gene trap	0	No	475 ± 34	2 ± 1	12 ± 5	0
S75F	22	NA	232 ± 20 *	28 ± 7	3 ± 4 *	0 *
A80T	51	NA	307 ± 39 *	11 ± 3 *	2 ± 1 *	0 *
G139S	112	Yes	175 ± 30 *	93 ± 15	22 ± 3	20 ± 1 *
S427R	103	Yes	146 ± 23 *	100 ± 22	32 ± 1 *	35 ± 3 *
KDD359-361 FSY	34	Yes	45 ± 25 *	75 ± 10	47 ± 5	35 ± 8 *

Table 3. Distinct role of Ofd1 in centriole length control.

Comparison of the functions of four proteins implicated in centriole length control (Keller et al., 2008; Kohlmaier et al., 2009; Schmidt et al., 2009; Tang et al., 2009). MC, mother centriole. DC, daughter centriole. PC, procentrioles. ND, no data.

Keller, L.C., Geimer, S., Romijn, E., Yates, J., 3rd, Zamora, I., and Marshall, W.F. (2008). Molecular Architecture of the Centriole Proteome: The Conserved WD40 Domain Protein POC1 Is Required for Centriole Duplication and Length Control. Mol Biol Cell.

Kohlmaier, G., Loncarek, J., Meng, X., McEwen, B.F., Mogensen, M.M., Spektor, A., Dynlacht, B.D., Khodjakov, A., and Gonczy, P. (2009). Overly long centrioles and defective cell division upon excess of the SAS-4-related protein CPAP. Curr Biol *19*, 1012-1018.

Schmidt, T.I., Kleylein-Sohn, J., Westendorf, J., Le Clech, M., Lavoie, S.B., Stierhof, Y.D., and Nigg, E.A. (2009). Control of centriole length by CPAP and CP110. Curr Biol *19*, 1005-1011.

Tang, C.J., Fu, R.H., Wu, K.S., Hsu, W.B., and Tang, T.K. (2009). CPAP is a cell-cycle regulated protein that controls centriole length. Nat Cell Biol *11*, 825-831.

Table 3

Protein	Centriolar Localization	Required for Centriole Duplication?	Elongation defects upon	Abnormal length of	Morphology of elongated centrioles	Character of elongated portion	Other
Ofd1	Distal MC, DC, PC	No	Loss	MC, DC	Complete walls and microtubules, appendage proteins expanded along elongated portion	Distal	Required for distal appendage formation
CP110	Distal MC, DC, PC, not always present	Yes	Depletion	MC, DC, PC	Incomplete walls and microtubule extensions, appendages in middle	Proximal?	
CPAP	Proximal MC, DC, PC	Yes	Overexpression	MC, DC, PC	Incomplete walls and microtubule extensions, appendages in middle, extra PC nucleation	Proximal	
Poc1	Proximal MC, DC, PC	Yes	Overexpression	ND	ND	ND	

Table 4. MGI nomenclature for alleles.

Allele	MGI nomenclature
Ofd1$^{IRESOfd1myc\text{-}S75F}$	*Ofd1*$^{Gt(RRF427)Byg.tm4(Ofd1mycS75F)Reit}$
Ofd1$^{IRESOfd1myc\text{-}A80T}$	*Ofd1*$^{Gt(RRF427)Byg.tm5(Ofd1mycA80T)Reit}$
Ofd1$^{IRESOfd1myc\text{-}G139S}$	*Ofd1*$^{Gt(RRF427)Byg.tm6(Ofd1mycG139S)Reit}$
Ofd1$^{Ofd1myc\text{-}S437R}$	*Ofd1*$^{Gt(RRF427)Byg.tm7(Ofd1mycS437R)Reit}$
Ofd1$^{Ofd1myc\text{-}KDD359\text{-}361FSY}$	*Ofd1*$^{Gt(RRF427)Byg.tm8(Ofd1mycKDD359\text{-}361FSY)Reit}$

Chapter 3: Perspectives: Floxin technology and study of gene function

SUMMARY AND CONCLUSION

Understanding gene function requires studying the phenotypes caused by knockout and replacement alleles of a specific gene. The Floxin technology is unique in that it encompasses both aspects of gene targeting within one system, and allows study of phenotypes on a cellular and organismal level. Our investigation of *Ofd1* function showed how the Floxin technology can be used to model a human disease, permitting creation of cell lines with targeted alleles in a quantity that was prohibitive with traditional methods. As this approach was successful in defining a role for *Ofd1* in a basic cell biological process, and identifying the molecular basis of a human disease, we hope to see other similar applications in the future.

Many centrosomal and ciliary genes have Floxin-compatible gene trap lines, so models of other ciliopathies could be created. Floxin is also particularly suited for studying gene function in ES cells, as genes expressed in this cell type are likely to be trapped. Finally, autosomal dominant and X-linked diseases are amenable to modeling with Floxin.

We see the Floxin technology as complementary to traditional methods for gene targeting. We hope that the capability to generate targeted alleles in a high throughput fashion in mammalian cells will aid in the detailed understanding of gene function, and creation of cellular and animal models of disease.

Publishing Agreement

It is the policy of the University to encourage the distribution of all theses, dissertations, and manuscripts. Copies of all UCSF theses, dissertations, and manuscripts will be routed to the library via the Graduate Division. The library will make all theses, dissertations, and manuscripts accessible to the public and will preserve these to the best of their abilities, in perpetuity.

Please sign the following statement:

I hereby grant permission to the Graduate Division of the University of California, San Francisco to release copies of my thesis, dissertation, or manuscript to the Campus Library to provide access and preservation, in whole or in part, in perpetuity.

3/26/2010